Modelling Pair Production of Top Squarks with Decays via Tau Sleptons in the pMSSM

Ludwig-Maximilians-Universität München

Faculty of Physics

Master Thesis

submitted by

Christoph Ames

Munich, 30.10.2020

Supervisor: PD Dr. Alexander Mann

Modellierung der Paarerzeugung von Top-Squarks mit Zerfälle nach Tau-Sleptonen im pMSSM

Ludwig-Maximilians-Universität München
Fakultät für Physik

Masterarbeit

vorgelegt von
Christoph Ames
München, 30.10.2020

Betreuer: PD Dr. Alexander Mann

Abstract

Supersymmetry is a theoretical framework that extends the Standard Model of Particle Physics and solves some of its shortcomings. The phenomenological Minimal Supersymmetric Standard Model (pMSSM) is a simplified supersymmetric model that allows for a systematic probing of its parameter space due to its heavily reduced number of parameters.

This work focuses on the comparison of three simplified models in the context of the pMSSM, in which a stop ($\tilde{t}_1$) decays via either a stau ($\tilde{\tau}_1$) or a tau-sneutrino ($\tilde{\nu}_\tau$). The lightest supersymmetric particle (LSP) is either a gravitino ($\tilde{G}$) or a neutralino ($\tilde{\chi}_1^0$). These models are used to get an understanding of how different particle decays are influenced by the parameters of the pMSSM, and to find the boundaries for each model's phase space. Decay modes that compete with the simplified models are also studied to determine how to suppress them. These comparisons are performed using generated model points, which are configurations of particle masses and decay modes uniquely defined by sets of pMSSM parameter values. The phase space of the model generation has been adjusted to increase the likelihood that the model points will contain the simplified models, whilst still allowing for an uncompromising study.

A secondary goal is to understand which of these models would be best suited for a study using real data. For this, the influence of the simplified models on the dark matter relic density and the mass of the Higgs boson is studied. Model points, in which the simplified models with a gravitino as LSP could be measured, are generally within the boundaries of the dark matter relic density. The models with the neutralino as LSP tended to have a relic density that is too large. The models are able to produce Higgs bosons within 122–128 GeV, but only within limited regions of the total phase space. While all three simplified models seem promising in the context of the pMSSM, clear advantages for the model with the gravitino as LSP can be identified.

Zusammenfassung

Supersymmetrie ist ein theoretisches Gerüst, welches das Standardmodell der Teilchenphysik erweitert und manche der offenen Fragen des Standardmodells beheben kann. Das phänomenologische Minimale Supersymmetrische Standard Modell (pMSSM) ist ein vereinfachtes supersymmetrisches Model, dessen Parameterraum aufgrund der stark reduzierten Parameteranzahl eine systematische Erforschung ermöglicht.

Der Schwerpunkt dieser Arbeit liegt im Vergleich von drei vereinfachten Modellen im Kontext des pMSSM's, in denen ein Stop ($\tilde{t}_1$) über einen Stau ($\tilde{\tau}_1$) oder einen Tau-Sneutrino ($\tilde{\nu}_\tau$) zerfällt. Das leichteste supersymmetrische Teilchen ist entweder ein Gravitino ($\tilde{G}$) oder ein Neutralino ($\tilde{\chi}_1^0$). Diese Modelle werden genutzt, um ein Verständnis vom Einfluss der Parameter des pMSSM auf verschiedene Teilchenzerfälle, zu bekommen. Dabei werden auch die Grenzen der Phasenräume der Modelle aufgedeckt. Zerfallsmoden, die mit den vereinfachten Modellen konkurrieren, werden ebenfalls untersucht, um sie unterdrücken zu können. Diese Vergleiche werden mit generieten Modellpunkten durchgeführt. Modellpunkte sind Konfigurationen von Teilchenmassen und Zerfallsmoden, die durch die Werte der pMSSM Parameter einzigartig bestimmt werden. Der Phasenraum der Generierung der Modellpunkte wird an die vereinfachten Modelle angepasst, um die Wahrscheinlichkeit, dass ein Modellpunkt eines der vereinfachten Modelle beinhaltet, erhöht wird.

Ein sekundäres Ziel ist es, herauszufinden, welches der Modelle für eine Studie mit experimentellen Daten am besten geeignet wäre. Dafür werden, unter anderem, die Einflüsse der Modelle auf die Restmenge von Dunkler Materie und auf die Masse des Higgs Bosons geprüft. Modellpunkte, in denen die vereinfachten Modelle mit Gravitino als LSP gemessen werden könnten, sind in der Regel innerhalb der Grenzen der Reliktdichte von Dunkler Materie. Die Modellpunkte mit Neutralino als LSP neigen dazu, eine zu groe Reliktdichte zu haben. Die Modelle können Higgs Bosonen innerhalb 122–128 GeV produzieren, aber nur innerhalb eingeschränkter Regionen des kompletten Phasenraums. Während alle drei vereinfachten Modelle vielversprechend im Kontext des pMSSM's sind, können eindeutige Vorteile für das Modell mit dem Gravitino als LSP identifiziert werden.

Contents

1 Introduction **1**

2 Theory **3**

2.1 The Standard Model . . . 3

2.1.1 Mathematical description . . . 3

2.1.2 Particle content . . . 7

2.2 Supersymmetry . . . 10

2.2.1 Mathematical Description . . . 10

2.2.2 Soft Symmetry Breaking . . . 10

2.2.3 The Hierarchy Problem . . . 11

2.2.4 Gauge Coupling Unification . . . 12

2.2.5 Dark Matter and R-Parity . . . 13

2.2.6 Minimal Supersymmetric Standard Model . . . 14

2.2.7 phenomenological Minimal Supersymmetric Standard Model . . . 16

2.3 Simplified Models . . . 17

3 Experimental Set-up **21**

3.1 Detectors . . . 21

3.2 Software and Model Generation . . . 22

3.3 Unphysical Model Points . . . 23

4 ATLAS-stau **25**

4.1 Particle Masses and Mixtures . . . 25

4.2 Competing Decay Modes . . . 28

4.3 Influence on the Mass of the Higgs Boson . . . 32

4.3.1 $tan(\beta)$ - Ratio of Higgs Field VEVs . . . 32

4.3.2 A_t - Trilinear Coupling Constant . . . 36

4.3.3 μ - Higgsino Mass Parameter . . . 37

4.4 Dark Matter Relic Density 39

5 CMS-stau and CMS-sneutrino **41**

5.1 CMS-stau 41

5.2 Competing Decay Modes 50

5.3 Influence on the Mass of the Higgs Boson 53

5.4 Dark Matter Relic Density 53

5.5 CMS-sneutrino 55

5.5.1 Phase Space 55

5.5.2 Comparison between CMS-sneutrino and CMS-stau 55

6 Conclusion **59**

Bibliography **61**

Appendix A **65**

Chapter 1

Introduction

The field of particle physics focuses on the study of some the most fundamental aspects of our universe: Which particles exist and how do they interact with one another? Many experiments requiring hundreds and thousands of researchers using some of the largest and most precise machines in the world have been performed to try to answer these questions. This has lead to the construction of a theoretical model known as the Standard Model of Particle Physics (SM). The SM is likely the most well researched physical theory to date. It describes all known elementary matter particles and explains the origin of three of the four known forces. Over the second half of the 20^{th} century, many of the particles predicted by the SM were found, with the final discovery being that of the Higgs boson in 2012 [1]. This verified the SM as a self-contained theory that could be used as a very good model for explaining most known phenomena in particle physics.

However, there are still open questions that can not be explained by the SM: What is dark matter? How are the loop corrections to the Higgs boson's mass being cancelled? How can gauge coupling unification at high energies be explained theoretically? It has become quite clear that theories that extend the SM are necessary. One class of theories is Supersymmetry (SUSY), which introduces new partner particles for all SM fermions and bosons. The potential discovery of these partner particles has become a great topic of interest, with large scale searches being performed by multiple collaborations using the Large Hadron Collider at CERN. So far, no traces of SUSY particle have been found.

A SUSY model can take on various forms, one of which being the phenomenological Minimal Supersymmetric Standard Model (pMSSM), which is a simplified version of the MSSM and is described by 19 parameters. This work focuses on getting a better understanding of how the different parameters influence the pMSSM's particle spectrum by studying three different simplified models within the pMSSM using generated models. After an introduction to the theoretical background required for this analysis, an overview of the model generation is given. How the simplified models are dependant on each pMSSM parameter is discussed in detail in the main section of this work.

Chapter 2

Theory

This following section will briefly cover the theoretical principles and models upon which this analysis is built. The Standard Model of Particle Physics (SM), along with it is short-comings, will be discussed and an overview of Supersymmetry (SUSY), a theoretical framework that extends the SM, will be given. Finally, the phenomenological Minimal Supersymmetric Standard Model (pMSSM), the SUSY model that this analysis focuses on, will be introduced.

2.1 The Standard Model

2.1.1 Mathematical description

Quantum field theory

The following mathematical description of the SM follows [2, 3, 4]

Classically, objects in space are described by their time-dependent spatial coordinates: $\boldsymbol{x}(t)$. Here, $\boldsymbol{x}(t)$ is a 3-vector, which is denoted by the bold font. An example of this would be the calculation of the path of a single water particle in a turbulent body of water. In contrast to this, field theory takes a metaphorical step backwards and tries to describe a region of space as a whole system. Therefore, fields are functions of position and time ($\phi_i(\boldsymbol{x}, t)$) and particles are excitations of a field. In the previous analogy, a field would describe the motion of the turbulent body of water as a system, throughout time. Or, for more of a particle physics related example, the electric potential V is a field.

A Lagrangian density $\mathcal{L}$ (often simply referred to as a *Lagrangian*, as in the following) is a function of fields ϕ_i and their derivatives in time and space $\partial_\mu \phi_i \equiv \frac{\partial \phi_i}{\partial x^\mu}$. In field theory, the action S is defined as the integral over a Lagrangian:

$$S = \int \mathcal{L}\left(\phi_i, \partial_\mu \phi_i\right) d^4x. \tag{2.1}$$

The principle of least action states that if a system can evolve over time, it will always do so in a way that the action S remains minimal; mathematically expressed as $\delta S = 0$. From this follows the Euler-Lagrange equation

$$\partial_\mu \left(\frac{\partial \mathcal{L}}{\partial \left(\partial_\mu \phi_i \right)} \right) = \frac{\partial \mathcal{L}}{\partial \phi_i}, \tag{2.2}$$

which provides the equations of motion for the system. Quantum field theory focuses on describing the behaviour of quantum particles with fields.

Phase invariance and gauge symmetry

Gauge invariance implies that the Lagrangian doesn't change when it undergoes a phase transformation. Specifically, the two types transformations in question are global phase transformations and local phase transformations. A global phase transformation, described as

$$\psi \to e^{i\alpha} \psi, \tag{2.3}$$

is independent of spacetime. An important property of global gauge invariance is that the new phase doesn't affect the derivative of the field

$$\partial_\mu \psi \to e^{i\alpha} \partial_\mu \psi, \tag{2.4}$$

which also means that the Lagrangian is not affected by the transformation. An anecdote for this would be a universe-wide potential being changed by a equally-large flat amount, everywhere. This shouldn't change the laws of physics, which is why a Lagrangian that describes elementary particles and forces must be globally gauge invariant. Generally, this is not problematic, as the global phase is independent of space-time and therefore not affected by the derivative during the construction of the Lagrangian. On the other hand, a local phase transformation, as the name implies, is dependent on spacetime and is described as

$$\psi \to e^{i\alpha(\boldsymbol{x})} \psi = \tilde{\psi}. \tag{2.5}$$

When applying the derivative to the transformed field, an additional term appears that doesn't exist for the non-transformed field

$$\partial_\mu \tilde{\psi} = \partial_\mu \left(e^{i\alpha(\boldsymbol{x})} \right) \psi + e^{i\alpha(\boldsymbol{x})} \partial_\mu \psi = i \left(\partial_\mu \alpha \left(\boldsymbol{x} \right) \right) e^{i\alpha(\boldsymbol{x})} \psi + e^{i\alpha(\boldsymbol{x})} \partial_\mu \psi. \tag{2.6}$$

Therefore, when constructing a Lagrangian to describe a physical theory, it must be expanded by an additional field that transforms such that it causes the additional term in Eq. 2.6 to be cancelled. This can be done by choosing the expansion of the field in a way that contains the local phase. A example of this can be performed with the Dirac Lagrangian [1]

[1]Using natural units: $\hbar = 1$, $c = 1$

$$\mathcal{L} = i\bar{\psi}\gamma^{\mu}\partial_{\mu}\psi - m\bar{\psi}\psi \tag{2.7}$$

where $\bar{\psi}$ is the adjoint spinor of ψ[2]. If the field in 2.7 transformed like Eq. 2.5, then the derivative of the field in the first part of the Lagrangian transforms like Eq. 2.6, resulting in

$$\mathcal{L} \rightarrow \mathcal{L} - \left(\partial_{\mu}\alpha\left(\boldsymbol{x}\right)\right)\bar{\psi}\gamma^{\mu}\psi \tag{2.8}$$

which clearly is not invariant under local phase transformation. To ease the choice of how the new field (with which the Lagrangian will be expanded) should transform locally, the phase $\alpha\left(\boldsymbol{x}\right)$ can be defined as

$$\alpha\left(\boldsymbol{x}\right) = -q\lambda\left(\boldsymbol{x}\right) \tag{2.9}$$

which redefines the local phase transformation to

$$\psi \rightarrow e^{-iq\lambda(\boldsymbol{x})}\psi \tag{2.10}$$

and results in Eq. 2.8 being rewritten as

$$\mathcal{L} \rightarrow \mathcal{L} + q\bar{\psi}\gamma^{\mu}\psi\partial_{\mu}\lambda\left(\boldsymbol{x}\right). \tag{2.11}$$

The Lagrangian clearly is not invariant under transformation. To reconcile this problem, a vector field A_{μ} (referred to as a 'gauge" field) is introduced that transforms locally with

$$A_{\mu} \rightarrow A_{\mu} + \partial_{\mu}\lambda. \tag{2.12}$$

Implementing Eq. 2.9 into Eq. 2.6 results in

$$\partial_{\mu}\psi = e^{-iq\lambda(\boldsymbol{x})}\left(\partial_{\mu} - iq\left(\partial_{\mu}\lambda\right)\right)\psi. \tag{2.13}$$

Since the transformation of the gauge field was chosen so that it contains $\partial_{\mu}\lambda$, a substitution for the partial derivative can be introduced, known as the "covariant derivative"

$$\mathcal{D}_{\mu} = \partial_{\mu} + iqA_{\mu} \tag{2.14}$$

which transforms with

$$\mathcal{D}_{\mu} \rightarrow \partial_{\mu} + iq\left(A_{\mu} + \partial_{\mu}\lambda\right) \tag{2.15}$$

and has the property

$$\mathcal{D}_{\mu}\psi \rightarrow e^{-iq\lambda(\boldsymbol{x})}\mathcal{D}_{\mu}\psi. \tag{2.16}$$

[2] $\bar{\psi} \equiv \psi^{\dagger}\gamma^{0}$, where γ^{0} is the time-like gamma-matrix

In other words, with a specific choice of gauge field (and with the help of the redefined phase to simplify matters), a new derivative can be constructed that makes the Dirac Lagrangian invariant under local phase transformation (note the similarity between Eq. 2.16 and Eq. 2.4). As a result, the Dirac Lagrangian takes on a new form

$$\mathcal{L} = i\bar{\psi}\gamma^\mu\partial_\mu\psi - m\bar{\psi}\psi + \left(q\bar{\psi}\gamma^\mu\psi\right) A_\mu \tag{2.17}$$

it is important to realise that the redefinition of the phase and the introduction of the gauge field do not just serve mathematical purposes. As with all terms in a Lagrangian, the new term seen in Eq. 2.17 has a physical interpretation: it introduces both the electromagnetic field A_μ and the electromagnetic charge q. However, it doesn't include the free term for the gauge field. Since the gauge field is a vector field, the free term can be described by the Proca Lagrangian

$$\mathcal{L} = -\frac{1}{16\pi}F^{\mu\nu}F_{\mu\nu} + \frac{1}{8\pi}m_A^2 B^\nu A_\nu. \tag{2.18}$$

The first term includes the electromagnetic tensor, which is defined as $F_{\mu\nu} = \partial^\mu A^\nu - \partial^\nu A^\mu$ and is local phase invariant under the aforementioned transformation of A_μ in Eq. 2.12. The second term, specifically $A^\nu A_\nu$, is not local phase invariant and the only way to solve this problem is by setting the mass parameter m_A to 0, eliminating the second term entirely. This means that the gauge field B_μ was introduced and its mediating particle, which at this point looks like the photon, must be massless. This results in a $U(1)$ gauge symmetry, and is the basis of quantum electrodynamics (QED). It should be noted, that in the example with the Dirac Lagrangian it looks like local gauge invariance was demanded first and then the origin of the electromagnetic force conveniently followed. However, it is the other way around: to be able to construct a Lagrangian describing the electromagnetic force, it is required that local gauge invariance is introduced.

The $U(1)_{QED}$ gauge symmetry is not the only symmetry that can come from implementing a gauge field to achieve local phase invariance. The same can be done for $SU(2)$ and $SU(3)$[3], though the local gauge transformations are not as simple as with the Dirac Lagrangian, as more fields are involved.
The $SU(3)$ gauge symmetry, which introduces gluons, quarks and the colour charge, is known as quantum chromodynamics (QCD). The process for its derivation is similar to that of the $U(1)_{QED}$ gauge symmetry.
The $SU(2)$ gauge symmetry describes the weak interaction with the gauge bosons $W_\mu^1, W_\mu^2, W_\mu^3$. It has the problem that the gauge bosons for the weak interaction would have to be massless to ensure local gauge symmetry, but it has been proven experimentally that they have mass [6, 7]. The $U(1)_{QED}$ and $SU(2)$ gauge symmetries can be combined to form the $SU(2)_L \times U(1)_Y$ symmetry, which describes the electroweak symmetry. Since the weak part only interacts with particles with a left-handed chirality, the $SU(2)$ group is denoted with the L subscript. The $U(1)_Y$ group is not quite the same as the $U(1)_{QED}$ group: the Y refers to the weak hypercharge from the Gell-Mann-Nishijima formula $Y = 2(Q - I_3)$, where Q is the electric charge and I_3 is the

[3]Strictly speaking, according to Yang and Mills [5], this can be done with any $SU(n)$ group.

third component of the weak isospin. The gauge bosons of $U(1)_{QED}$ and $SU(2)$ mix, to create the $W^{\pm}$ bosons, the Z^0 boson and the photon A_μ

$$W^+ = \frac{1}{\sqrt{2}}\left(W^1_\mu - iW^2_\mu\right) \tag{2.19}$$
$$W^- = \frac{1}{\sqrt{2}}\left(W^1_\mu + iW^2_\mu\right) \tag{2.20}$$
$$Z^0 = \cos\left(\theta_W\right) \cdot W^3_\mu - \sin\left(\theta_W\right) \cdot B_\mu \tag{2.21}$$
$$A_\mu = \sin\left(\theta_W\right) \cdot W^3_\mu + \cos\left(\theta_W\right) \cdot B_\mu \tag{2.22}$$
$$\tag{2.23}$$

where θ_W is the weak mixing angle. During this process, with the introduction of the Higgs mechanism, the $W^{\pm}$ and Z^0 bosons gain mass. The Higgs field is a complex scalar field

$$\phi(x) = \frac{1}{\sqrt{2}}\left(\phi_1(x) + i\phi_2(x)\right) \tag{2.24}$$

and introduces a new potential

$$V(\phi) = -\mu^2(\phi^*\phi) + \lambda(\phi^*\phi)^2 \tag{2.25}$$

where μ^2 and λ are positive constants. It can be shown that the minimum of this potential is degenerate, meaning that there are an infinite number of states that achieve the minimum potential. The minimum is known as the vacuum expectation value (VEV). The first term on the right side of Eq. 2.25, $-\mu^2(\phi^*\phi)$, looks like it represents a mass term, but the minus sign would mean that the mass is negative. This would be unphysical, therefore the mass term would have to be set to 0. However, this problem can be solved by considering fluctuations around the minimum, which results in the spontaneous breaking of the symmetry of the system (meaning without influence from an outside system). This ultimately introduces the Higgs boson, a scalar particle with mass $m_H = \sqrt{2\lambda v^2}$ $\left(= \sqrt{2}\mu\right)$ and when implemented into the SM, it gives the electroweak gauge bosons, $W^{\pm}$ and Z^0, mass.

2.1.2 Particle content

The following section is based on [2, 8, 9]

All known elementary particles can be split into two groups: fermions, which have a half-integer spin and bosons, which have an integer spin.

Fermions

Fermions have a spin of $S_Z = \pm\frac{1}{2}$, follow the Pauli principle and and get their name from following the Fermi-Dirac statistics. They consist of all of the known matter particles and can be split into two groups: leptons and quarks.

Leptons come from the $SU(2)$ gauge symmetry involving the weak interaction. They are generated as three doublets (see Tab. 2.1) which, in this case, means that each charged lepton has an associated neutral lepton (neutrino). Whilst they all have a weak isospin of $I = 1$, the third component of the weak isospin is $I_3 = \frac{1}{2}$ for charged leptons and $I_3 = -\frac{1}{2}$ for neutral leptons. They all interact via the weak interaction, but only the charged leptons interact electromagnetically. According to the SM, neutrinos are massless, but evidence of flavour oscillation implies that some neutrinos must be massive [10]. Charged and neutral leptons can change into one another by either absorbing or emitting a $W^{\pm}$ boson, whereby the third component of their weak isospin is changed by ± 1 (thereby changing their electric charge via the Gell-Mann-Nishijima formula). This indicates that if not for the electric charge, one could think of the two particles of a doublet being two states of the same particle. A lepton and anti-lepton can eliminate to a Z^0 boson. Each generation has its own lepton number $L_i = 1$ (anti-leptons have -1), where i indicates the first, second or third generation. So far, total leptonic number conservation has been observed. For example, if a tau-lepton (τ) decays, then the total lepton number of the end state particles would have to equal $L_1 = 0$, $L_2 = 0$, $L_3 = 1$.

Generation	Flavour	Electric charge [e]	Mass
1	e	-1	0.511 MeV
	ν_e	0	< 1.1 eV
2	μ	-1	105.7 MeV
	ν_μ	0	< 0.19 MeV
3	τ	-1	1776.9 MeV
	ν_τ	0	< 18.2 MeV

Table 2.1: SM leptons. Natural units. Masses taken from [8].

Quarks come from the $SU(3)$ gauge symmetry involving the colour charge. The colour charge, which appears in the form of either *red*, *green* or *blue* (or the associated anti-colours), allows multiple quarks of the same flavour to bind together. Without the colour charge, the Pauli exclusion principle would seem to be broken for particles such as Δ^{++}, which consists of three strange-type quarks. The configuration of quarks has to be colour neutral (also called colourless or "white"), meaning there must be a red, green and blue charge for particles made of three quarks (known as baryons), or there must be a colour charge plus anti-colour charge of the same colour for particles made of a quark and an anti-quark (mesons). As a result, quarks can never be found by themselves and hadronise[4] when separated. The quarks themselves come in six flavours, split into three generations of doublets (see Tab. 2.2). Like with the leptons, the doublets are defined by their weak isospin, where each doublet has an isospin of $I = \frac{1}{2}$ and the upper quarks have a third component of weak isospin $I_3 = \frac{1}{2}$ and the lower quarks $I_3 = -\frac{1}{2}$. Also like the leptons, their electric charge differs by a total value of 1[5], but it is split differently. The upper quarks have a value of $Q = +\frac{2}{3}$, whereas the lower quarks have $Q = -\frac{1}{3}$, which allows for the creation of negative and positive particles.

[4] New quarks are spontaneously created and bind to create a colourless particle.

[5] In units of e

Generation	Flavour	Electric charge [e]	Mass [MeV]
1	u	$+\frac{2}{3}$	2.16
	d	$-\frac{1}{3}$	4.67
2	c	$+\frac{2}{3}$	$1.27 \cdot 10^3$
	s	$-\frac{1}{3}$	93
3	t	$+\frac{2}{3}$	$172.78 \cdot 10^3$
	b	$-\frac{1}{3}$	$4.18 \cdot 10^3$

Table 2.2: SM quarks. Natural units. Masses taken from [8].

Bosons

Bosons have spin $S_z = 1$ (apart from the Higgs boson) and follow Bose-Einstein statistics. They consist of the gauge bosons that mediate the known forces between matter particles.

The **gluon** g mediates the strong force, the interaction between quarks. it is massless and has no electric charge, but it has eight different colour charge states, known as the colour octet.

The **photon** γ is the neutral gauge boson of the electromagnetic interaction. it is massless, has spin $s = 1$ and conserves angular momentum. The lack of mass is a result of setting $m_A = 0$ in Eq. 2.18.

The $\boldsymbol{W^\pm}$ bosons and the $\boldsymbol{Z^0}$ boson are the mediators of the weak force. The $W^\pm$ bosons have a weak isospin of ± 1 and only couple to left-handed helicity states of quarks and leptons. They allow for quarks to change their flavour and for charged and neutral leptons to interact with one-another. The Z^0 boson mediates chargeless interactions (known as weak neutral currents) between leptons, conserving momentum and spin, and has a weak isospin of 0.

The **Higgs boson** has spin $S_Z = 0$. It gives mass to the $W^\pm$ and Z^0 bosons and it is coupling strength with other SM particles depends on the particle's mass. For this reason, it is strongest coupling is with the top-quark, followed by the $W^\pm$ and Z^0 bosons.

Boson	Mass [GeV]
g	0
γ	0
$W^\pm$	80.379
Z^0	91.1876
H	125.10

Table 2.3: SM bosons. Natural units. Masses taken from [8].

2.2 Supersymmetry

The basic idea of SUSY is that symmetry is constructed between fermions and bosons. For the Minimal Supersymmetric Standard Model (MSSM), the simplest complete SUSY model, this means that every fermion has a bosonic, supersymmetric partner particle (superpartner) that has the same quantum numbers (apart from the spin), and every boson has a fermionic superpartner. First, some of the shortcomings of the SM will be highlighted along with their SUSY solutions. Then, the simplest complete SUSY model, the MSSM and a simplification of this model, the phenomenological MSSM (pMSSM), which this work focuses on, will be presented.

The following section is based off of [11, 8].

2.2.1 Mathematical Description

In SUSY, fermionic states are transformed into bosonic states, and vice-versa. The transformation is performed with the fermionic operator Q, which is an anti-commuting spinor [11], with

$$Q\,|boson\rangle = |fermion\rangle\,, \qquad Q\,|fermion\rangle = |boson\rangle\,. \tag{2.26}$$

Since Q is a spinor, its hermitian conjugate $Q^\dagger$ is also a symmetry generator. That fact that both Q and $Q^\dagger$ are fermionic operators means that they have a spin of 1/2, from which follows that SUSY is a spacetime symmetry. They follow the commutator and anti-commutator relations:

$$\{Q, Q^\dagger\} \propto P^\mu \tag{2.27}$$

$$\{Q, Q\} = \{Q^\dagger, Q^\dagger\} = 0 \tag{2.28}$$

$$[P^\mu, Q] = [P^\mu, Q^\dagger] = 0, \tag{2.29}$$

where P^μ is the four-momentum generator of spacetime translations [11]. Each particle and its superpartner are represented together as a *supermultiplets* in the SUSY algebra. As a result of Eq. 2.29, the SUSY generators also commute with $-P^\mu$, which is the operator that produces a particle's squared mass. This means that a particle and their superpartner must have the same mass, as it doesn't matter whether the particle is transformed into its superpartner before squared mass operator is applied. Also, because Q and $Q^\dagger$ commute with generators of gauge transformations, it follows that the particles and their superpartners have the same quantum numbers (apart from spin).

2.2.2 Soft Symmetry Breaking

If SUSY were to be a perfect symmetry, then sparticles would have the same mass as particles (as discussed in Sec. 2.2.1). The general assumption is that if this were the case, then the SUSY-particles should be measurable with the currently achieved energy levels in particle accelerators. The fact that SUSY has not been confirmed means that if SUSY particles do exist, then their masses are heavier than previously thought. Therefore, sparticle masses must be greater than particle masses, breaking the symmetry. To take this "soft" breaking into account, the SUSY Lagrangian has to be extended by an additional term:

$$\mathcal{L} = \mathcal{L}_{SUSY} + \mathcal{L}_{soft}. \tag{2.30}$$

2.2.3 The Hierarchy Problem

Quantum gravitational effects become important at an energy scale known as the reduced Planck scale M_P, which is in the order of magnitude of around 10^{18} GeV. it is generally assumed that M_P functions as a sort of upper bound for the SM and that new physics must exist beyond it. Another energy scale that is used to describe the SM is the electroweak scale M_W, which defined is by the VEV of the Higgs field and is in the order of 10^2 GeV. It is generally seen as quite odd that two energy scales that seem fundamental for the SM are at completely different orders of magnitude and becomes problematic when looking at higher order corrections to the Higgs boson's (squared) mass, which according to the SM are dependant on these energy scales. These corrections come from particles coupling to the Higgs field. The larger the mass of a coupling particle is, the larger the correction is as well.

An example is a correction to ${m_h}^2$ from a loop involving a fermion f that has the mass m_f and a coupling parameter λ_f [11]:

$$\Delta {m_H}^2 = -\frac{|\lambda_f|^2}{8\pi^2}\Lambda_{UV}^2 + \dots\ . \tag{2.31}$$

The *ultraviolet momentum cut-off* Λ_{UV}^2 is the energy scale that is used to regulate the loop integral (to stop divergences) and should be understood as the energy scale at which new physics need to be introduced to describe behaviours at high energies. If Λ_{UV}^2 is taken to be M_P, then the corrections to the Higgs mass become incredibly large; many orders of magnitude larger than the Higgs mass itself. More corrections can come from a coupling to a hypothetical heavy complex scalar particle S with mass m_S [11]:

$$\Delta {m_h}^2 = \frac{\lambda_S}{16\pi^2}\left(\Lambda_{UV}^2 + 2{m_S}^2 ln\left(\frac{\Lambda_{UV}}{m_S}\right) + \dots\right). \tag{2.32}$$

These corrections need to be eliminated to get a Higgs boson with a mass in the order of GeV. For the λ_S and $|\lambda_f|^2$ terms to cancel each other, the coupling parameters require the relation $\lambda_S = 2|\lambda_f|^2$. It is not possible to eliminate all other appearing terms without having to introduce some sort of tuning to specifically counter them, referred to as *fine-tuning*, but this is considered unphysical. The idea that all of these extremely large corrections just so happen to cancel each other in a way that leaves the Higgs mass around the same order of magnitude as the other SM particles is generally seen as "unnatural". This is what is referred to as the hierarchy problem.

Figure 2.1: Interaction between the Higgs boson and (a) a fermion and (b) a scalar particle [11].

The general assumption is that there must be a new physical model that somehow regulates these corrections. This is where SUSY comes into play: the corrections that the Higgs boson receives from fermions and bosons are countered by corrections from their superpartners. Since the electric charge, colour charge and weak isospin are the same, the absolute value of the corrections are the same, but they have the opposite signs due to the different spins. This is one of the stronger motivations for discovering a SUSY-model.

2.2.4 Gauge Coupling Unification

it is believed that the strong, weak and electromagnetic forces are actually different parts of the same force. If this were the case, then the individual coupling constants of the forces would be the same at high energies (the coupling constants are not actually constants, but are dependent on the energy of the system). Unfortunately, the SM does not provide such a unification (depicted as dashed lines in Fig. 2.2). Through the introduction of new particles, new corrections are applied to the coupling constants and the MSSM allows for a unification at about $1.5 \cdot 10^{16}$ GeV (coloured lines in Fig. 2.2). The corrections start to have a stronger effect at around 3 TeV, which is where the coloured lines in Fig. 2.2 deviate from the dashed.

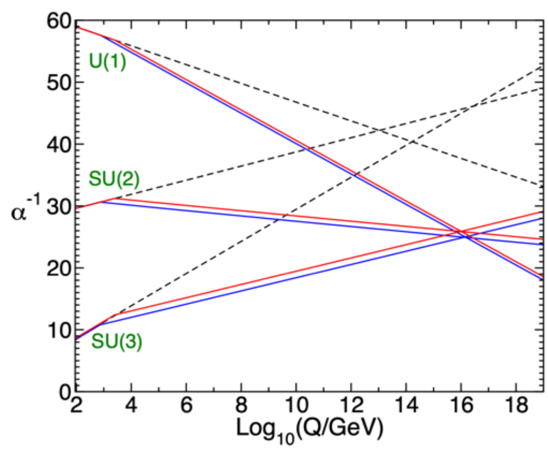

Figure 2.2: Strength of the coupling constants depending on energy scale for the SM (dashed) and the MSSM (coloured) [11].

2.2.5 Dark Matter and R-Parity

The are many experimental observations that hint at the existence of non-baryonic dark matter, a few examples being gravitational lensing, stellar velocity dispersion and rotation curves in asymmetric systems [8]. A big problem with the SM is that does not provide an explanation for what dark matter could be. However, a mechanism that can be implemented in SUSY models to solve a problem with baryon and lepton number conservation can also result in particles that fulfil the requirements for dark matter: R-parity.

A problem that can arise when constructing a SUSY Lagrangian is the possibility of introducing terms that break baryon and lepton number conservation. The conservation is intrinsic to the SM and a breaking of this conservation has not been observed. This issue can be resolved by introducing R-parity conservation. R-parity is defined as

$$P_R = (-1)^{3(B-L)+2s}, \tag{2.33}$$

where B is the baryon number, L the lepton number and s the spin. As a result, SM-particles have an even R-parity ($P_R = +1$) and SUSY-particles have an odd R-parity ($P_R = -1$). This has important consequence: every interaction needs to involve an even number of SUSY-particles. Therefore, if a SUSY-particle decays, then it is required to decay to an odd number of SUSY-particles (usually just one). That means that the lightest SUSY-particle (LSP) is stable, as it is unable to decay to any other SUSY-particles. If the LSP is also electrically neutral, then it becomes a candidate for dark matter.

Relic Density

We can assume that there are two types of interactions: interactions that change the abundance of a given particle type (annihilation, production) and interactions that do not. Once the rate of a particle species' number-changing interactions Γ has fallen below the Hubble constant H, the species is considered *chemically decoupled* [8] and the number of abundance-changing interactions is approximated to be negligible. This limit is estimated by calculating the *freeze-out temperature* $T_{f.o.}$. It is defined as the temperature where $H(T_{f.o.}) \sim \Gamma(T_{f.o.})$. Doing so provides a density of the given particle species that is constant throughout time, also known as a relic density (this assumes that the entropy is conserved between $T_{f.o.}$ and today, which is not given).

The relic densities calculated for theoretical models that describe new forms of particles and particle interactions must coincide with the experimentally measured values. When it comes to dark matter, the relic density calculated in this fashion is referred to as the cold dark matter relic density. Models that propose an interaction that creates a dark matter candidate must take into consideration that the interaction must not be so common as to violate this relic density. The cold dark matter relic density itself is given as $\Omega_c h^2$, where h is a normalised version of the Hubble constant H and is used to make the density Ω_c unitless.

Names	Spin	P_R	Gauge Eigenstates	Mass Eigenstates
Higgs bosons	0	$+1$	$H_u^0\ H_d^0\ H_u^+\ H_d^-$	$h^0\ H^0\ A^0\ H^\pm$
squarks	0	-1	$\widetilde{u}_L\ \widetilde{u}_R\ \widetilde{d}_L\ \widetilde{d}_R$	(same)
			$\widetilde{s}_L\ \widetilde{s}_R\ \widetilde{c}_L\ \widetilde{c}_R$	(same)
			$\widetilde{t}_L\ \widetilde{t}_R\ \widetilde{b}_L\ \widetilde{b}_R$	$\widetilde{t}_1\ \widetilde{t}_2\ \widetilde{b}_1\ \widetilde{b}_2$
sleptons	0	-1	$\widetilde{e}_L\ \widetilde{e}_R\ \widetilde{\nu}_e$	(same)
			$\widetilde{\mu}_L\ \widetilde{\mu}_R\ \widetilde{\nu}_\mu$	(same)
			$\widetilde{\tau}_L\ \widetilde{\tau}_R\ \widetilde{\nu}_\tau$	$\widetilde{\tau}_1\ \widetilde{\tau}_2\ \widetilde{\nu}_\tau$
neutralinos	1/2	-1	$\widetilde{B}^0\ \widetilde{W}^0\ \widetilde{H}_u^0\ \widetilde{H}_d^0$	$\widetilde{N}_1\ \widetilde{N}_2\ \widetilde{N}_3\ \widetilde{N}_4$
charginos	1/2	-1	$\widetilde{W}^\pm\ \widetilde{H}_u^+\ \widetilde{H}_d^-$	$\widetilde{C}_1^\pm\ \widetilde{C}_2^\pm$
gluino	1/2	-1	$\widetilde{g}$	(same)
goldstino (gravitino)	1/2 (3/2)	-1	$\widetilde{G}$	(same)

Table 2.4: Particle content of the MSSM. Sfermion mixing is assumed negligible for the first two families. Table taken from [11].

According to the Planck 2018 results [12], the current combined measurement for the cold dark matter relic density is $\Omega_c h^2 = 0.120 \pm 0.001$. The dark matter relic density of a model point is not required to be exactly this value to be acceptable — it can also be lower. If a model point does reach this value, then that would mean that this model point can explain the existence of all dark matter currently in the universe, as it is able to produce enough dark matter to achieve the measured density. If the dark matter relic density of a model point is lower than the measured value, then the model point does not produce enough dark matter to explain all current dark matter in the universe, meaning that there would have to be other processes that also produce dark matter.

2.2.6 Minimal Supersymmetric Standard Model

SUSY-particles are described by introducing new parameters, but how this is implemented depends of the model. The Minimal Supersymmetric Standard Model (MSSM) requires the smallest number of new parameters necessary to construct a SUSY-model. The MSSM can be constructed to contain R-parity, in which case it is able to produce a candidate for dark matter. The particles and supersymmetric particles of the MSSM are represented in supermultiplets, of which there are two kind: chiral and gauge.

The chiral supermultiplets contain fermions and their superpartners, which are referred to as scalar fermions, or *sfermions*. They have the prefix “s-” and are denoted with a tilde. As stated, the spin of the sfermions is 0, hence the name “scalar”. The left-handed and right-handed parts of a fermion have their own superpartners, which themselves are *not* left-handed or right-handed, since they are scalar. The L and R as seen in Tab. 2.4 merely indicate whether they are the superpartners of the left-handed or right-handed part of a fermion.

There is a second type of supermultiplets, which contains gauge bosons and their superpartners, known as the *gauginos*. Gauginos have a spin of 1/2 and are denoted as $\tilde{W}^0$, $\tilde{W}^{\pm}$ (*winos*) and $\tilde{B}^0$ (*binos*). The gluon also forms a gauge supermultiplet with its superpartner, the *gluino*. When the electroweak symmetry is broken, along with the W and Z bosons becoming massive, five scalar Higgs mass eigenstates appear.

The scalar Higgs bosons are associated with two chiral supermultiplets. The electroweak gauge symmetry is a bit more complicated in SUSY models, which leads to the MSSM requiring more that one Higgs boson. As a result, there are two supermultiplets with Higgs bosons.The first supermultiplets $(H_u^+,\ H_u^0)$ has $Y = +1/2$ and the second $(H_d^-,\ H_d^0)$ has $Y = -1/2$. Each supermultiplet has its own VEV: v_u and v_d. The superpartners of these Higgs bosons are called higgsinos which belong to gauge supermultiplets. The suffix applied to a spin-1/2 superpartner is "-ino". They are denoted as $\tilde{H}_u^+$, $\tilde{H}_u^0$, $\tilde{H}_d^-$ and $\tilde{H}_d^0$.

There are two are CP-even neutral scalars h^0 and H^0, where h^0 is lighter than H^0. h^0 represents the Higgs boson that has been measured. There is one CP-odd neutral scalar A^0 and there are two charged scalars, H^+ and H^-.

Another effect of electroweak symmetry breaking is the mixing of higgsinos with gauginos to form new mass eigenstates. The neutral higgsinos $\tilde{H}_u^0$ and $\tilde{H}_d^0$ with the neutral gauginos $\tilde{W}^0$ and $\tilde{B}$ mix to form four mass eigenstates called *neutralinos*, denoted in Tab. 2.4 as N_i $(i = 1, 2, 3, 4)$. The charged higgsinos and gauginos $\tilde{H}_u^+$, $\tilde{H}_d^+$, $\tilde{W}^+$ and $\tilde{W}^-$ mix to form four mass eigenstates called *charginos*, denoted in Tab. 2.4 as C_i $(i = 1, 2, 3, 4)$. An alternative notation exists for both neutralinos and charginos, which is used in this work. Neutralinos are denoted as $\tilde{\chi}_i^0$ $(i = 1, 2, 3, 4)$ and charginos as $\tilde{\chi}_i^+$ $(i = 1, 2, 3, 4)$. Neutralinos and charginos are ordered by their masses, with $i = 1$ being the lightest. It should be noted that the mass of a charginos or neutralinos can have a negative phase. Although this phase has no effect on physical interactions, the absolute values of the masses of the neutralinos and charginos are used in this analysis.

Generally, the lightest neutralino $\tilde{\chi}_1^0$ is the LSP of an MSSM model. However, it is possible to have a different LSP by constructing a model that includes the superpartner to the graviton, the *gravitino* $\tilde{G}$. The mass of the gravitino is not well defined, so it can be chosen to be lighter than the $\tilde{\chi}_1^0$ and therefore be the LSP.

Notation in this Work

Throughout this work, the particles $\tilde{t}_1$, $\tilde{\tau}_1$, $\tilde{\chi}_1^+$ and $\tilde{\chi}_1^0$ are often referred to as "stop", "stau", "chargino" and "neutralino" instead of using the notation to ease the readability. Although these terms are not quite accurate, as there are individually two different stops and staus and four different charginos and neutralinos, this work will almost exclusively be discussing the lightest form of each particle. It will be made clear if one of the heavier versions is being referred to, by using the proper notation.

The mixtures of the stop and the stau are mixtures of a right-handed and a left-handed state. To keep things simple, if the mixtures lean towards being mostly right-handed, the stop or stau will be referred to as being "right-like". Similarly, stops and staus with a mostly left-handed mixture will be referred to as being "left-like".

When SPheno (see Sec. 3.2) calculates whether a decay mode for a particle is possible, it lumps the decay mode and the anti-decay mode together. There is no differentiation between $X \to Y + Z$ and $\bar{X} \to \bar{Y} + \bar{Z}$. Generally speaking this shouldn't matter, as the branching ratios should be the same, but questions could be raised when it comes to the chargino. $\tilde{\chi}_1^+$ and $\tilde{\chi}_1^-$ have two different mixing matrices, yet the resulting differences are extremely small. Because of this, the notation of the charge is omitted for all particles throughout this work, except to differentiate the chargino ($\tilde{\chi}_1^+$) from the neutralino ($\tilde{\chi}_1^0$).

In the MSSM there are multiple Higgs bosons, but this analysis only studies one of them: h^0. Throughout the rest of this work, it will be referred to as the "Higgs boson".

2.2.7 phenomenological Minimal Supersymmetric Standard Model

The MSSM has 124 [8] parameter, which is the smallest amount of parameters needed for a SUSY-model. It is necessary to understand how all of these parameters interact with and influence each other to understand how the MSSM functions, but this is very difficult to do with 124 parameters. Therefore, a simplified version of the MSSM is introduced: the phenomenological Minimal Supersymmetric Standard Model (pMSSM). The pMSSM includes new assumptions that align with observations[13]:

- All parameters are real (no CP violation through SUSY)
- No flavour-changing neutral currents
- First and second generation sfermions are degenerate and have negligible Yukawa couplings (based on experimental constraints)

These additional constraints reduce the number of parameters to 19 [13]:

- $\tan(\beta)$, which is defined as the ratio of the VEVs: $\tan(\beta) = \frac{v_u}{v_d}$
- m_A: mass of the CP-odd Higgs boson A^0
- μ: the higgsino mass parameter
- $M_1,\ M_2,\ M_3$: the bino, wino and gluino mass parameters
- $m_{Q_{L1}},\ m_{u_R},\ m_{d_R},\ m_{e_L},\ m_{e_R}$: mass parameters for the first and second sfermion generations
- $m_{Q_{L3}},\ m_{t_R},\ m_{b_R},\ m_{\tau_R},\ m_{\tau_L}$: mass parameters for the third sfermion generation
- $A_t,\ A_b,\ A_\tau$: third generation trilinear coupling constants

The gravitino's mass has to be set by hand, acting as a 20th parameter, as it can not be calculated with the given parameters. It is possible to scan this reduced parameter space, which will provide a better understanding of how the parameters influence particle masses, mixing ratios, branching ratios, etc. To a degree, this information will be extendible to the MSSM.

2.3 Simplified Models

The idea of a simplified model is to focus on only a few particles and interactions, instead of trying to understand all aspects of a more complete model at once. This allows for a targeted analysis on the boundaries of sensitivity of specific interactions, which can then be used to limit broader searches [14]. The goal of this work is to look into similar simplified models, to get a better understanding of how large of an effect the pMSSM parameters have on each particle and their interactions, but also to figure out which model would be better suited for an expansive search with real experimental data.

The first model (Fig. 2.3) has been chosen by the ATLAS Collaboration [15]. Here, the stop decays via (what is assumed to be) an off-shell $\tilde{\chi}_1^+$ (not depicted) to a stau ($\tilde{\tau}_1$), a tau-neutrino (ν_τ) and a b-quark (b). The stau then decays to a $\tilde{G}$, which is the LSP, and a tau (τ). Throughout this work, this model is dubbed the "ATLAS-stau" model.

The second (Fig. 2.4a) and third (Fig. 2.4b) models have been chosen by the CMS Collaboration [16]. In this work, they have been named the "CMS-stau" model and the "CMS-sneutrino" (sometimes shortened to "CMS-sneu") model. The CMS-stau model differentiates itself from the ATLAS-stau model in two main ways: first, the stop decays to an on-shell chargino ($\tilde{\chi}_1^+$) and a b-quark (b). The $\tilde{\chi}_1^+$ then decays to a $\tilde{\tau}_1$ and a ν_τ, and the $\tilde{\tau}_1$ decays to a $\tilde{\chi}_1^0$ and a τ. Second, the LSP is a neutralino instead of a gravitino. The CMS-sneutrino model differs only slightly from the CMS-stau model: instead of the $\tilde{\chi}_1^+$ decaying to a $\tilde{\tau}_1$ and a ν_τ, it decays to a tau-sneutrino $\tilde{\nu}_\tau$ and a τ. The $\tilde{\nu}_\tau$ then decays to a $\tilde{\chi}_1^0$ and a ν_τ. The CMS-sneutrino model has been chosen for this analysis to find out if there are any noticeable differences between the $\tilde{\chi}_1^+$ decaying to a $\tilde{\tau}_1$ or a $\tilde{\nu}_\tau$.

As stated in Sec. 2.2.7, the mass of the gravitino has to be implemented by hand.

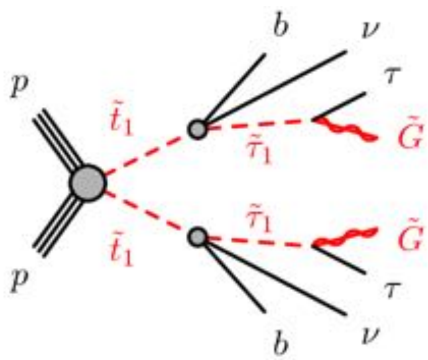

Figure 2.3: ATLAS-stau simplified model [15]

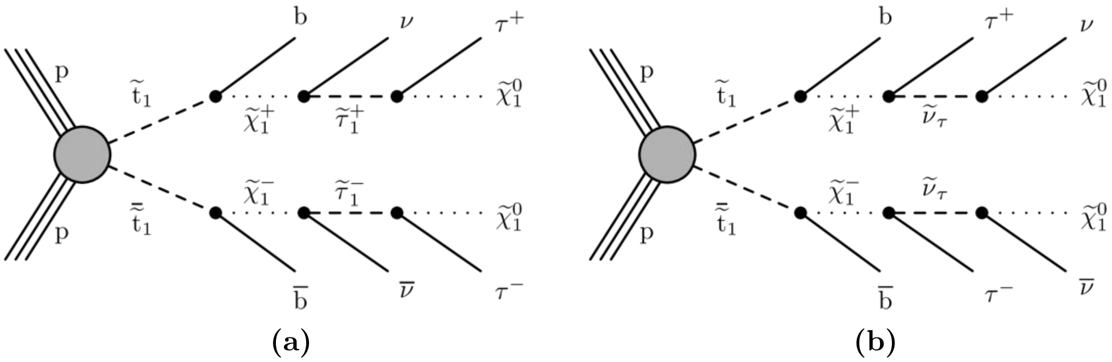

Figure 2.4: (a) CMS-stau simplified model, (b) CMS-sneutrino simplified model [16]

Since the ATLAS-stau model has the gravitino as the LSP, the mass has been chosen to be very light (m($\tilde{G}$) = 10^{-9} GeV). For the CMS-stau and CMS-sneutrino models, the gravitino's mass is chosen to be extremely heavy (m($\tilde{G}$) = 10^{19} GeV), so that the possibility of another particle decaying to it is eliminated.

A model point is a unique set of values of the pMSSM parameters, plus the physical masses and branching ratios of each particle, which are determined by the values of the parameters and are therefore also unique to that model point. By generating many model points, a variety of different configurations of particle masses and decay modes are created, which can be compared to one another. Throughout this work, model points are often referred to as "containing" one of the simplified models. This references whether specific criteria regarding the simplified model are upheld within the model point.

The following criteria are used to determine whether a model point contains the ATLAS-stau model:

- model point has to be physical: `SPheno` does not return an error and `FeynHiggs` returns $\mathrm{m}(h) > 0$ (see Sec. 3.2)
- $\mathrm{m}(\tilde{t}_1) > (\mathrm{m}(\tilde{\tau}_1) + \mathrm{m}(b) + \mathrm{m}(\nu_\tau))$
- $\mathrm{m}(\tilde{\tau}_1) > (\mathrm{m}(\tilde{G})+\mathrm{m}(\tau))$
- $\tilde{G}$ is the LSP
- $\mathrm{BR}(\tilde{t}_1 \to \tilde{\tau}_1\ b\ \nu_\tau) \cdot \mathrm{BR}(\tilde{\tau}_1 \to \tilde{G}\ \tau) > 0.1$[6]

The following selection criteria are for the CMS-stau model:

- model point is physical
- $\mathrm{m}(\tilde{t}_1) > \big(\mathrm{m}(\tilde{\chi}_1^+) + \mathrm{m}(b)\big)$
- $\mathrm{m}(\tilde{\chi}_1^+) > (\mathrm{m}(\tilde{\tau}_1)+\mathrm{m}(\nu_\tau))$

[6] BR stands for "branching ratio"

- $\mathrm{m}(\tilde{\tau}_1) > (\mathrm{m}(\tilde{\chi}_1^0)+\mathrm{m}(\tau))$
- $\tilde{\chi}_1^0$ is the LSP
- $\mathrm{BR}(\tilde{t}_1) \to \tilde{\chi}_1^+ \, b) \cdot \mathrm{BR}(\tilde{\chi}_1^+ \to \tilde{\tau}_1 \, \nu_\tau) \cdot \mathrm{BR}(\tilde{\tau}_1 \to \tilde{\chi}_1^0 \, \tau) > 0.1$

The following selection criteria are for the CMS-sneutrino model:

- model point is physical
- $\mathrm{m}(\tilde{t}_1) > \big(\mathrm{m}(\tilde{\chi}_1^+) + \mathrm{m}(b)\big)$
- $\mathrm{m}(\tilde{\chi}_1^+) > (\mathrm{m}(\tilde{\nu}_{\tau_1})+\mathrm{m}(\tau))$
- $\mathrm{m}(\tilde{\nu}_{\tau_1}) > (\mathrm{m}(\tilde{\chi}_1^0)+\mathrm{m}(\nu_\tau)))$
- $\tilde{\chi}_1^0$ is the LSP
- $\mathrm{BR}(\tilde{t}_1) \to \tilde{\chi}_1^+ \, b) \cdot \mathrm{BR}(\tilde{\chi}_1^+ \to \tilde{\nu}_{\tau_1} \, \tau) \cdot \mathrm{BR}(\tilde{\nu}_{\tau_1} \to \tilde{\chi}_1^0 \, \nu_\tau) > 0.1$

Regarding the last condition, the combined branching ratio being greater than 0.1 comes from the secondary objective of this analysis: determining which simplified model is best suited for a study using real data. If the combined branching ratio is too small in a model point, then it becomes unlikely that the simplified model would be measurable. Therefore, the lower bound of 0.1 has been set. As a result, a model point in which any of the individual decay steps has a branching ratio below 0.1 does not pass the selection criteria. This means that not every model point that is physical contains one of the simplified models. On some occasions, the selection criteria of a plot will be referred to a simplified model's mass hierarchy. This means that the all the criteria of the simplified model except for any selections on the branching ratios are applied. The goal of this selection criteria is to have model points in which the decay steps of the simplified model are kinematically possible, but they do not have to be present. For example, a model point with $\mathrm{m}(\tilde{t}_1) > (\mathrm{m}(\tilde{\tau}_1) + \mathrm{m}(b) + \mathrm{m}(\nu_\tau))$ allows for the decay $\tilde{t}_1) \to \tilde{\chi}_1^+ \, b$ kinematically, but $\mathrm{BR}(\tilde{t}_1) \to \tilde{\chi}_1^+ \, b) = 0$ is still possible.

Chapter 3

Experimental Set-up

3.1 Detectors

The ATLAS and CMS detectors are located on the Large Hadron Collider (LHC). The LHC is a proton-proton ring collider with a circumference of roughly 27 km and beam energy of 13 TeV [17]. It is located at CERN, crossing the boarder between Switzerland and France.

The ATLAS detector is a general-purpose detector. The inner detector consists of semi-conductor pixel and strip detectors, which together are capable of pattern recognition, momentum and vertex measurements, and electron identification. The outer part of the inner detector has a transition radiation tracker. The inner detector is immersed in a 2 T solenoidal magnetic field. Outside of the inner detector is an electromagnetic and a hadronic calorimeter, the latter being split into multiple parts. The caps of the detector have toroid magnets and the outer layer consists of a muon detection system [18].

The CMS detector is also a general-purpose detector [19]. At the centre is the tracking system. consisting of a silicon pixel detector and a silicon strip tracker. Next are the calorimeters, first the electromagnetic followed by the hadronic calorimeter. These

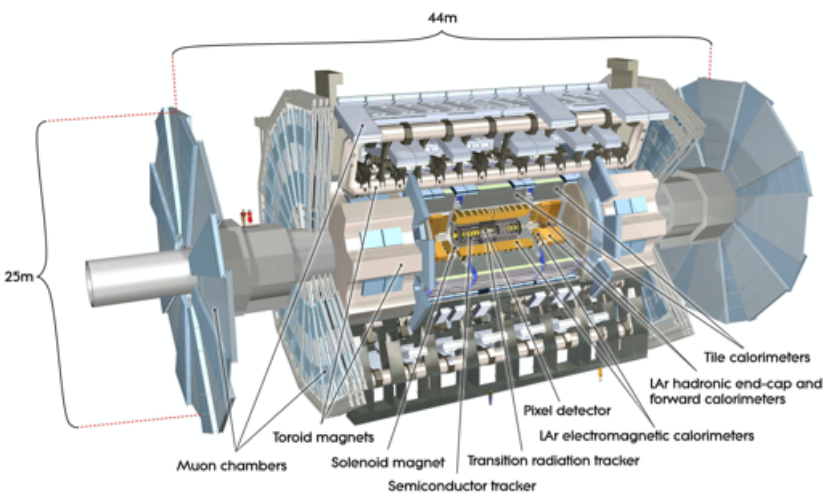

Figure 3.1: ATLAS detector, taken from [18]

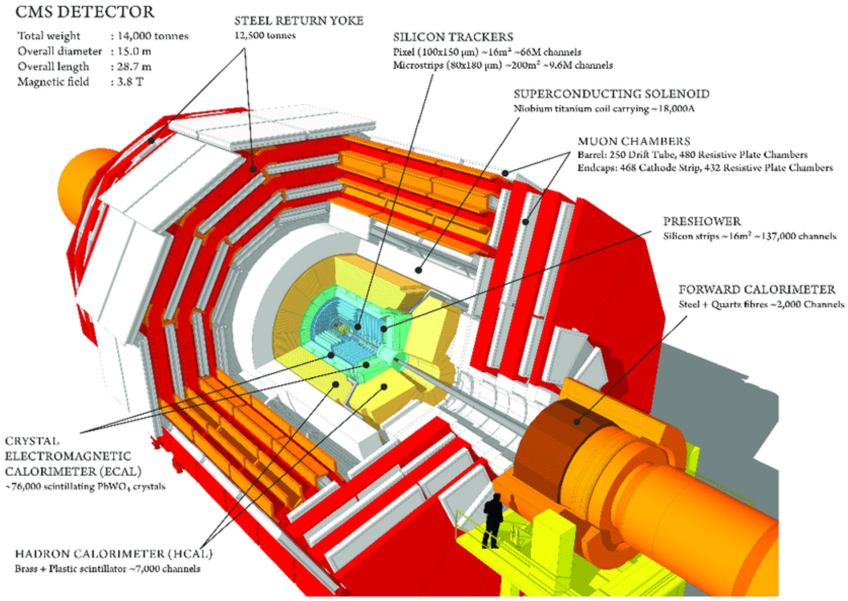

Figure 3.2: CMS detector, taken from [19]

layers are all within a superconducting solenoid magnet, which provides a magnetic field of 3.8 T. Outside of the solenoid magnet is the muon detection system, which is embedded within an steel yoke which serves as the absorber plates for the muon system [20]. The ends of the detector have hadronic forward calorimeters.

3.2 Software and Model Generation

The simulated data is generated using multiple programs. The first is `EasyScan_HEP v.1.0.0` [21], which functions as a wrapper for the following programs, but is also used to randomly generate parameter values. One run of `EasyScan_HEP` generates one random value for each of the 19 pMSSM parameters, and this set of parameter values is referred to as a model point. These values can be used to calculate all particle masses, mixtures, decay modes, etc. that are allowed within the pMSSM model. The intervals from which each value is chosen are user defined, allowing for targeted simulation (see Tab. 4.1 and Tab. 5.1). The configuration for `EasyScan_HEP` , which includes the configurations for `SoftSusy` and `SPheno`, can found in App. A.1.

The output file is then fed to both `SoftSusy v.4.1.8` [22] and to `SPheno v.4.0.4` [23, 24], which both perform the aforementioned calculations. Afterwards, the mass of the Higgs boson is calculated with `FeynHiggs v.2.15.0` [25, 26, 27, 28, 29, 30, 31, 32] and the dark matter relic density provided by `MicrOMEGAS v.5.0.8` [33]. The output files of `SoftSusy`, `SPheno`, `FeynHiggs` and `MicrOMEGAS` are in the form of SUSY Les Houches Accord (SLHA) files [34]. The SLHA files are read by `PySLHA v.3.2.0` [35], which is used to save the data as `.root` files.
The model points are either read from the `.root` files with `ROOT v.6.20/04` [36] and plotted with `ROOT` or they are read with `uproot v.3.11.3` [37] and plotted with `MatplotLib v.2.2.5` [38]. Wide-scale comparisons between multiple parameters were

performed with `Seaborn` [39].

`SoftSusy` is used for its error generation, since not all model points are physical. Sometimes, the values of the pMSSM parameters are randomly chosen such that they generate unphysical phenomenons, such as tachyons. In these cases, `SoftSusy` raises an error related to the type of unphysical problem and the run is aborted. If `SoftSusy` completes successfully, then `SPheno` calculates the data that is used for this analysis' studies. `SPheno` was chosen over `SoftSusy`, because `SoftSusy` was not able to produce any model points that contained the decay mode $\tilde{t}_1 \to \tilde{\tau}_1\ b\ \nu_\tau$. It is possible that this was due to a user error when configuring `SoftSusy`.
When `SPheno` calculates the branching ratios of a particle's decay modes, only branching ratios greater than 10^{-4} are saved to the output file (user defined, see App. A.1).

3.3 Unphysical Model Points

In the previous section, model points that do not cause `SoftSusy` to return an error have been regarded as physical. However, for this analysis, another minor condition is applied for a model point to count as physical: the Higgs boson mass $\mathrm{m}(h)$, as calculated by `FeynHiggs`, is required to be positive ($\mathrm{m}(h) > 0$). How this affects the number of physical model points can be seen in Tab. 3.1.

Comparing unphysical model points with physical model points (e.g., Fig. 3.3) already provides a lot of information on the pMSSM. Only a few parameters have much of an impact by themselves (see App. A.2). m_{t_R} and $m_{Q_{L3}}$ have a very strong influence, where the likelihood of a physical model increases as the parameter's values increase. This means that light stops become problematic for the pMSSM (bound by the phase space of the simulations). The gluino mass parameter M_3 has the reverse effect: the larger it gets, the less physical model points there are. Other notable parameters are A_t and M_2, where the number of physical points decreases for larger absolute values, but to a much larger degree for A_t. Interestingly, A_τ and A_b are the only parameters that have seemingly no effect at all, since the other parameters that influence the sleptons and squarks (apart from the stop) all drop-off at small values. It is unknown why this decline in physical points at small values appears for these parameters.

There is no considerable difference in the shapes of the distributions when comparing the physical model points with a light gravitino to the points with a heavy gravitino. Therefore, the conclusion can be made that the mass of the gravitino doesn't have a tangible effect on whether a model point is physical or not. The difference in the

Table 3.1: Overview of the number of physical and unphysical model points. The selection regarding the Higgs mass is only performed on model points that were deemed physical by `SoftSusy`.

Model Set	Generated	Unphysical (Error)	Unphysical (Higgs Mass)	Physical
light $\tilde{G}$	500000	417121	1747	81132
heavy $\tilde{G}$	500000	414560	1846	83594

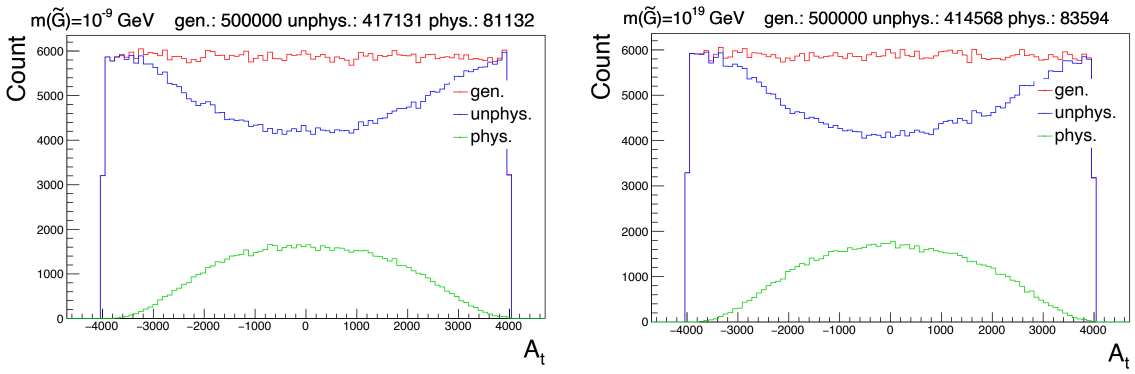

(a) (b)

Figure 3.3: Distribution of A_t for physical models points with (a) $\mathrm{m}(\tilde{G}) = 10^{-9}$ GeV and (b) $\mathrm{m}(\tilde{G}) = 10^{19}$ GeV.

number of physical model points with a light or with a heavy gravitino is most likely a statistical fluctuation.

Chapter 4

ATLAS-stau

The main objective of this thesis is to improve our understanding of how the pMSSM parameters influence variables such as particle masses, mixing ratios, decay modes, etc. To achieve this, the behaviours of various simplified models are examined using the previously discussed generated model points.

4.1 Particle Masses and Mixtures

The complete phase space used for generating models points with m($\tilde{G}$) = 10^{-9} GeV can be seen in Tab. 4.1.

Table 4.1: Phase space used to generate model points with m($\tilde{G}$) = 10^{-9} GeV.

$tan\,(\beta)$	1 – 60
$\lvert A_t\rvert$, $\lvert A_b\rvert$, $\lvert A_\tau\rvert$	0– 4000 GeV
m_{t_R}, $m_{Q_{L3}}$, m_{τ_L}, m_{τ_R}	100 – 1200 GeV
$\lvert M_1\rvert$, $\lvert M_2\rvert$	0 – 3000 GeV
μ	0 – 3000 GeV

M_3, m_A, m_{u_R}, m_{d_R}, $m_{Q_{L1}}$, m_{b_R}, m_{e_L}, m_{e_R}	100 – 3000 GeV

The mass of each particle in the pMSSM is influenced by specific parameters. The ATLAS detector is not sensitive to $\tilde{t}_1$ with masses over 1 TeV, therefore the mass of the simulated stops are limited to around 1 TeV. This is done by setting the upper bounds for m_{t_R} and $m_{Q_{L3}}$ to 1.2 TeV. Since the simplified model requires a certain mass hierarchy, the parameters m_{τ_L} and m_{τ_R} are also set to maximally be 1.2 TeV, generating staus up to around 1 TeV. The reason 1.2 TeV is chosen as the maximum,

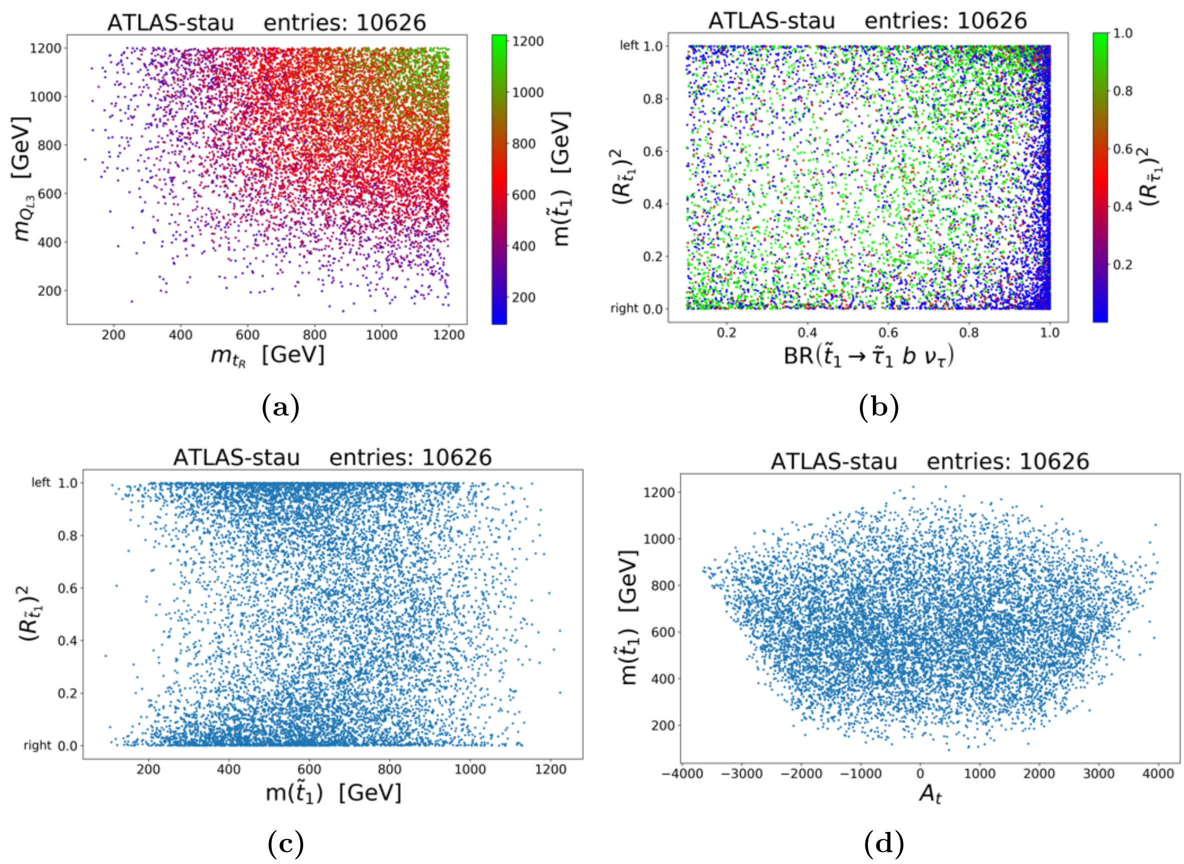

Figure 4.1: $\tilde{t}_1$ mass parameters and mixture. Selection criteria: ATLAS-stau Simplified Model. (a) Mass parameters. (b) Mixture ($\left(R_{\tilde{t}_1}\right)^2$) with relation to the branching ratio for $\tilde{t}_1 \rightarrow \tilde{\tau}_1\ b\ \nu_\tau$. $(R_{\tilde{t}_1})^2 = 1$ represents a left-handed mixture. (c) Mixture with relation to the mass. (d) Stop trilinear coupling constant with relation to the mass.

and not 1 TeV, is that it makes it more likely to generate model points in which the masses of the stop and stau are around 1 TeV. There will be some model points in which they are heavier than 1 TeV, but there are not many, as this requires both m_{t_R} and $m_{Q_{L3}}$ to be large, which is less likely. The parameters that are generated in the range of 100–3000 GeV are mass parameters for particles that are not directly involved in the ATLAS-stau simplified model, which means that their upper bounds can be chosen to be large without having any significant effects on model points that contain the simplified model. Their lower boundaries have been set to 100 GeV, as model points generated with lower values were unphysical. The coupling constants A_t, A_τ and A_b also have a very broad phase space, as it is not clear how large their impact on the simplified model is. $tan(\beta)$ is also given a large phase space for the same reason. Since the chargino is off-shell and there are no neutralinos in this simplified model, M_1, M_2 and μ can also have a large range. It should be noted that μ is chosen to be positive, as model points with negative μ did not produce SM Higgs bosons with $m(h) = 125 \pm 3$ GeV during early tests (see section 4.3.3). The boundaries for $m(h)$ have been chosen to be broad, because not very many model points produce Higgs bosons with masses close to 125 GeV. Therefore, to have enough statistics to be able to make conclusions on which regions of the phase space are likely to have Higgs bosons with a mass near the observed value, a room for error of ± 3 GeV has been implemented.

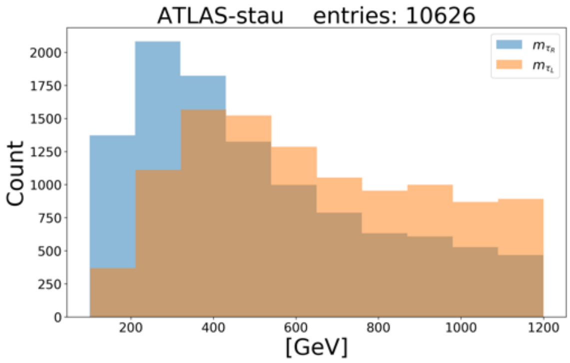

Figure 4.2: Distributions of m_{τ_R} and m_{τ_L}. Selection criteria: ATLAS-stau simplified model.

In Fig. 4.1a, the influence of m_{t_R} and $m_{Q_{L3}}$ on the mass of the stop can be seen for model points that contain the ATLAS-stau simplified model. Unsurprisingly, stops with heavy masses are preferred. Only in model points in which m_{t_R}, $m_{Q_{L3}} > 1000$ GeV are some stops heavier than 1 TeV, which is a small section of the phase space. Many model points with a stop under 1 TeV have either $m_{Q_{L3}} > 1000$ GeV with $m_{t_R} < 1000$ GeV, or vice-versa. Some points, in which both parameters are over 1000 GeV, still produce stops with masses of around 800 − 1000 GeV, which implies that the mass is also influenced by at least one other parameter. It can be safely assumed that m_{t_R} and $m_{Q_{L3}}$ have the largest impact. The mixture also hardly plays a role when it comes to influencing either the mass or the branching ratio for $\tilde{t}_1 \rightarrow \tilde{\tau}_1\ b\ \nu_\tau$ (see Fig. 4.1b). For larger branching ratios (> 0.6), there seems to be slightly more model points with left-handed mixtures, but the difference is very small.
A_t is the trilinear coupling constant for the stop. While a very distinct distribution can be seen in Fig. 4.1d, it mimics the distribution of A_t in physical model points, where there are less physical models points the larger $|A_t|$ gets (see. App. A.1). It's unclear why model points with small $|A_t|$ are able to produce heavier stops than those with large $|A_t|$.

The stau generally is not much heavier than around 700 GeV (see Fig. 4.3a), apart from a few model points. There are much fewer points with $m_{\tau_L} < 200$ GeV compared to $m_{\tau_R} < 200$ GeV. This is supported by the distributions of m_{τ_L} and m_{τ_R} (see Fig. 4.2). The fact that m_{τ_R} tends towards smaller values while m_{τ_L} tends to larger values suggests that there are more model points with right-like staus. Most staus have either a mostly right- or mostly left-like mixture; in very few points is it evenly balanced (see Fig. 4.3c). The branching ratio for $\tilde{\tau}_1 \rightarrow \tilde{G}_1\ \tau$ is almost exclusively 1 in model points that contain the simplified model (see Fig. 4.3b). It differs in a few points, but even then it is by an extremely small amount. The only other particles that are sometimes lighter than the $\tilde{\tau}_1$ are the $\tilde{\nu}_{\tau_1}$ and the $\tilde{\chi}_1^0$. However the mass difference is very small in these model points, meaning that the kinematic phase space for a decay to one of these particles becomes much less likely than a decay to the gravitino. This is likely why the decay to a gravitino is so strongly preferred. The branching ratio tends to differ more for left-like mixtures, which is likely due to decays to the $\tilde{\nu}_{\tau_1}$, which is strictly left-handed.

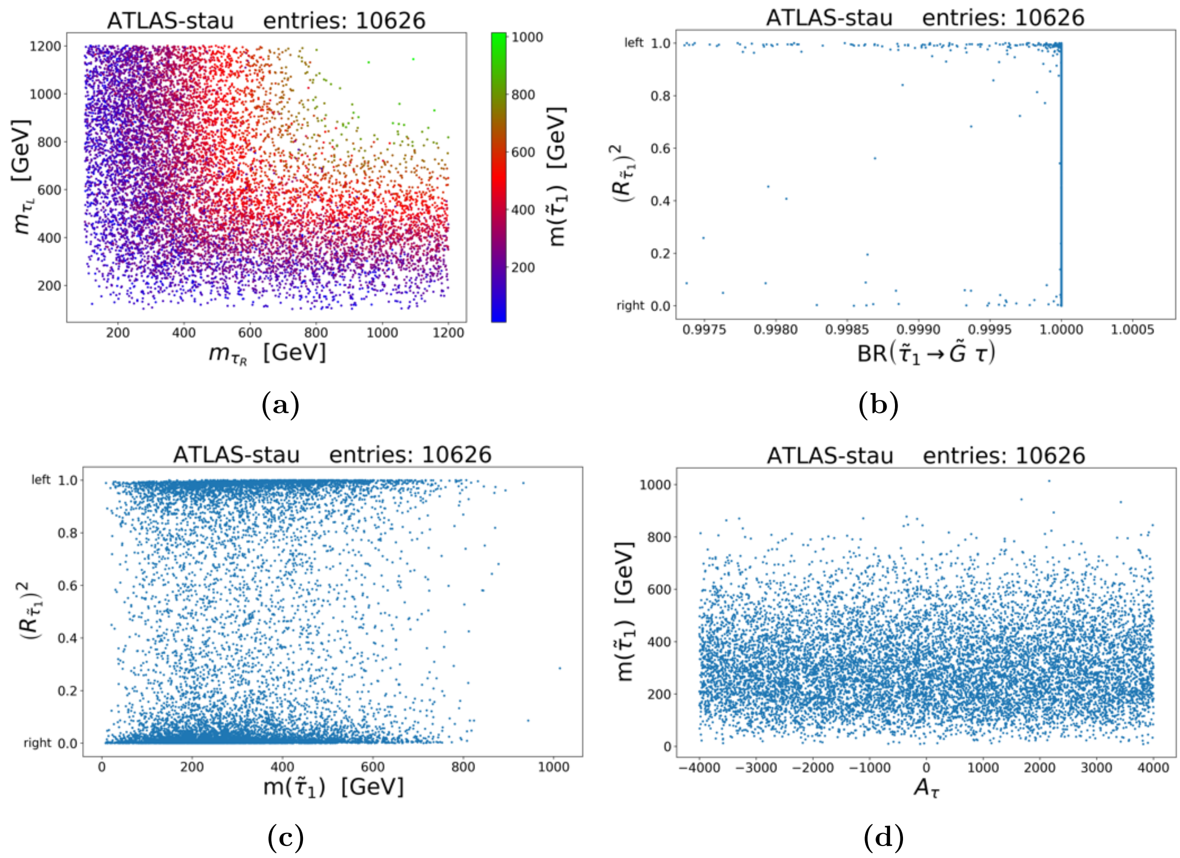

Figure 4.3: $\tilde{\tau}_1$ mass parameters and mixture. Selection criteria: Simplified Model. (a) Mass parameters. (b) Mixture with relation to the branching ratio for $\tilde{\tau}_1 \to \tilde{G}_1\ \tau$. $(R_{\tilde{\tau}_1})^2 = 1$ represents a left-like mixture. (c) Mixture with relation to the mass. (d) Stau trilinear coupling constant with relation to the mass.

4.2 Competing Decay Modes

When looking into how a simplified model works, the decay modes that compete with the simplified model have to be taken into account. The goal is to be able to suppress other decay modes that particles in the simplified model could have. For example, in the following snippet from a `SPheno` output file, it can be seen that the decay $\tilde{t}_1 \to \tilde{\tau}_1\, b\, \tau$ has a branching ratio of around 0.69, where as the decay $\tilde{t}_1 \to \tilde{G}t$ (which should be avoided) has a branching ratio of around 0.31.

```
DECAY    1000006     1.02394943E-08    # ~t_1
#     BR                 NDA       ID1       ID2
      3.09970616E-01     2      1000039       6    # BR(~t_1 -> ~G t)
#     BR                 NDA       ID1       ID2        ID3
      6.90029384E-01     3     -1000015      16        5    # BR(~t_1 -> ~tau^+_1 nu_tau b)
```

This is more of a fine-tuning step, as the idea is to further optimise the phase space of model points that already contain the ATLAS-stau simplified model.

The most common competing decay is where the $\tilde{t}_1$ directly decays to a gravitino (Fig. 4.4a). The differences in the parameters, particle mass and mixtures were compared

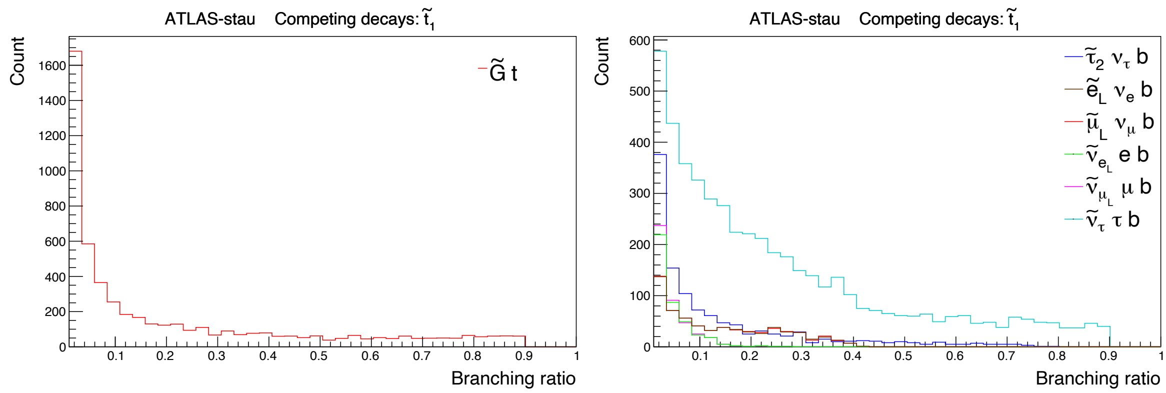

(a) **(b)**

Figure 4.4: Competing decays for $\tilde{t}_1 \rightarrow \tilde{\tau}_1\ b\ \nu_\tau$. Selection criteria contains the mass hierarchy and the simplified model with a combined branching ratio > 0.1. Separated into (a) and (b) for readability.

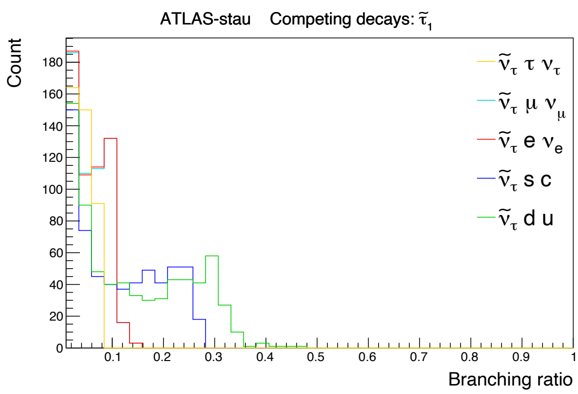

Figure 4.5: Competing decays for $\tilde{\tau}_1 \rightarrow \tilde{G}\ \tau$. Selection criteria: mass hierarchy and simplified model with a combined branching ratio > 0.1. Light blue graph heavily overlaps with the red graph.

between model points that contain the ATLAS-stau simplified model with BR($\tilde{t}_1 \rightarrow \tilde{G}\ \tau$) < 0.1, and model points that contain the ATLAS-stau simplified model with BR($\tilde{t}_1 \rightarrow \tilde{G}\ \tau$) > 0.7. Only the mass difference between $\tilde{t}_1$ and $\tilde{\tau}_1$ has a clear impact on the likelihood of $\tilde{t}_1 \rightarrow \tilde{G}\ \tau$ having a large branching ratio, displayed in Fig. 4.6. Most model points with BR($\tilde{t}_1 \rightarrow \tilde{G}\ \tau$) > 0.7 have m($\tilde{t}_1$)$-$m($\tilde{\tau}_1$) < 300 GeV. Many model points with small a mass difference also allow for small branching ratios. Clearly, other parameters are influencing the branching ratio, but a clear combination of parameter values that separates large branching ratios from small ones has not been found for this decay mode.

Apart from the direct decay to a gravitino, the competing decay modes consist of a slepton, a lepton and a b-quark (see Fig. 4.4b). Their distributions all have a similar shape to the decay to a gravitino, but their counts are lower. The most prominent of these decay modes is the decay to $\tilde{\nu}_\tau$, τ and b. Like with $\tilde{t}_1 \rightarrow \tilde{G}\ \tau$, to understand this mode the model points have been split via BR($\tilde{\tau}_1 \rightarrow \tilde{\nu}_{\tau_1}\ \tau\ b$) < 0.1 and BR($\tilde{\tau}_1 \rightarrow \tilde{\nu}_\tau\ \tau\ b$) > 0.7 (see Fig. 4.7). Clearly, this decay mode prefers staus that are strongly left-like, which most likely has to do with the fact that the $\tilde{\nu}_\tau$ is strictly left-handed.

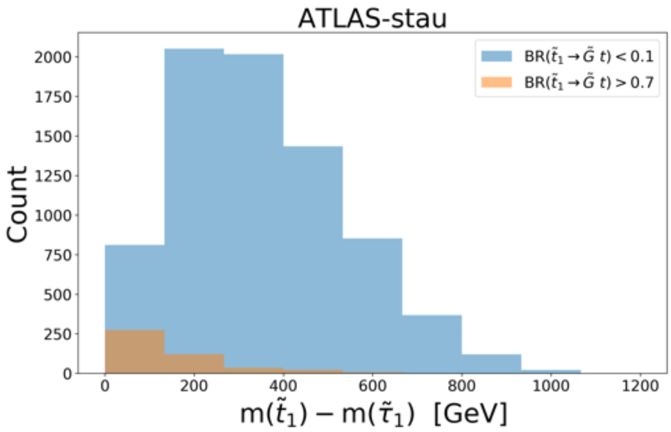

Figure 4.6: The mass difference between $\tilde{t}_1$ and $\tilde{\tau}_1$ has the largest impact on the separation between large and small branching ratios for $\tilde{t}_1 \to \tilde{G}\ \tau$. Selection criteria: ATLAS-stau simplified model, branching ratio denoted by the colour.

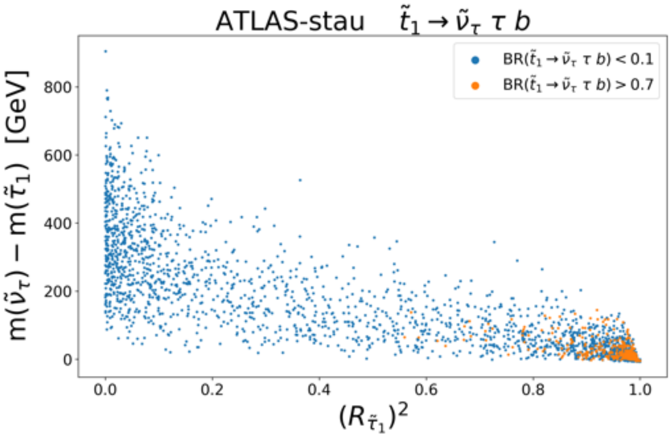

Figure 4.7: Most significant parameters differentiating between small and large branching ratios for $\tilde{\tau}_1 \to \tilde{\nu}_\tau\ \tau\ b$. Selection criteria: ATLAS-stau simplified model with BR($\tilde{t}_1 \to \tilde{G}\ \tau$) > 10^{-4} [1].

Also, the closer the mass of the $\tilde{\nu}_\tau$ is to that of the stau, the greater the chance for a large branching ratio is. There are model points in which the mass difference is negative (in other words, the tau-sneutrino is lighter than the stau), but in these cases the difference is very small.
There are obviously other parameters that influence the branching ratio, as there are also model points with left-like staus and small mass differences which have small branching ratios. No other individual parameter has as significant of an effect as the mass difference or the stau mixture. Therefore, it must be a combination of multiple parameters that has a strong effect on the branching ratio, which is hard to detect, as there are many possible combinations.

The competing decays for $\tilde{\tau}_1 \to \tilde{G}\ \tau$ do not have very high branching ratios (Fig. 4.5). Unlike the competing decays for the $\tilde{t}_1$, which peak around 0 and then fall off, these cases generally have secondary peaks after which the count falls to 0. The exact reason

[1] 10^{-4} is the minimum branching ratio required for a decay mode to be added to the data of a model point.

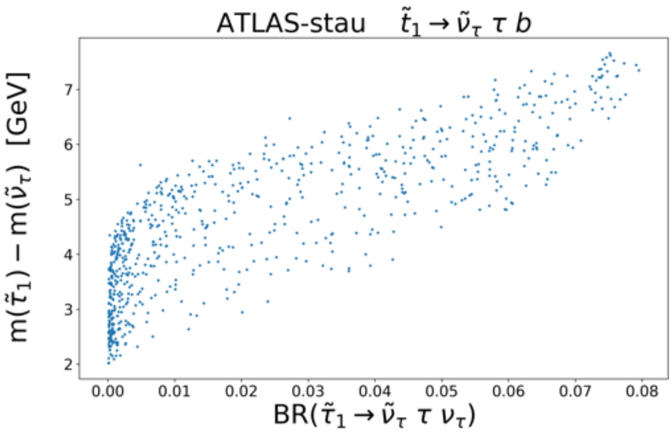

Figure 4.8: Influence of the mass difference between the stau and the tau-sneutrino on the branching ratio $\tilde{\tau}_1 \to \tilde{\nu}_\tau\ \tau\ \nu_\tau$. Selection criteria: ATLAS-stau simplified model with $\mathrm{BR}(\tilde{\tau}_1 \to \tilde{\nu}_\tau\ \tau\ \nu_\tau) > 10^{-4}$.

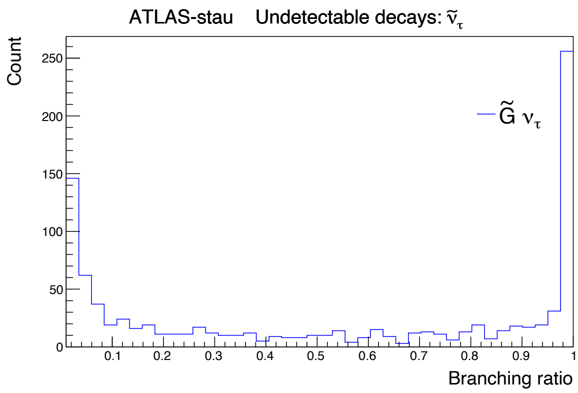

(a)

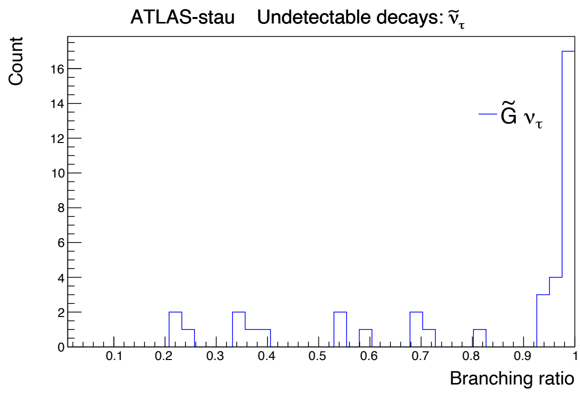

(b)

Figure 4.9: Decay modes for $\tilde{\nu}_\tau$ in model points that contain the ATLAS simplified model. Selection criteria: Simplified Model. (a) Decay chain: $\tilde{t}_1 \to \tilde{\nu}_\tau\ \tau\ b$, $\tilde{\nu}_\tau \to \tilde{G}\ \nu_\tau$. (b) Decay chain: $\tilde{t}_1 \to \tilde{\tau}_1\ \nu_\tau\ b$, $\tilde{\tau}_1 \to \tilde{\nu}_\tau\ \tau\ \nu_\tau$, $\tilde{\nu}_\tau \to \tilde{G}\ \nu_\tau$.

for the sudden drop-off in each distribution once the branching ratios reach certain values is unclear. Although the mass difference is very small in these model points, the branching ratio increases as the stau gets heavier compared to the tau-sneutrino (see Fig. 4.8). There is not an obvious reason as to why the branching ratio should increase as the tau-sneutrino gets heavier relative to the stau.

The competing decays $\tilde{t}_1 \to \tilde{\nu}_\tau\ b\ \tau$ and $\tilde{\tau}_1 \to \tilde{\nu}_\tau\ \tau\ \nu_\tau$ are a bit problematic: if the $\tilde{\nu}_\tau$ were to further decay to undetectable particles (which would result in missing energy in a detector), then the signal in a detector would look like the simplified model. Therefore, further studies on how to kinematically differentiate a measurement of this decay mode from $\tilde{t}_1 \to \tilde{\tau}_1\ b\ \nu_\tau$ would be required.

Since only decay chains which result in a tau, a b-quark and undetectable particles are of interest, both the cases $\tilde{t}_1 \to \tilde{\nu}_\tau\ b\ \tau$ and $\tilde{t}_1 \to \tilde{\tau}_1\ b\ \nu_\tau$, $\tilde{\tau}_1 \to \tilde{\nu}_\tau\ \tau\ \nu_\tau$ require the tau-sneutrino to decay to undetectable particles. Only decay modes involving the gravitino turn out to be significant (see Fig. 4.9). The first case (which is the ATLAS equivalent to the CMS-sneutrino simplified model) has a low count, bearing in mind that there are 10626 model points that contain the ATLAS-stau simplified model. The second case, in which a $\tilde{\tau}_1$ decays to a $\tilde{\nu}_\tau$, which in return decays to a gravitino, turns out to be extremely unlikely (see Fig. 4.9b), as hardly any of the ATLAS-stau model points contain this decay chain. Therefore, the chance to get the same detector signal whilst measuring a different model is very small.

4.3 Influence on the Mass of the Higgs Boson

For a model point to have a particle spectrum that could represent reality, the mass of the Higgs boson (m(h)) is required to have the observed value of m(h) = 125.10 ± 0.14 GeV [8]. Therefore, it is important to understand which parameters have the greatest influence over the Higgs boson mass and how their allowed regions of phase space overlap with the phase space of the simplified models. The parameters that have the strongest impact are $tan(\beta)$, A_t and μ. This isn't surprising, as all three parameters are heavily linked to the Higgs boson: $tan(\beta)$ is the ratio of the VEVs of the Higgs fields, A_t is the coupling constant for the $\tilde{t}_1$, which is generally very heavy, and μ is the higgsino mass parameter.
The selection criteria imposed in the following is set in three steps: first, a look each parameters' physical phase space by looking at physical model points. Second, the selection $122 < \text{m}(h) < 128$ GeV is applied to the physical model points, to determine which sections of the parameter's phase space allow for Higgs bosons with masses around 125 GeV. The upper and lower boundaries have been chosen to be rather large, since not many model points fulfil this criteria. The third selection criteria is for model points that contain the ATLAS-stau simplified model and have have $122 < \text{m}(h) < 128$ GeV.

The following section will mostly use violin plots instead of scatter plots, as they make subtle differences within distributions easier to see. The top and bottom of a bar represents the highest and lowest values of the parameter on the y-axis, whereas the width indicates how many model points are around a certain value of the y-axis (the wider the bar, the more points). This means that a bin with 1000 entries could have a bar with the same shape and size as a bin with only 100 entries, but the width would represent a different number of model points. The number in parentheses underneath a bin represents the number of entries in the bin.

4.3.1 $tan(\beta)$ - Ratio of Higgs Field VEVs

The parameter $tan(\beta)$ has influence over the masses of various particles, amongst them the $\tilde{t}_1$, $\tilde{\tau}_1$ and the Higgs boson. These three particles are mass eigenstates that are formed through the mixing of gauge eigenstates, in which $sin(\beta)$ and $cos(\beta)$ play a role. It is therefore possible that the phase space of $tan(\beta)$ will most likely be limited by the simplified models.

While the distribution of the $\tilde{t}_1$ mass doesn't vary too strongly amongst all values of $tan(\beta)$ (see Fig. 4.10), the bins for higher and lower values of $tan(\beta)$ tend to have fewer entries.

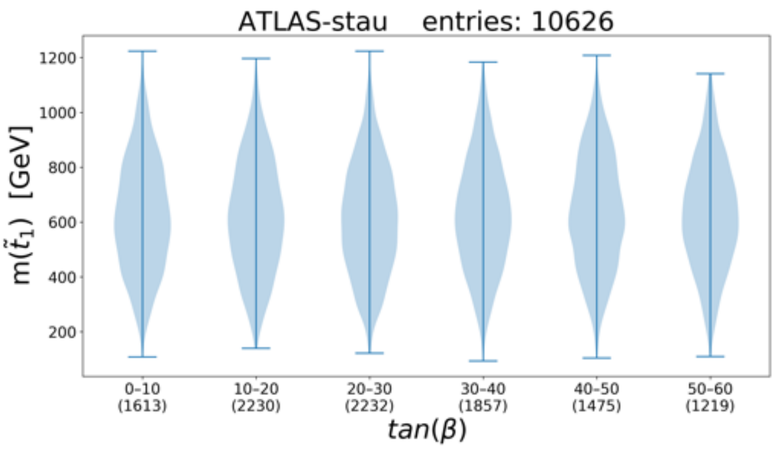

Figure 4.10: Effect of $tan(\beta)$ on the mass of $\tilde{t}_1$. Selection criteria: ATLAS-stau simplified model.

Regarding $\tilde{\tau}_1$, both its mass and the mass difference between $\tilde{\tau}_1$ and $\tilde{\tau}_2$ are of interest. Looking at the mass (see Fig. 4.11), it would appear at first that model points with higher values of $tan(\beta)$ are more inclined to have heavier $\tilde{\tau}_1$. However, in every bin there are very few model points containing heavy $\tilde{\tau}_1$ (indicated by the thin part of the bar). Therefore, it is very well possible that this difference could arise from statistical fluctuations. Overall, most model points have $\tilde{\tau}_1$ with masses around 150–450 GeV.

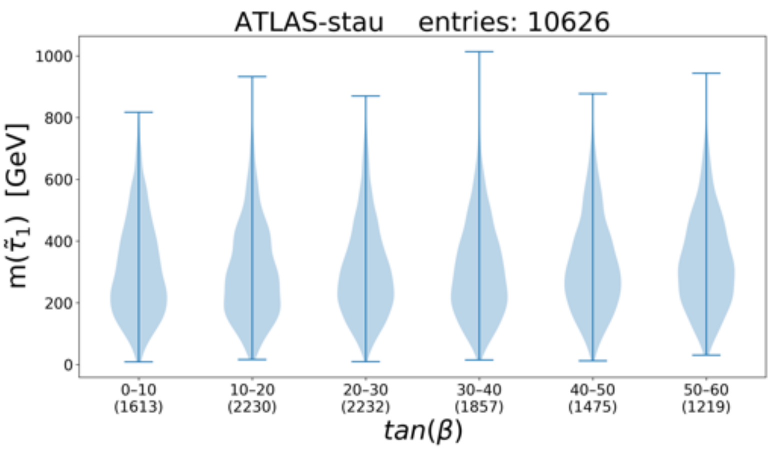

Figure 4.11: Effect of $tan(\beta)$ on the mass of $\tilde{\tau}_1$. Selection criteria: ATLAS-stau simplified model.

The mass difference between $\tilde{\tau}_1$ and $\tilde{\tau}_2$ is interesting, for when its close to 0, the likelihood that the $\tilde{t}_1$ will decay to a $\tilde{\tau}_2$ increases. The difference is not very large for most model points (see Fig. 4.12). As a result, the mass of $\tilde{\tau}_2$ is often lighter than $\tilde{t}_1$, which can be seen in Fig. 4.13. This means that it possible for a competing decay mode of $\tilde{t}_1 \rightarrow \tilde{\tau}_2 + X$ to take place (as seen in Sec. 4.2).

The influence of $tan(\beta)$ on the mass of the Higgs boson can be seen in Fig. 4.14. Model points with small values of $tan(\beta)$ mostly contain very light Higgs bosons and even the

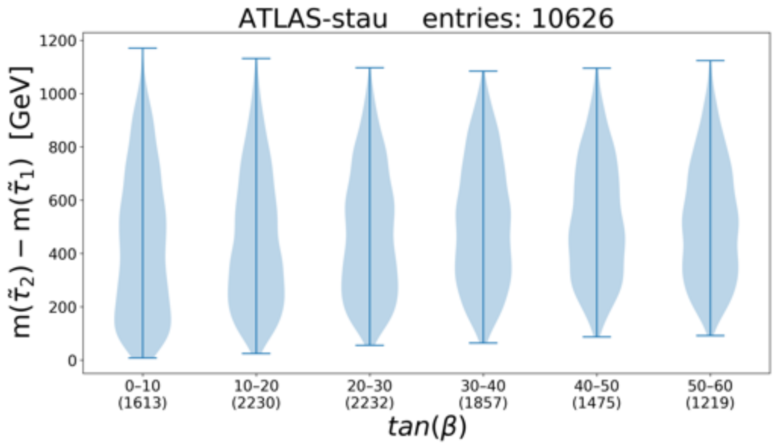

Figure 4.12: Effect of $tan(\beta)$ on the difference in mass between $\tilde{\tau}_1$ and $\tilde{\tau}_2$. Selection criteria: ATLAS-stau simplified model.

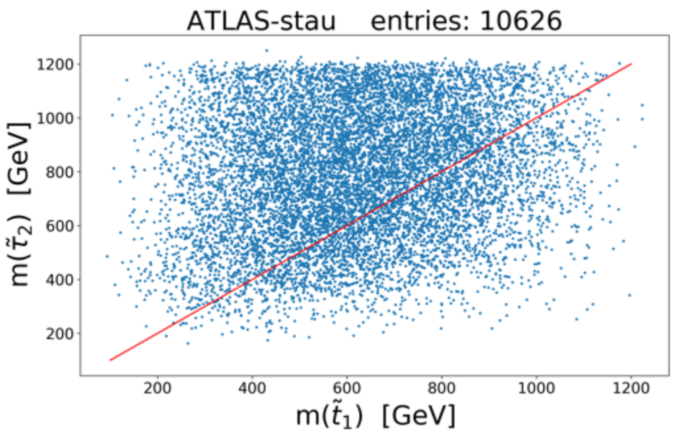

Figure 4.13: Mass of $\tilde{t}_1$ compared to $\tilde{\tau}_2$. Selection criteria: ATLAS-stau simplified model. Red line indicates equal masses. Below the line equates m($\tilde{t}_1$) > m($\tilde{\tau}_2$).

heaviest bosons for $tan(\beta) \leq 10$ are barely heavier than 120 GeV. For a model point to have a phase space that could reflect reality, a model point has to have a Higgs boson with a mass that is equal to the measured value.

In Fig. 4.15, the selection criteria includes all physical points where the mass of the Higgs boson is between $122 < \mathrm{m}(h) < 128$ GeV. Whilst lower values for $tan(\beta)$ are hardly able to generate Higgs bosons within the these bounds, higher values also have very few points around 125 GeV. This is problematic for the secondary objective of this analysis: to optimise the phase space to generate model points that fulfil modern observations. Ideally, the selection criteria for the mass of the Higgs boson would be much closer to 125 GeV, but to be able to make any significant conclusions much more data would need to be generated.

In Fig. 4.16, the selection criteria for the simplified model is combined with the limitation on the Higgs boson mass to $122 < \mathrm{m}(h) < 128$ GeV. The only remaining bins that have a model point with $\mathrm{m}(h) \approx 125$ GeV are those with $tan(\beta) \geq 40$, but this could be a result of statistical fluctuations. Even though there are a small number of model points that pass the selection criteria, it is quite clear that values of $tan(\beta) < 10$ are very unlikely to produce model points that reflect real observations.

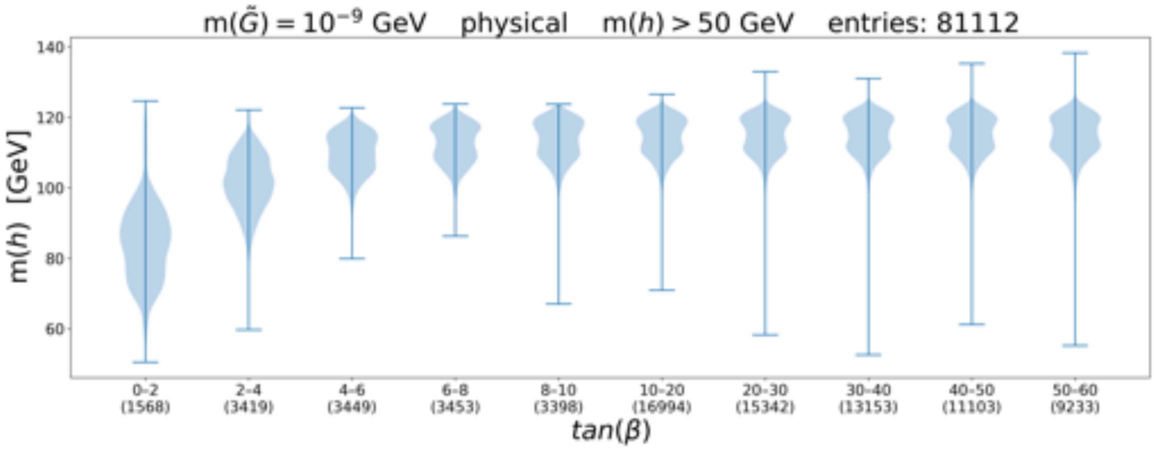

Figure 4.14: Effect of $tan(\beta)$ on m(h). Selection criteria: physical model points with $50 <$ m(h) < 140 GeV. Lower values split into multiple brackets for better visualisation.

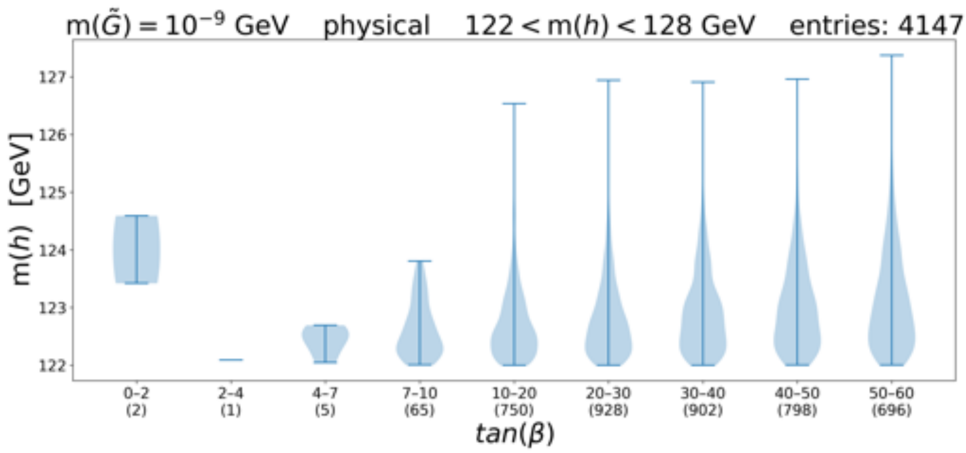

Figure 4.15: Effect of $tan(\beta)$ on m(h). Selection criteria: physical model points with m(h): $122 <$ m(h) < 128 GeV

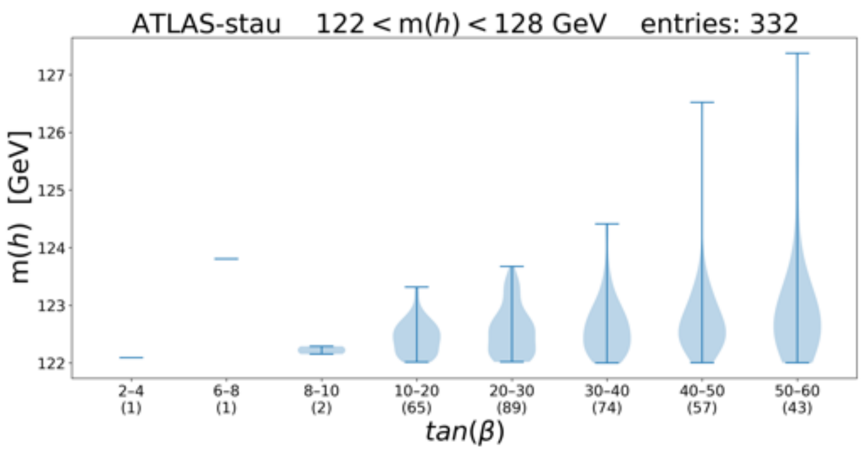

Figure 4.16: Effect of $tan(\beta)$ on m(h). Selection criteria: ATLAS-stau simplified model with m(h): $122 <$ m(h) < 128 GeV. Missing bins contain no entries.

4.3.2 A_t - Trilinear Coupling Constant

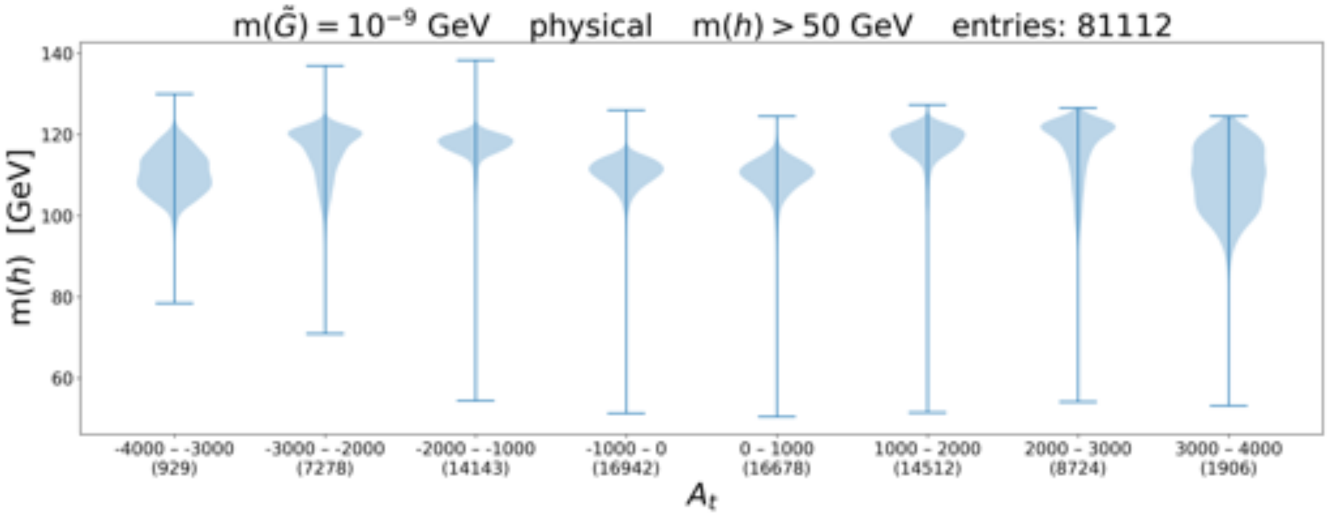

Figure 4.17: Violin plot of A_t by m(h) (ATLAS). Number in brackets represent the number of entries in each bin. Selection criteria: Physical model points.

A_t is the trilinear coupling parameter that links the Higgs boson to $\tilde{t}_1$ and $\tilde{t}_2$. In Fig. 4.17, the influence of A_t on the Higgs boson's mass can be seen for physical model points. Although the distribution is not quite symmetric, it is clear that both large and small absolute values tend to generate Higgs bosons that are too light. Also, while the bins with $A_t < |1000|$ have the most entries, there are very few model points that make it past 120 GeV. The outer bins ($A_t > |3000|$) have very broad distributions and are more likely to produce Higgs bosons that are close to 100 GeV. While there are much fewer entries in these bins compared to the others, they seem to have taken on a distinctly different shape. It should be reminded that the lack of entries for larger absolute values has to do with the generation of physical points, not to do with any selection criteria.

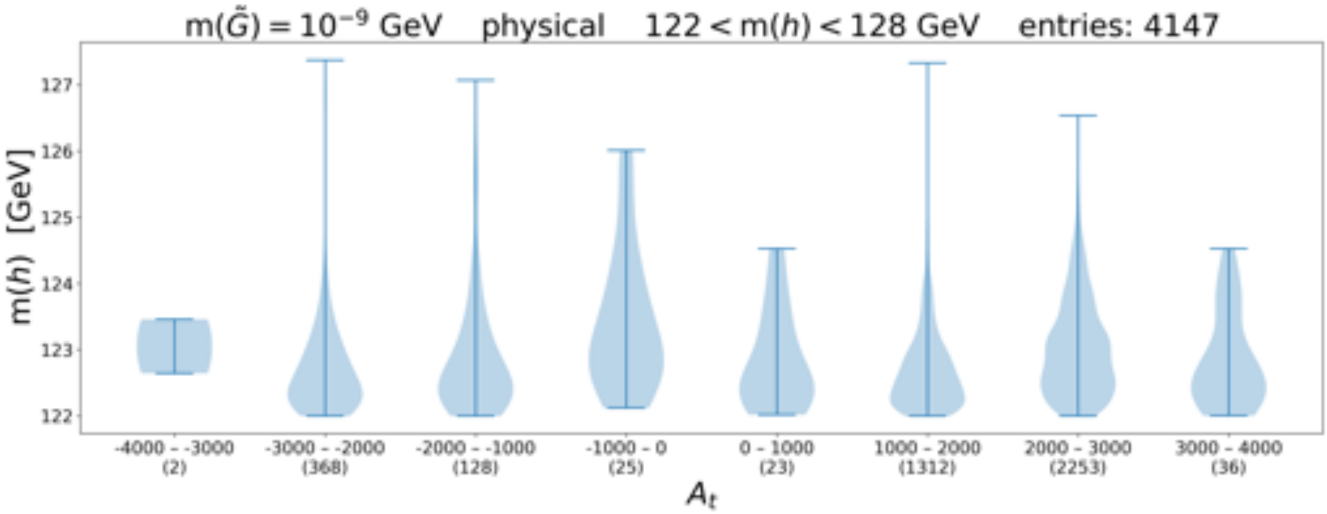

Figure 4.18: Violin plot of A_t by m(h) (ATLAS). Selection criteria: Physical model points with 122 < m(h) < 128 GeV.

By implementing an additional cut on the mass of the Higgs boson (see Fig. 4.18), one can see that the bins 1000–2000 and 2000–3000 have many more entries compared to the others. Particularly, there are relatively many Higgs bosons with m(h) ≈ 125 GeV in the 2000–3000 range. Even though the most physical model points were generated for $A_t < |1000|$, very few have passed the cut.

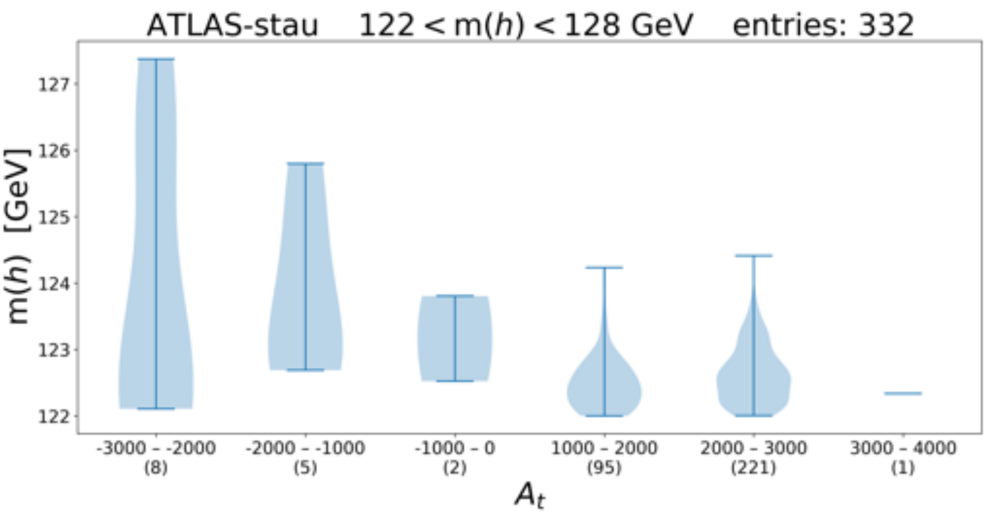

Figure 4.19: Violin plot of A_t by m(h) (ATLAS). Selection criteria: Simplified Model with 122 < m(h) < 128 GeV. Missing bins have no entries.

Implementing the selection for the simplified model results in an interesting distribution (see Fig. 4.19). About two thirds of the remaining model points are in the bin 2000–3000, whereas almost all of the reset are in 1000–2000. None of the model points in either of these bin contain a Higgs mass of m(h) ≈ 125 GeV. Negative values for A_t, on the other hand, are able to generate heavy SM Higgs bosons. Since the statistics are so low for these bins, it is not possible to say if the heavy SM Higgs bosons are fluctuations, or if the distribution does in fact tend to have more heavy SM Higgs bosons. Since `EasyScan_HEP` requires a single interval from which values will be randomly chosen for the generation, the phase space could be reduced to $A_t < |3000|$ to increase the likelihood of generating a model point that would pass this criteria, but model points with $A_t < |1000|$ are not able to be avoided.

4.3.3 μ - Higgsino Mass Parameter

As stated in Sec. 4.1, the reason only positive values for the higgsino mass parameter μ have been generated, is because negative values weren't able to produce model points with 122 < m(h) < 128 GeV. Therefore, only positive values were chosen to increase the number of model points that pass the selection criteria regarding m(h). The distribution of m(h) is pretty much the same for all bins in Fig. 4.20, so it does not seem to have an effect on physical model points.

When limiting the physical model points with 122 < m(h) < 128 GeV, it becomes clear that lower values of μ are more likely to produce heavier Higgs bosons. Not only do more model points pass the selection criteria, but there are also more points with m(h) ≈ $125 GeV$.

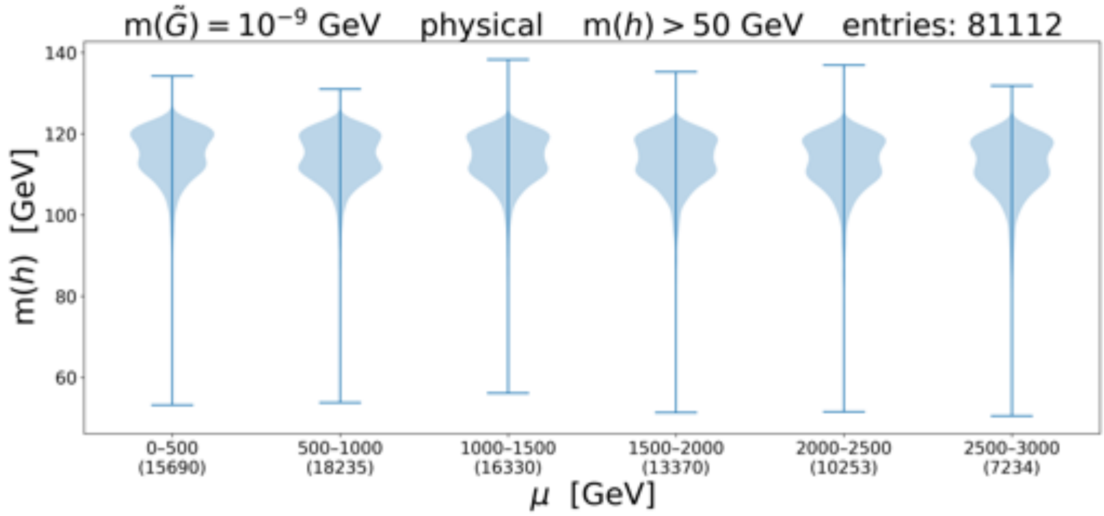

Figure 4.20: Violin plot of μ by m(h). Selection criteria: physical model points.

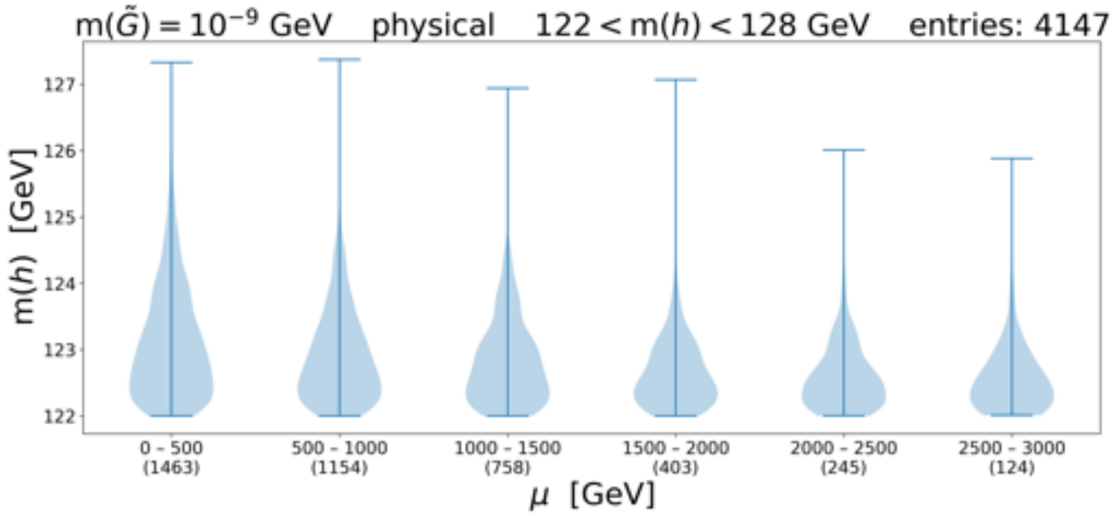

Figure 4.21: Violin plot of μ by m(h). Selection criteria: physical model points with $122 < \mathrm{m}(h) < 128$ GeV.

This changes when also applying the selection of the ATLAS-stau simplified model (See Fig. 4.22): the range of 0–500 GeV is much less likely to contain the simplified model. Instead, model points with $1000 < \mu < 1500$ GeV are the most common, followed by $500 < \mu < 1000$ GeV.

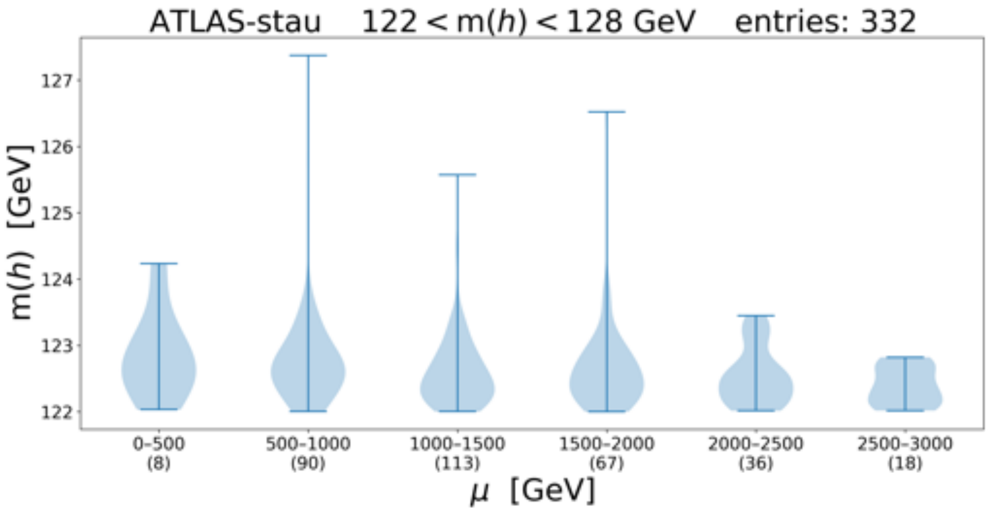

Figure 4.22: Violin plot of μ by m(h). Selection criteria: ATLAS-stau simplified model with $122 < \mathrm{m}(h) < 128$ GeV.

4.4 Dark Matter Relic Density

The distribution of the dark matter relic density for the ATLAS-stau simplified model can been seen in Fig. 4.23a. The model points have been inclusively split by the combined branching ratio of the simplified model to see if the branching ratio has any effect on the dark matter relic density. Of the 10626 model points that contain the ATLAS-stau simplified model with a branching ration > 0.1, 9110 points have a relic density below 0.3 and most of those points are well below the measured value of $\Omega_c h^2 \approx 0.12$, which makes the ATLAS-stau model very promising in terms of fulfilling the requirements of not producing too much dark matter.
One interesting question is what influence the mass of the LSP has on the distribution of the relic density. To see the effect of the mass of the gravitino, two more sets of data were generated, one with $m_{\tilde{G}} = 10^{-8}$ GeV (Fig. 4.23b) and one with $m_{\tilde{G}} = 10^{-7}$ GeV (Fig. 4.23c). Both of these cases only have around half the number of model points that contain the ATLAS-stau simplified model, but the shapes of the distributions of the relic densities hardly changes. The dark matter relic density seems to not be strongly influenced by variances in the mass of light gravitinos.

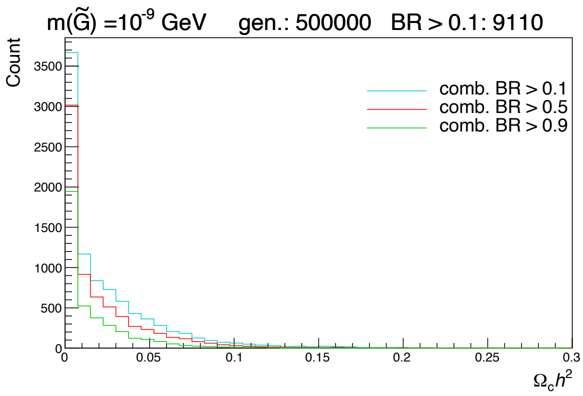

(a)

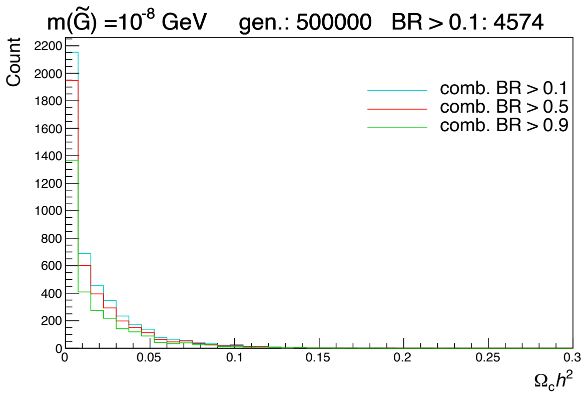

(b)

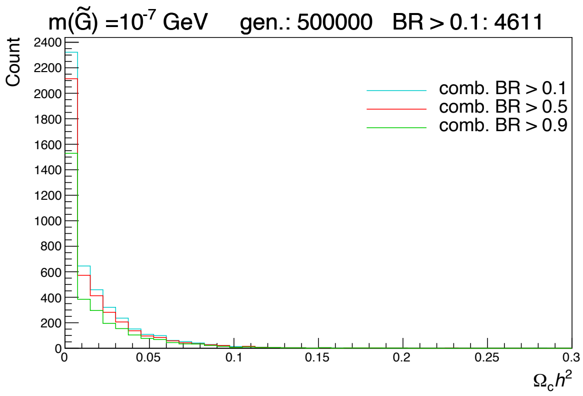

(c)

Figure 4.23: Dark matter relic density for the ATLAS model. Selection criteria: ATLAS-stau simplified model (a) m($\tilde{G}$) = 10^{-9} GeV, (b) m($\tilde{G}$) = 10^{-8} GeV, (c) m($\tilde{G}$) = 10^{-7} GeV

Chapter 5

CMS-stau and CMS-sneutrino

5.1 CMS-stau

The complete phase space used for generating models points with m($\tilde{G}$) = 10^{19} GeV can be seen in Tab. 5.1.

Table 5.1: Phase space used to generate model points with m($\tilde{G}$) = 10^{19} GeV.

$tan\,(\beta)$	1 – 60
$\lvert A_t\rvert$ $\lvert A_b\rvert$ $\lvert A_\tau\rvert$	0 – 4000 GeV
m_{t_R} $m_{Q_{L3}}$ m_{τ_L} m_{τ_R}	100 – 1200 GeV
$\lvert M_1\rvert$	0 – 1000 GeV
$\lvert M_2\rvert$	0 – 3000 GeV
μ	0 – 3000 GeV

M_3 m_A m_{u_R} m_{d_R} $m_{Q_{L1}}$ m_{b_R} m_{e_L} m_{e_R}	100 – 3000 GeV

To get a better comparison between the ATLAS-stau and CMS-stau model, the $\tilde{t}_1$ generated in model points with heavy gravitinos are also limited to 1.2 TeV. The $\tilde{\tau}_1$ are limited to 1.2 TeV for the same reasons as discussed with the ATLAS-stau model. Like the stau, the $\tilde{\chi}_1^+$ needs to be lighter than the stop. Regulating the chargino's mass is more complicated, as it is influenced by M_2 and μ (the wino and higgsino mass parameters) which also influence the mass of the $\tilde{\chi}_1^0$ (alongside M_1). Therefore, the phase spaces of M_2 and μ are chosen to be broad for the generation and as a result, the chargino's mass can go up to 3 TeV. $|M_1|$ has been limited to 1 TeV, as early tests showed that increasing the boundary reduced the chance of generating a model points that surpassed the CMS-stau simplified model's selection criteria, yet the distributions for all other parameters maintained the same shapes. A more in-depth look as to why this is the case is discussed later whilst looking at the mass and mixture of the neutralino. The parameters generated in the range of 100–3000 GeV have had their

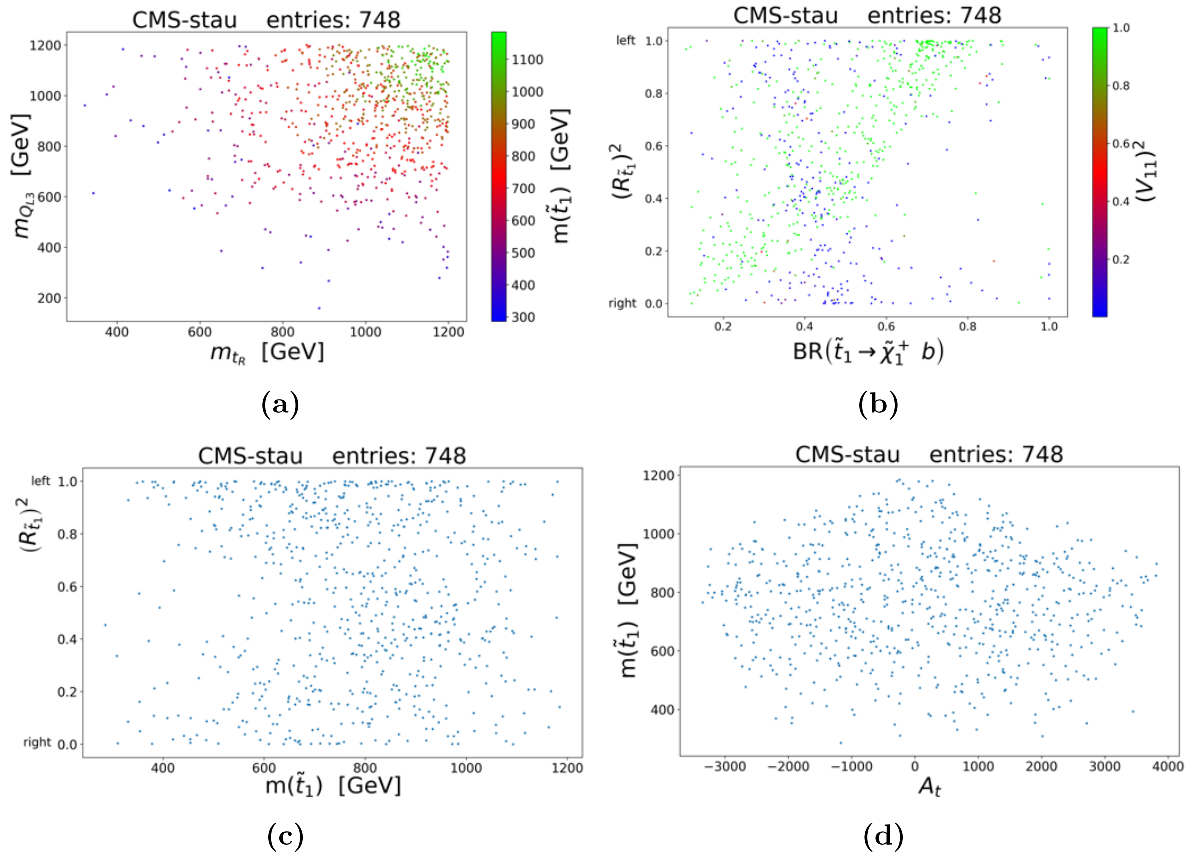

Figure 5.1: $\tilde{t}_1$ mass parameters and mixture. Selection criteria: Simplified Model. (a) Mass parameters. (b) Stop mixture with relation to the branching ratio for $\tilde{t}_1 \rightarrow \tilde{\chi}_1^+ b$. $(R_{\tilde{t}_1})^2 = 1$ represents a left-like stop. $(V_{11})^2$ represents the chargino mixture: $(V_{11})^2 \approx 1$ wino-like, $(V_{11})^2 \approx 0$ higgsino-like. (c) Mixture with relation to the mass. (d) Stop trilinear coupling constant with relation to the mass of the $\tilde{t}_1$.

upper and lower boundaries set for the same reasons as for the ATLAS-stau model: the upper bounds can be chosen to be large without having any significant effects on model points that contain the simplified model and any lower than 100 GeV produces unphysical model points.

In Fig. 5.1a, the influence of m_{t_R} and $m_{Q_{L3}}$ on the mass of the stop can bee seen for model points that contain the CMS-stau simplified model. Unsurprisingly, heavy stops are preferred. Only in model points with m_{t_R}, $m_{Q_{L3}} > 1000$ GeV have stops heavier than 1 TeV, which is a small section of the phase space. Many model points with a stop under 1 TeV have either $m_{Q_{L3}} > 1000$ GeV with $m_{t_R} < 1000$ GeV, or vice-versa, much like the ATLAS-stau model. The distribution in Fig. 5.1b shows that model points that have a high branching ratio for BR($\tilde{t}_1 \rightarrow \tilde{\tau}_1\ b\ \nu_\tau$) tend to have stops with a left-like mixture. For lower branching ratios, there seems to be a slight bias towards right-like stops, but this could be due to low statistics. There is a very clear relationship between the mixture of the stop, the mixture of the chargino and the branching ratio $\tilde{t}_1 \rightarrow \tilde{\chi}_1^+ b$. Model points with left-like stops have small branching ratios when the chargino is higgsino-like, and large branching ratios when the chargino is wino-like. For right-like stops it is the other way around.

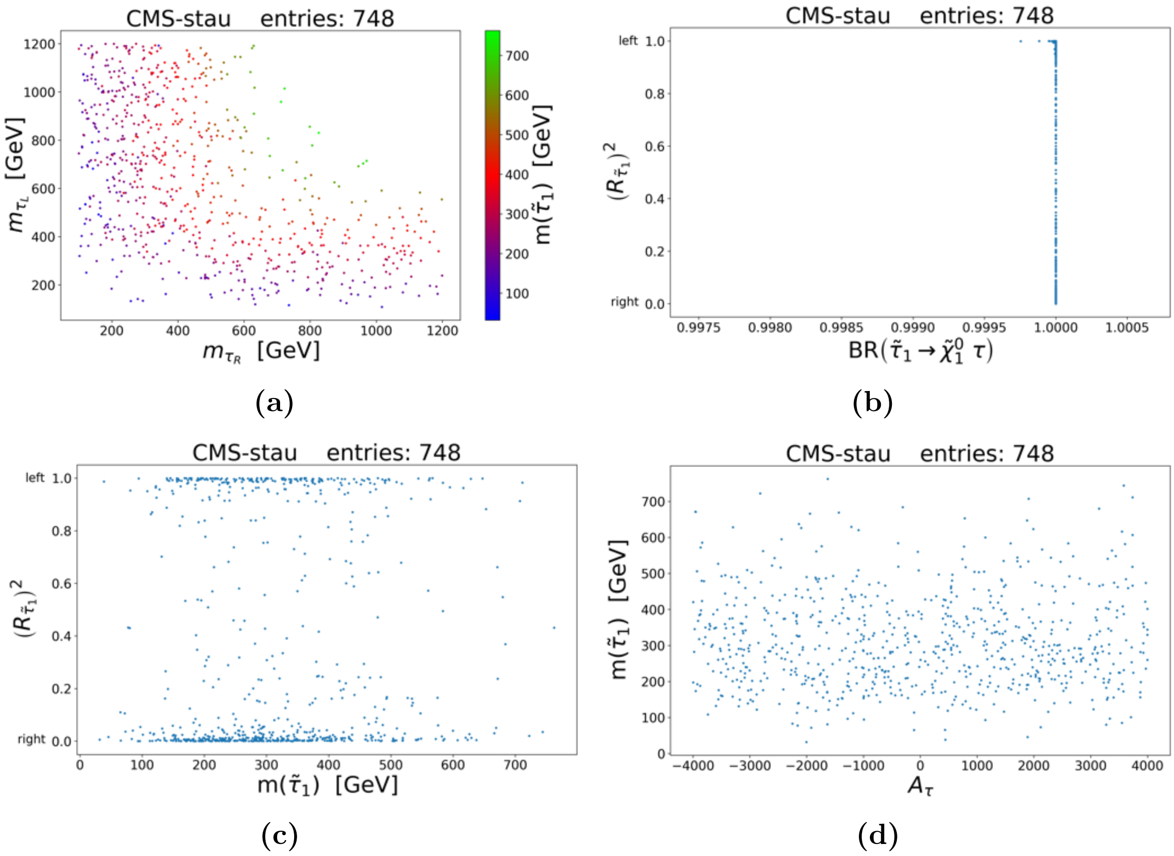

Figure 5.2: $\tilde{\tau}_1$ mass parameters and mixture. Selection criteria: Simplified Model. (a) Mass parameters. (b) Stau mixture with relation to the branching ratio for $\tilde{\tau}_1 \to \tilde{\chi}_1^+ b$. $(R_{\tau_1})^2 = 1$ represents a left-handed mixture. (c) Mixture with relation to the mass. (d) Stau trilinear coupling constant with relation to the mass.

The mass of the stau is limited by the mass of the chargino. As a result, the heaviest staus are around 700 GeV (see Fig. 5.2a), but there are only very few. In almost all model points either m_{τ_L} or m_{τ_R} is below 600 GeV, whereas the other parameter can still go up to 1200 GeV. Therefore, in most model points the stau has either a strong left- or right-like mixture (see Fig. 5.2c). The mixture has almost no effect on the branching ratio of the decay $\tilde{\tau}_1 \to \tilde{\chi}_1^0\ \tau$ and almost all points have a branching ratio of 1. There are some cases where staus with left-like mixtures have branching ratios slightly below 1, but the difference is so small that it is negligible.

In Fig. 5.3a, M_2 and μ are shown and the mass of the chargino is represented by the colour. The selection criteria only allows for model points that contain the CMS-stau simplified model. Clear boundaries are visible, showing that if either M_2 or μ is over 1 TeV, then the other parameter has to be under 1 TeV. As can be seen in Fig. 5.3b, if both parameters are over around 1 TeV, then the chargino will become heavier than the stop and the simplified model won't be able to exist. The lack of points with very small values of either M_2 and μ is partially a consequence of requiring the chargino to be lighter than the stau, but this is also heavily influenced by the $\tilde{\chi}_1^0$.

M_1, M_2 and μ all influence the mass (and mixture) of the $\tilde{\chi}_1^0$. The mixture of the $\tilde{\chi}_1^0$ in model points that contain the CMS-stau simplified model is almost always bino-like (see Fig. 5.4). Whether a neutralino is categorised as bino-, wino- or higgsino-like

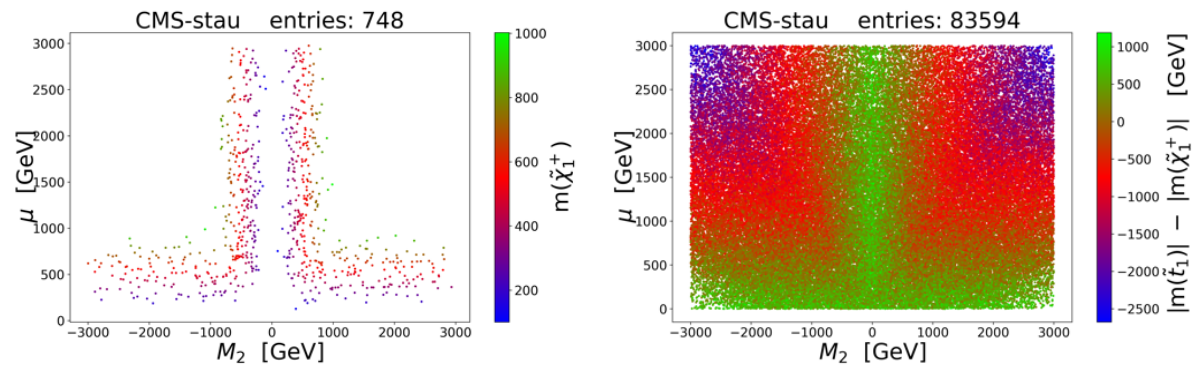

(a) (b)

Figure 5.3: $\tilde{\chi}_1^+$ mass parameters. (a) Selection criteria: CMS-stau simplified model, (b) Green dots represent model points where the $\tilde{\chi}_1^+$ is lighter than the $\tilde{t}_1$. Selection criteria: physical points

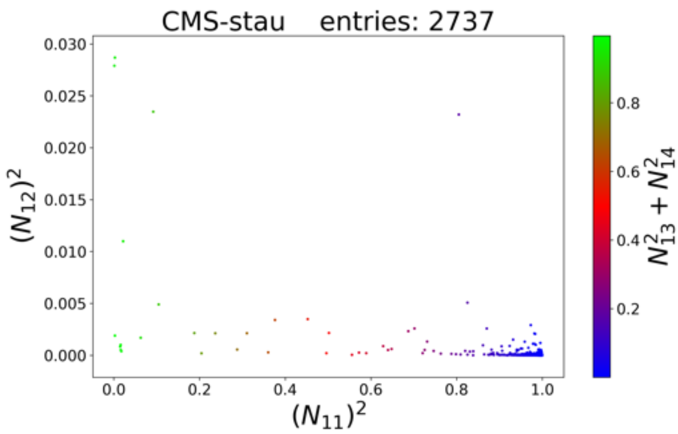

Figure 5.4: $\tilde{\chi}_1^0$ mixture. Selection criteria: CMS-stau mass hierarchy. Most model points are eliminated solely by this criteria and mostly those with bino-like $\tilde{\chi}_1^0$ are left.

depends on the mixing components N_{11} (bino), N_{12} (wino) and N_{13}, N_{14} (higgsino). In this analysis, if $(N_{11})^2 > (N_{12})^2 + ((N_{13})^2 + (N_{14})^2)$, then the neutralino is labelled bino-like. The definition for wino-like is similar and for higgsino-like, $((N_{13})^2 + (N_{14})^2)$ has to be the largest.

The mixtures and masses of both the neutralino and the chargino are influenced by M_2 and μ. Therefore, it can be assumed that there could be a connection between the almost strict bino-like mixture of the remaining neutralinos and the mass and mixture of the chargino. In Fig. 5.5, the mass of the chargino is compared to the mixture and mass of the neutralino. The selection criteria for these plots requires $\mathrm{m}(\tilde{t}_1) > \big(\mathrm{m}(\tilde{\chi}_1^+) + \mathrm{m}(b)\big)$, $\mathrm{m}(\tilde{\chi}_1^+) > (\mathrm{m}(\tilde{\tau}_1) + \mathrm{m}(\nu_\tau))$. The neutralino is ignored, since a selection on either $\tilde{\tau}_1 \to \tilde{\chi}_1^0\, \tau$ or $\mathrm{m}(\tilde{\tau}_1) > \mathrm{m}(\tilde{\chi}_1^0)$ would result in almost exclusively bino-like neutralinos (such as in Fig. 5.4). In Fig. 5.5a, the green points represent model points with a neutralino that has a large bino-like mixture. The difference between the masses of the chargino and the neutralino is largest in these points, which means that it is more likely for a stau to exist with a mass that is between those of the chargino and neutralino. The higgsino-like neutralinos can be seen in Fig. 5.5c. The masses of

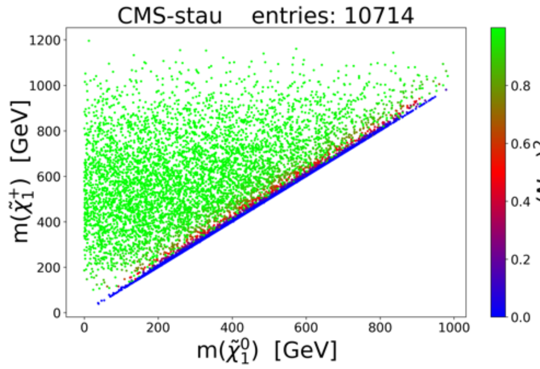

(a) Bino mixing parameter

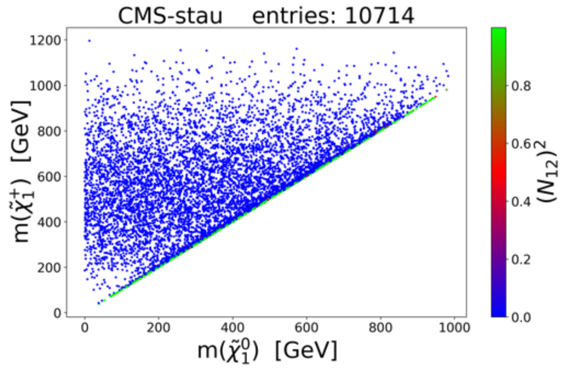

(b) Wino mixing parameter

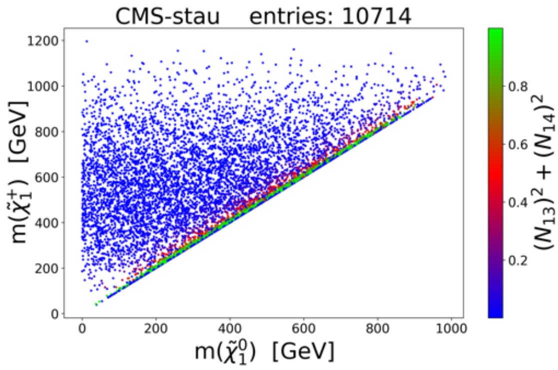

(c) Higgsino mixing parameters

Figure 5.5: Comparison between the masses of the chargino ($|\tilde{chi}_1^+$) and the mass of the ($|\tilde{chi}_1^0$), where the colour represents the (a) bino mixing parameter (b) wino mixing parameter (c) higgsino mixing parameters. Selection criteria: $\mathrm{m}(\tilde{t}_1) > \big(\mathrm{m}(\tilde{\chi}_1^+) + \mathrm{m}(b)\big)$, $\mathrm{m}(\tilde{\chi}_1^+) > (\mathrm{m}(\tilde{\tau}_1)+\mathrm{m}(\nu_\tau))$.

the chargino and neutralino are very close to one another in these points, but there is still a bit of a difference between them. This means that while it is unlikely for a stau to exist with a mass necessary for the CMS-stau simplified model, it is still going to appear in a few cases, which is what can be seen in Fig. 5.4. Finally, model points that have wino-like neutralinos (see Fig. 5.5b) have very small mass differences, to the point where it is extremely unlikely for a stau to fit in.
Something noticeable about these plots is the lack of model points where the neutralino is much heavier than the chargino. Although it looks like there is a cut-off at $\mathrm{m}(\tilde{\chi}_1^+) > \mathrm{m}(\tilde{\chi}_1^0)$, this is not the case; there are very few points in which the neutralino is heavier. It is unclear why the neutralino can only be marginally heavier than the chargino.

In Fig. 5.6, the phase space of M_1, M_2, and μ compared to one another can be seen with relation to the neutralino's mass. The complete mass hierarchy of the CMS-stau simplified model is used as the selection criteria (unlike in Fig.5.5) to get a better understanding of how each parameter affects the neutralino's mass. Decay modes are not of interest here, as the mass hierarchy alone defines which neutralino mixtures are allowed, since both the neutralino's mass and mixture are influenced by M_1, M_2, and μ.

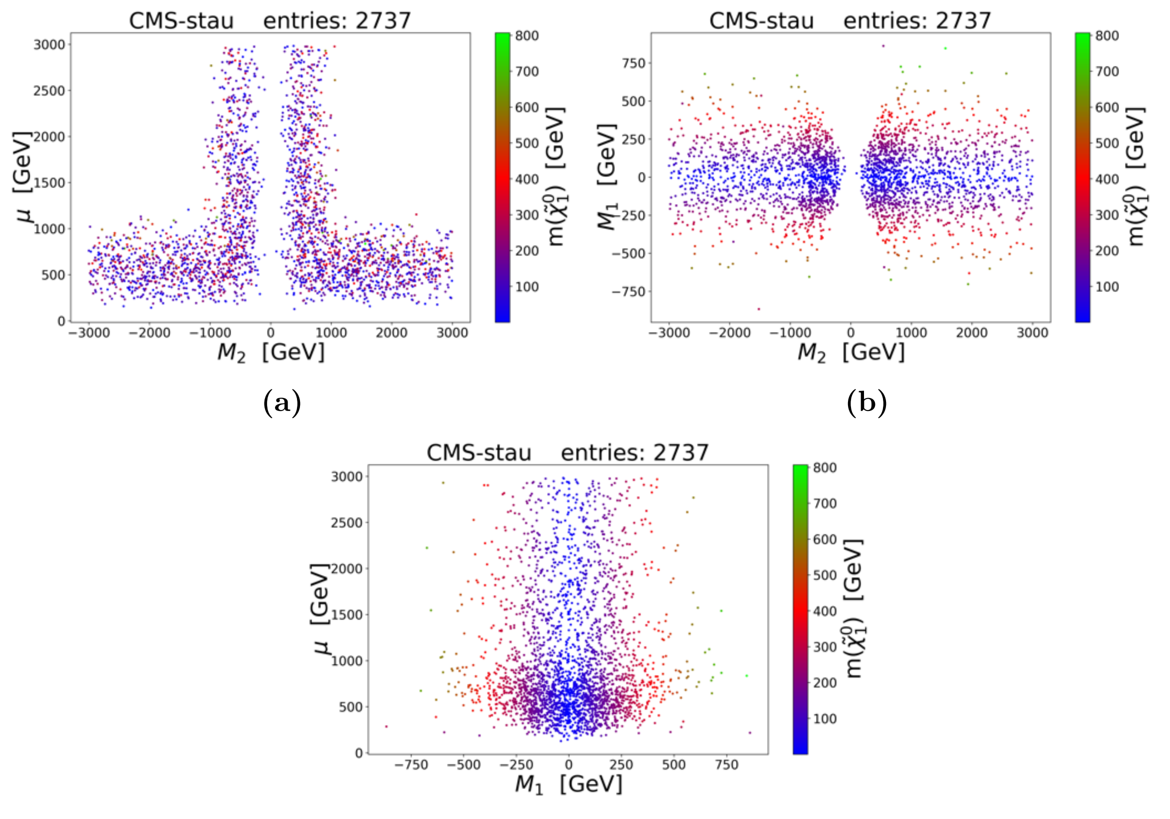

(a) **(b)**

(c)

Figure 5.6: Neutrino mixing parameters with relation to one another. Selection criteria:CMS-stau Mass Hierarchy.

According to Fig. 5.6b, it looks like there are not any model points with $|M_1|<|M_2|$. Further investigation shows that this is not quite true. In a few points, $|M_2|$ is smaller than $| M_1 |$, but then μ is smaller than $| M_2 |$, which leads to the neutralino being higgsino-like. However, there are a couple model points in which $|M_2|$ is smaller than both $|M_1|$ and μ, yet the neutralinos still have very strong bino-like mixtures. In these cases, $|M_2|$ is only marginally smaller than $|M_1|$, therefore, it is most likely higher order corrections that end-up having a larger influence on the mixture. A similar shape can be seen around $|M_1|< \mu$ in Fig. 5.6c, but it is not as sharp. This is not surprising, as it is more likely for a stau to have a mass between those of the chargino and neutralino in model points with a higgsino-like neutralino, since they have a slightly larger mass splitting compared to wino-like cases (see Fig. 5.5c). The two-dimensional phase space for M_2 and μ has the same shape as in Fig. 5.3a. There, it can clearly be seen that M_2 and μ have an influence on the mass of the chargino. However, the correlation between M_2, μ, and the neutralino's mass is not obvious. The lower bounds of $|M_2|$ and μ seem to be set by $|M_1|$, whereas the upper bounds are set by the mass of the chargino. This explains why model points with bino-like neutralinos can have such a large mass splitting between the neutralino and chargino: as long as $|M_1|$ has the lowest value of the three parameters, $|M_2|$ and μ can be as large as the bounds for the chargino mass allow. In wino- and higgsino-like cases, either $|M_2|$ or μ respectively has to have a small value, which inadvertently decreases the mass of the chargino.

At this point it still is not quite clear why M_1 has the dominant effect on the neu-

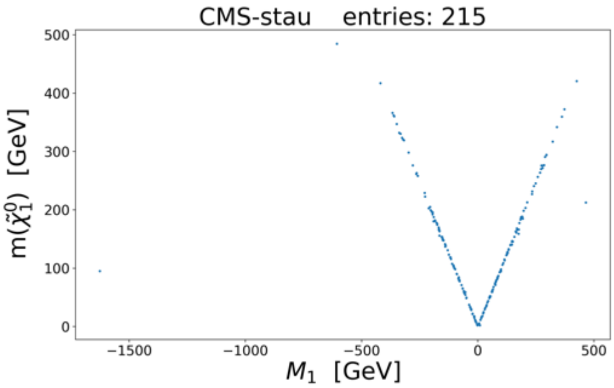

Figure 5.7: Relation between M_1 and the $\tilde{\chi}_1^0$ mass using a different set of simulated data with $|M_1| < 3000$. Selection criteria: Mass Hierarchy.

tralino's mass. When looking at Fig. 5.6b it is also unclear why $|M_1|$ is more or less bound to be smaller than 750 GeV. To answer the latter, more data was generated with $|M_1| < 3000$ and the connection between M_1 and the neutralino's mass was looked into. Fig. 5.7 shows two interesting things: first, M_1 is still limited to small values. Second, there seems to be a one-to-one correlation between M_1 and the neutralino's mass (evidence for this could already be seen in Fig. 5.6b by looking at the distribution of the colours). These two bits of information are related to one another; the mass hierarchy of the particles requires the neutralino to be lighter than the stau. The stau is required to be lighter than the stop, which is generated to have at most a mass of 1.2 TeV. Since $|M_1|$ has a linear correlation to the neutralino's mass, only small values will be able to generate a neutralino that is lighter than the stau.

The observation that $|M_1|$ has a linear correlation to the neutralino's mass has been predicted. Under the condition $m_Z \ll |\mu \pm M_1|$, $m_Z \ll |\mu \pm M_2|$, the masses of $\tilde{\tau}_1$, $\tilde{\tau}_2$, and $\tilde{\tau}_3/\tilde{\tau}_4$ can be simplified to M_1, M_2, and μ respectively (minus higher order corrections) [11]. Almost all model points, apart from a few outliers, that contain the CMS-stau simplified model can be described with this simplification.

Another aspect of the CMS-stau simplified model which needs to be taken into consideration is the relation between the mixture of the chargino and the mixture of the stau. Since model points with a bino-like neutralino have a relatively broad 2-D phase space for M_2 and μ (see Fig. 5.3a), the mixture of the chargino can be wino-like or higgsino-like. Also, the stau tends to be either left-like or right-like; there are not many model points where it is evenly mixed. As a result, the question about whether the combination of the mixtures has an effect on $\tilde{\chi}_1^+ \to \tilde{\tau}_1\, \nu_\tau$ arises.

In Fig. 5.8a, model points containing the CMS-stau simplified model can be seen, where the colour represents the branching ratio for $\tilde{\chi}_1^+ \to \tilde{\tau}_1\, \nu_\tau$. Model points in which the chargino is wino-like and the stau right-like have the highest branching ratios on average, generally above 0.9, whereas the combinations wino-left and higgsino-right are only around 0.5–0.6. It looks like there are not any model points with higgsino-left, but this comes from the requirement that the simplified model has a combined branching ratio > 0.1.

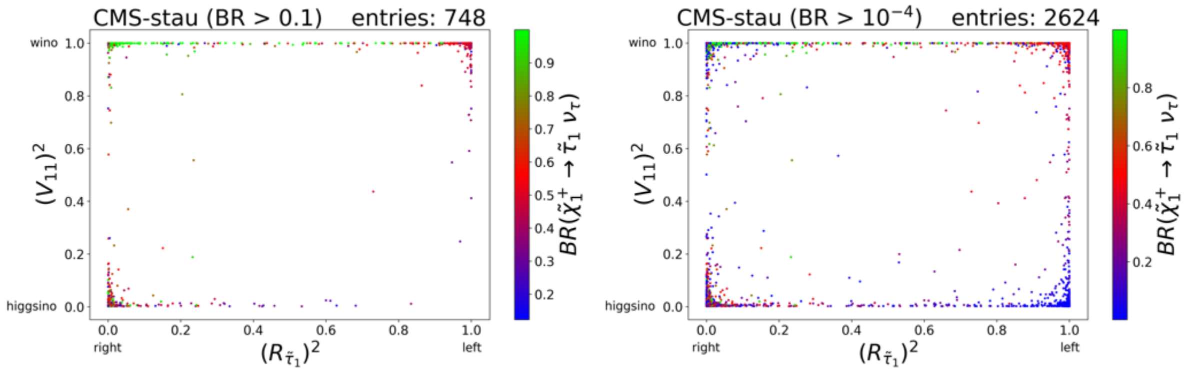

(a) **(b)**

Figure 5.8: V_{11} = chargino mixing angle, $R_{\tilde{\tau}_1}$ = stau mixing angle. Selection criteria: (a) CMS-stau Simplified Model, (b) CMS-stau Simplified Model, but selection on combined branching ratio reduced to $> 10^{-4}$.

Changing this selection to $> 10^{-4}$ [1] reveals that higgsino-left model points do exist, but are suppressed. Clearly, some other decay modes are competing with $\tilde{\chi}_1^+ \to \tilde{\tau}_1\ \nu_\tau$. Fig. 5.9 shows the main three competing decay modes, where each plot represents a different combination of the chargino and stau mixtures. Essentially, each plot focuses on model points from one of the four corners of Fig. 5.8. In Fig. 5.9a, 5.9b and 5.9c the combined branching ratio of the CMS-stau simplified model is > 0.1, whereas for Fig. 5.9d it is $> 10^{-4}$. The low statistics for $\tilde{\chi}_1^+ \to \tilde{b}_1\ t$ make it hard to make any meaningful conclusions about the shape of its distribution. One of the reasons this decay mode is much less likely to exist compared to the others has to do with the phase space over which the model points are generated: m_{b_R} can take values from $100 - -3000$ GeV, which means that the $\tilde{b}_1$ (sbottom) can be very heavy. As a result, the sbottom is often heavier than the chargino. The decay mode $\tilde{\chi}_1^+ \to \tilde{\chi}_1^0\ W$ tends to have higher branching ratios for higgsino-like charginos and $\tilde{\chi}_1^+ \to \tilde{\nu}_\tau\ \tau$ almost only appears for left-like staus. As a result, in higgsino-left model points the combination of these decay modes suppress the decay $\tilde{\chi}_1^+ \to \tilde{\tau}_1\ \nu_\tau$ heavily.

The distribution for the branching ratio for $\tilde{\chi}_1^+ \to \tilde{\nu}_\tau\ \tau$ in Fig. 5.9b takes on an interesting shape, as it mostly consists of a large peak around 0.5. This comes from the fact that the mixture of the $\tilde{\tau}_1$ is related to the mass of the $\tilde{\nu}_\tau$ (which is strictly left-handed). To look into this further and to see what role the mass of the chargino plays for this decay mode, the selection criteria for the scatter plots in Fig. 5.10 contain the existence of the CMS-stau simplified model and the decay mode $\tilde{\chi}_1^+ \to \tilde{\nu}_\tau\ \tau$. By not requiring on $(V_{11})^2$ or $(R_{\tilde{\tau}_1})^2$, such as in Fig. 5.9b, a bit more information about the influence of the particles' mixtures can be gained.
As can be seen in Fig. 5.10a, the more left-like the stau is, the closer the masses of the stau and $\tilde{\nu}_\tau$ get to one another, until the $\tilde{\nu}_\tau$ even becomes a little bit heavier. The mass of the chargino with relation to the branching ratio is depicted in Fig. 5.10b and it is remarkable that the mass does not have much of an impact until the branching ratio gets to around 0.52, where it suddenly drops rapidly. Because of this, the difference

[1] 10^{-4} is the minimum branching ratio required for a decay mode to be added to the data of a model point.

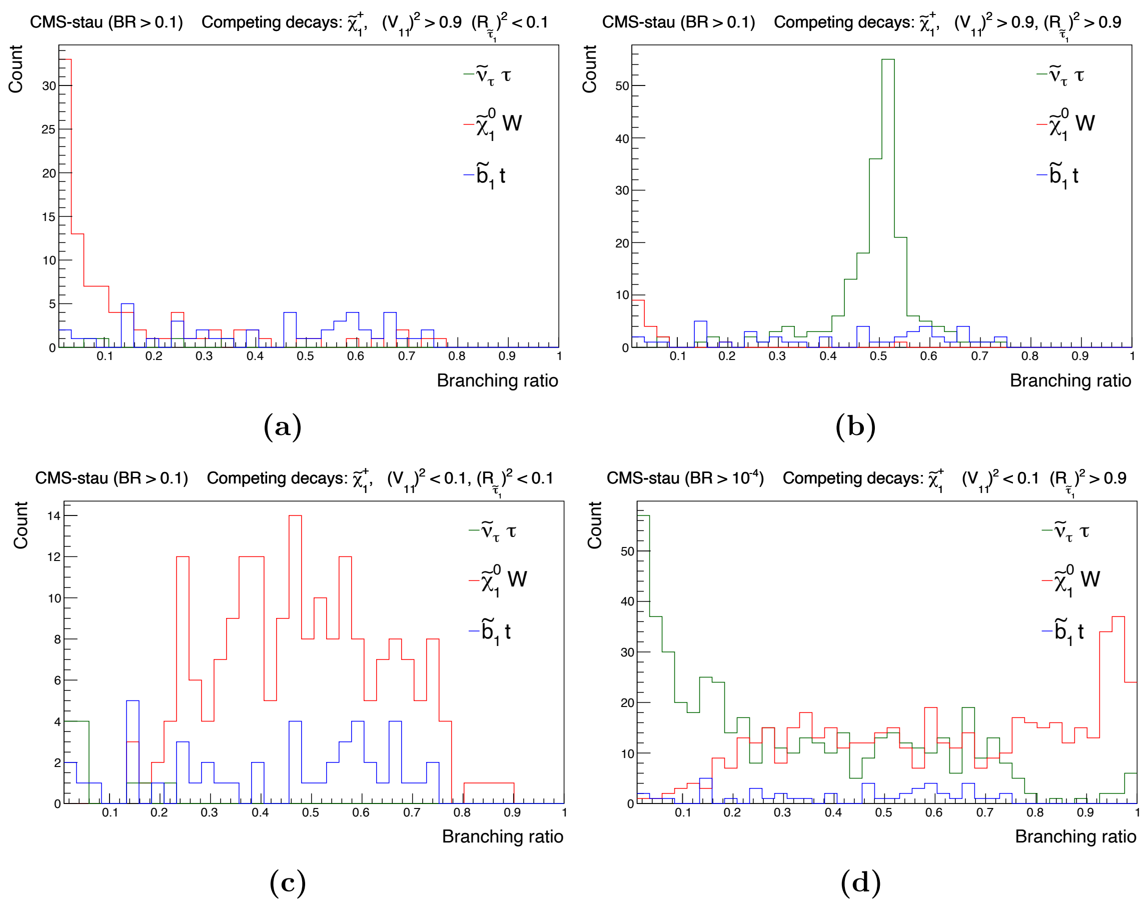

Figure 5.9: Competing decays for the different combinations of chargino and stau mixtures. The summed branching ratio of the depicted decay modes with $\tilde{\chi}_1^+ \to \tilde{\tau}_1\ \nu_\tau$ is nearly always ≈ 1. Selection criteria: CMS-stau Simplified Model with combined BR> 0.1, apart from (d), which has combined BR> 0.

in mass between the chargino and either the $\tilde{\tau}_1$ or $\tilde{\nu}_\tau$ also decreases (see Fig. 5.10c) to the point where the chargino's mass is barely larger.

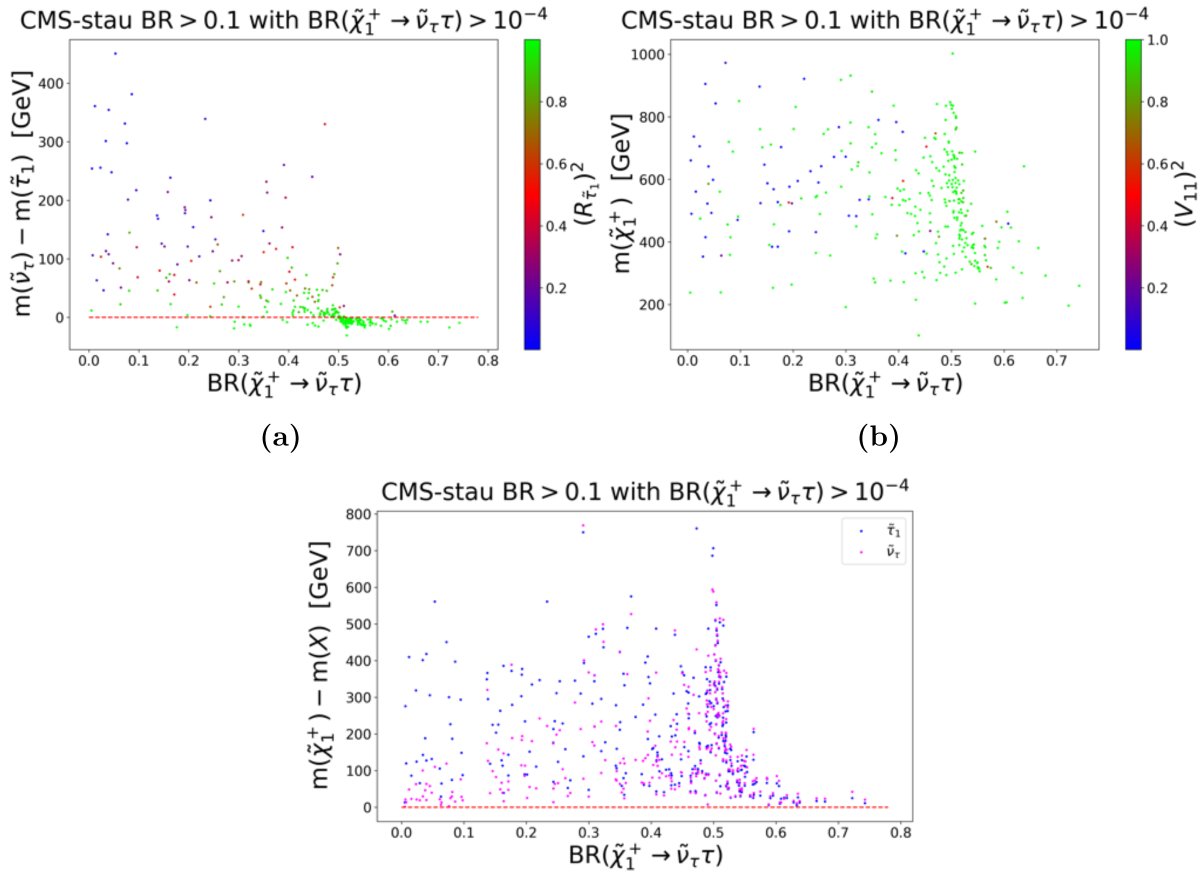

(c)

Figure 5.10: Entries: 314. Selection criteria: CMS-stau Simplified Model and BR($\tilde{\chi}_1^+ \to \tilde{\nu}_\tau\ \tau$) > 0 (a) Mass difference between $\tilde{\nu}_\tau$ and $\tilde{\tau}_1$ with relation to the branching ratio of $\tilde{\chi}_1^+ \to \tilde{\nu}_\tau\ \tau$. (b) Comparing the mass difference between $\tilde{\nu}_\tau$ and $\tilde{\chi}_1^+$ with $\tilde{\chi}_1^+$ and $\tilde{\tau}_1$. (c) Mass difference between $\tilde{\chi}_1^+$ and particle indicated by the colour with relation to the branching ratio of $\tilde{\chi}_1^+ \to \tilde{\nu}_\tau\ \tau$.

5.2 Competing Decay Modes

The CMS-stau simplified model has three decay steps: $\tilde{t}_1 \to \tilde{\chi}_1^+\ b$, $\tilde{\chi}_1^+ \to \tilde{\tau}_1\ \nu_\tau$ and $\tilde{\tau}_1 \to \tilde{\chi}_1^0\ \tau$.

The most common competing modes for the $\tilde{t}_1$ all consist of direct decays to a neutralino and a quark (see Fig. 5.11a). The flavour of the quark plays a large role in both how often the competing decay appears, but also how likely it is for the branching ratio to be large. The decay to $\tilde{\chi}_1^0\ b$ is far more likely to have a high branching ratio compared to the decay modes with heavier neutralinos and a t-quark. The decay mode to $\tilde{\chi}_2^+$, which is the heavier chargino, and a b-quark is not very common. This has to do with the particles' masses: $\tilde{\chi}_2^+$ is generally heavier than the $\tilde{t}_1$ (see Fig. 5.12), therefore this decay mode is suppressed.

One of the down-sides of having a neutralino as the LSP is that the stop will often directly decay to the neutralino. Although it is not necessary for either the CMS-stau or CMS-sneutrino model, the relation between the neutralino's mixture and the branching ratio of $\tilde{t}_1 \to \tilde{\chi}_1^0\ t$ is worth looking into. Fig. 5.13 shows that only model

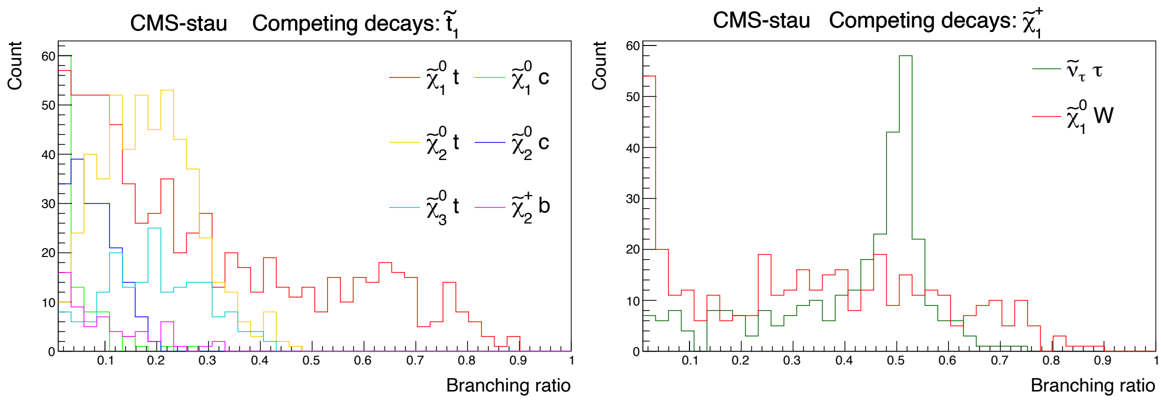

(a) (b)

Figure 5.11: (a) Competing decays for $\tilde{t}_1 \to \tilde{\chi}_1^+ \, b$. Selection criteria: mass hierarchy and simplified model with a combined branching ratio > 0.1. (b) Competing decays for $\tilde{\chi}_1^+ \to \tilde{\tau}_1 \, \nu_\tau$. Same selection criteria.

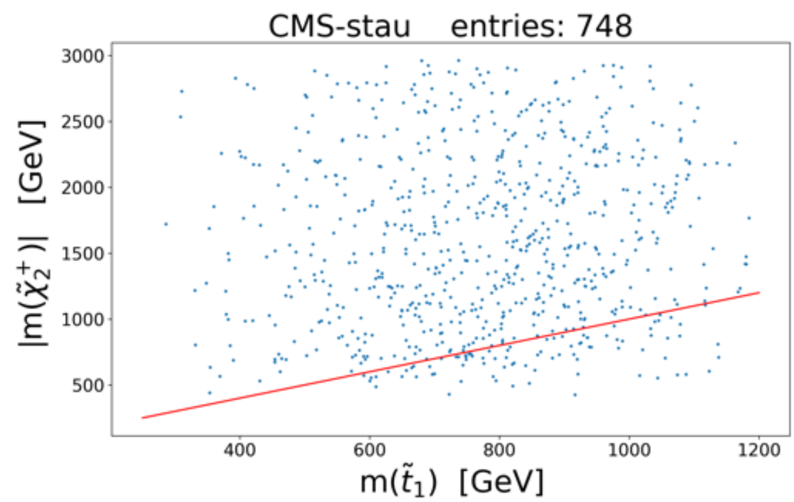

Figure 5.12: Comparison of the mass of the $\tilde{t}_1$ to the mass of the $\tilde{\chi}_2^+$. Selection criteria: CMS-stau Simplified Model. Red line indicates equal masses. The mass of the $\tilde{\chi}_2^+$ can have a negative phase, therefore the absolute value is taken.

points with bino-like neutralinos have large branching ratios. Yet, at the same same time, model points with small branching ratios are also mostly bino-like. Wino- and higgsino-like points tend to have a branching ratio of around 0.2–0.3. it is unclear why the branching ratio behaves so differently with bino-like neutralinos compared to wino- or higgsino-like neutralinos. Nevertheless, the CMS-stau model contains bino-like neutralinos, so it is important to find out what separates model points with small branching ratios for $\tilde{t}_1 \to \tilde{\chi}_1^0 \, t$ from model points with large ones.

Fig. 5.14 represents model points that contain the CMS-stau simplified model in which $\mathrm{BR}(\tilde{t}_1 \to \tilde{\chi}_1^0\,) > 10^{-4} t$. The colour of the histograms represents whether the branching ratio for $\tilde{t}_1 \to \tilde{\chi}_1^0 \, t$ is high or low. Clearly, model points with a left-like stop tend to have lower branching ratios for $\tilde{t}_1 \to \tilde{\chi}_1^0 \, t$ compared to right-like stop.This correlates with Fig. 5.1b, in which left-like stops are shown to be more likely to decay to a chargino and a b-quark with a high branching ratio. However, as discussed previously,

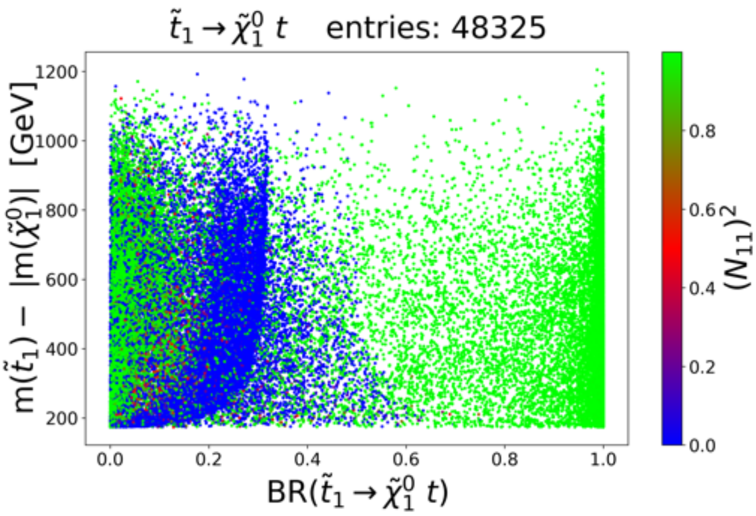

Figure 5.13: Branching ratio for $\tilde{t}_1 \to \tilde{\chi}_1^0\, t$ compared to the mass difference between the $\tilde{t}_1$ and the $\tilde{\chi}_1^0$. Selection criteria: $m(\tilde{t}) > (m(\tilde{\chi}_1^0)+m(t))$ and $\mathrm{BR}(\tilde{t}_1 \to \tilde{\chi}_1^0\, t) > 10^{-4}$.

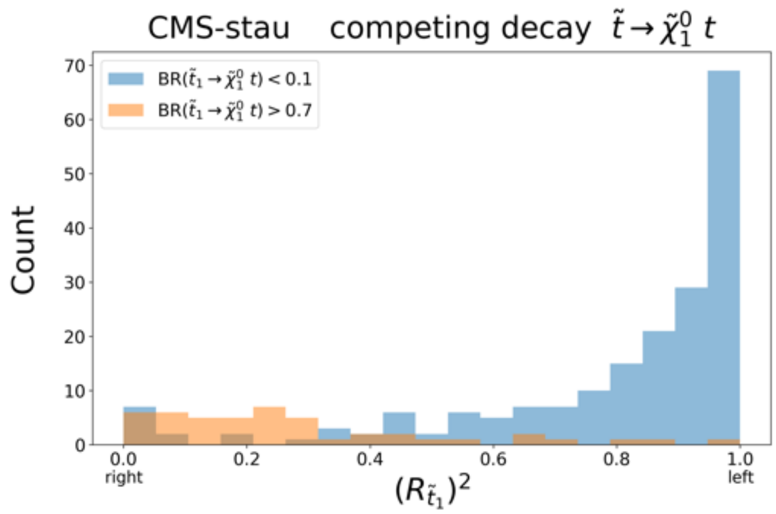

Figure 5.14: Relation between the stop mixture and the branching ratio for $\tilde{t}_1 \to \tilde{\chi}_1^0\, t$. Selection criteria: CMS-stau simplified model with $\mathrm{BR}(\tilde{t}_1 \to \tilde{\chi}_1^0\, t) > 10^{-4}$.

the mixture of the stop is also tied to the mixture of the chargino. Unfortunately, it is not clear whether the preference for right-like stops for the decay mode $\tilde{t}_1 \to \tilde{\chi}_1^0\, t$ is a result of the preference for left-like stops for $\tilde{t}_1 \to \tilde{\chi}_1^+\, b$, or if right-like stops somehow have a stronger connection to neutralinos than left-like stops.

There are only two competing decay modes for $\tilde{\chi}_1^+$ that stand out (see Fig. 5.11b). Both of these decays have already been discussed at the end of Sec. 5.1 whilst studying how the mixture of the chargino affects its decay modes.

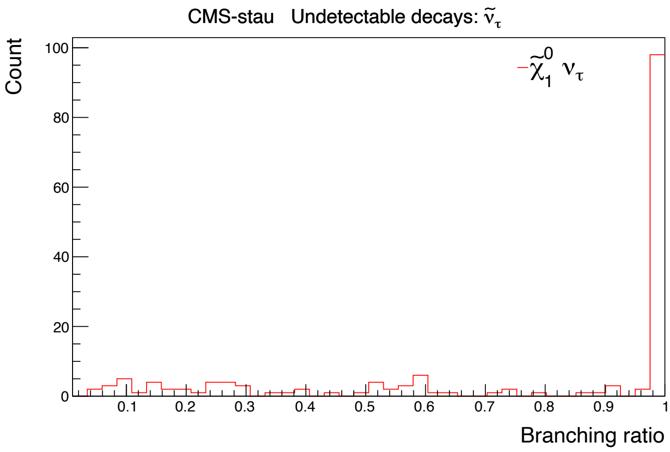

Figure 5.15: Decay modes for $\tilde{\nu}_\tau$ in model points that contain the CMS simplified model. Selection criteria: Simplified Model.

5.3 Influence on the Mass of the Higgs Boson

The parameters that influence the mass of the Higgs boson are independent of the simplified model. Therefore, $tan(\beta)$, A_t and μ still have the strongest influence over the Higgs boson's mass. The cross section between model points containing the CMS-stau simplified model and model points with $122 < \mathrm{m}(h) < 128$ GeV is small: only 63 of the 748 model points containing the simplified model come within $122 < \mathrm{m}(h) < 128$ GeV. The distributions of the parameters seem to take-on the same shapes as wit the ATLAS-stau model, however, this could be due to statistical fluctuations, since the statistics are very low.

5.4 Dark Matter Relic Density

It is not easy to make any significant claims for the CMS-stau simplified model. Most model points have dark matter relic densities much larger than the observed value of $\Omega_c h^2 \approx 0.12$. Only 564 model points are shown in Fig. 5.16b as a cut-off at $\Omega_c h^2 = 5$ has

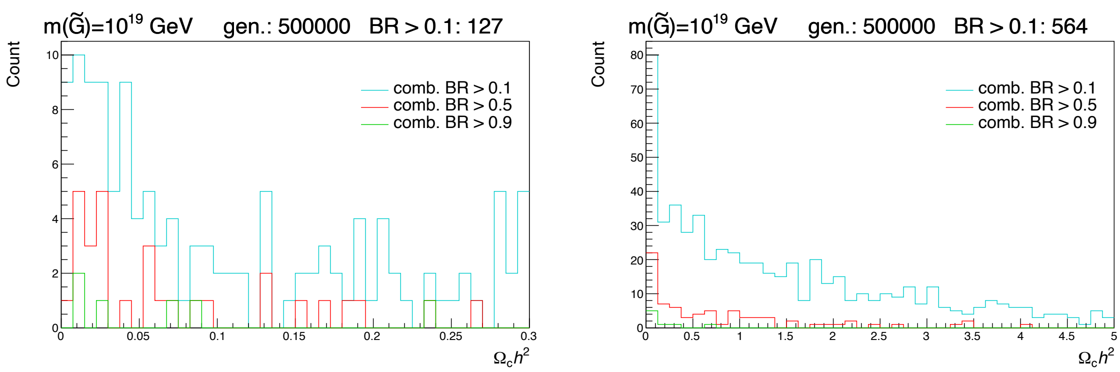

(a) (b)

Figure 5.16: Dark matter relic density for the CMS-stau model. Selection criteria: CMS-stau simplified model.

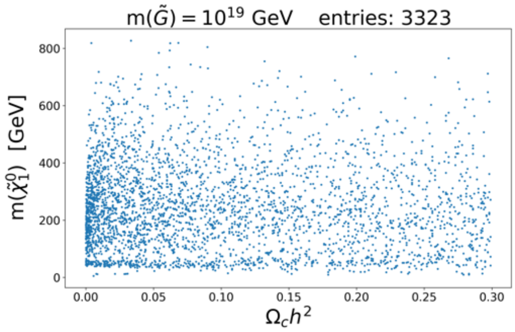

(a) Bino-like

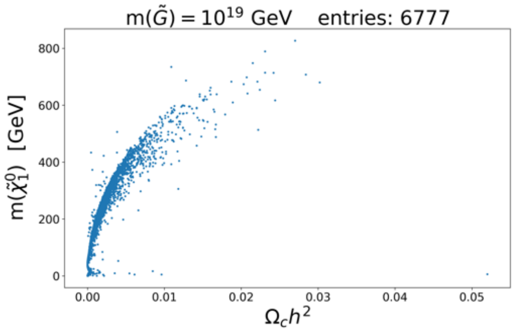

(b) Wino-like

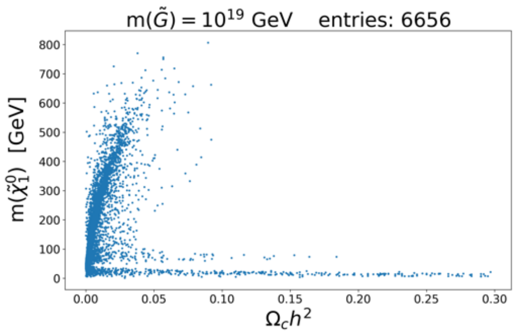

(c) Higgsino-like

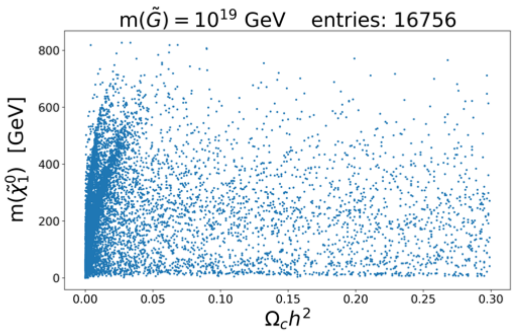

(d) Combined

Figure 5.17: Cold dark matter relic density depending on the mass and mixture of the $\tilde{\chi}_1^0$. Selection criteria: physical points with $\Omega_c h^2 < 0.3$.

been implemented to improve the readability. The model points have been inclusively split by the combined branching ratio of the simplified model to see if the branching ratio has any effect on the dark matter relic density. As only 127 models points, around a sixth of the model points that contain the CMS-stau simplified model, have a relic density lower than 0.3, the statistics are too low to be able to receive an insightful distribution.

A more distinguishable effect can be seen when looking at the different $\tilde{\chi}_1^0$ mixtures. As discussed in Sec. 5.1, the mass of the $\tilde{\chi}_1^0$ is strongly affected by its mixture. Therefore, by exclusively looking at single mixture types, a relation between the LSP mass and the dark matter relic density, alongside a relation between the mixture type and the relic density, can be established.

It was shown in Sec. 5.1 that with the current choice of phase space, only model points with bino-like $\tilde{\chi}_1^0$ pass the selection, because wino- and higgsino-like $\tilde{\chi}_1^0$ are almost always too heavy. This means that Fig. 5.17a represents the connection between the LSP mass and the dark matter relic density that applies to this analysis, which is very broad. The limits of the phase space could of course be extended, generating heavier particles which would allow for model points with heavier neutralinos to pass the selection. It could still be possible for the CMS-stau simplified model to exist with wino- or higgsino-like $\tilde{\chi}_1^0$ and it could have a very concise shape for the dark matter relic density, but that is outside of the scope of this work.

5.5 CMS-sneutrino

5.5.1 Phase Space

The CMS-sneutrino simplified model, in which the $\tilde{t}_1$ decay via $\tilde{\nu}_\tau$ instead of $\tilde{\tau}_1$, occupies a slightly different phase space. The search for this simplified model uses the same data as the CMS-stau simplified model, since the generation was performed over a broad phase space.
The two most significant differences between a $\tilde{\tau}_1$ and a $\tilde{\nu}_\tau$ are that the $\tilde{\nu}_\tau$ has no charge and that its mixture is strictly left-handed. The left-handedness strongly influences the phase space of m_{τ_L}. Model points with the CMS-sneutrino simplified model generally have small values for m_{τ_L} (see Fig. 5.18a), which coincides with previous examples of a particle's mixture generally being defined by the mixing parameter with the lowest value. m_{τ_R} occupies the same phase space as the CMS-stau simplified model. The mass of the $\tilde{\nu}_\tau$ is dependent of the mixture of the $\tilde{\tau}_1$, as shown with model points that contain the CMS-stau simplified model in Fig. 5.18c. In model points containing the CMS-sneutrino model, the $\tilde{\tau}_1$ generally has a left-like mixture, which causes the $\tilde{\nu}_\tau$ to be light.
Only 506 model points contain the CMS-sneutrino simplified model, which is about two thirds less than the CMS-stau simplified model. This can largely be explained by comparing Fig. 5.18a with Fig. 4.3a: because of the limitations to m_{τ_L}, only about two thirds of the phase space of the CMS-stau model is taken up by the CMS-sneutrino model.

5.5.2 Comparison between CMS-sneutrino and CMS-stau

To get a better idea of how each parameter affects the CMS-stau and the CMS-sneutrino simplified models differently, further comparisons are made by searching for the simplified models in model points in which both are kinematically possible. This means that the chargino has to be heavier than both the stau and the tau-sneutrino individually, which in return need to be heavier than the neutralino. It should be noted that this does not mean that both simplified models have to exist in each of these model points. it is possible, for example, that in one of these model points a chargino does not decay to a tau-sneutrino, when it does decay to a stau. As long as all decay modes from both simplified models are kinematically possible, the model point is accepted.

In Fig. 5.19, each graph represents model points in which both simplified models are kinematically possible, but only one of the models is searched for. Which model is search for is indicated by the colour. It is quite interesting to see that there are 485 model points containing the CMS-sneutrino simplified model compared to the 316 model points with the CMS-stau simplified model. Without the requirement that both simplified models are kinematically possible, there are 506 model points with CMS-sneutrino and 748 with CMS-stau. This means that almost all model points that contain the CMS-sneutrino simplified model also kinematically allow for the CMS-stau simplified model, whereas less than half of the model points with the CMS-stau simplified model kinematically allow the CMS-sneutrino model.

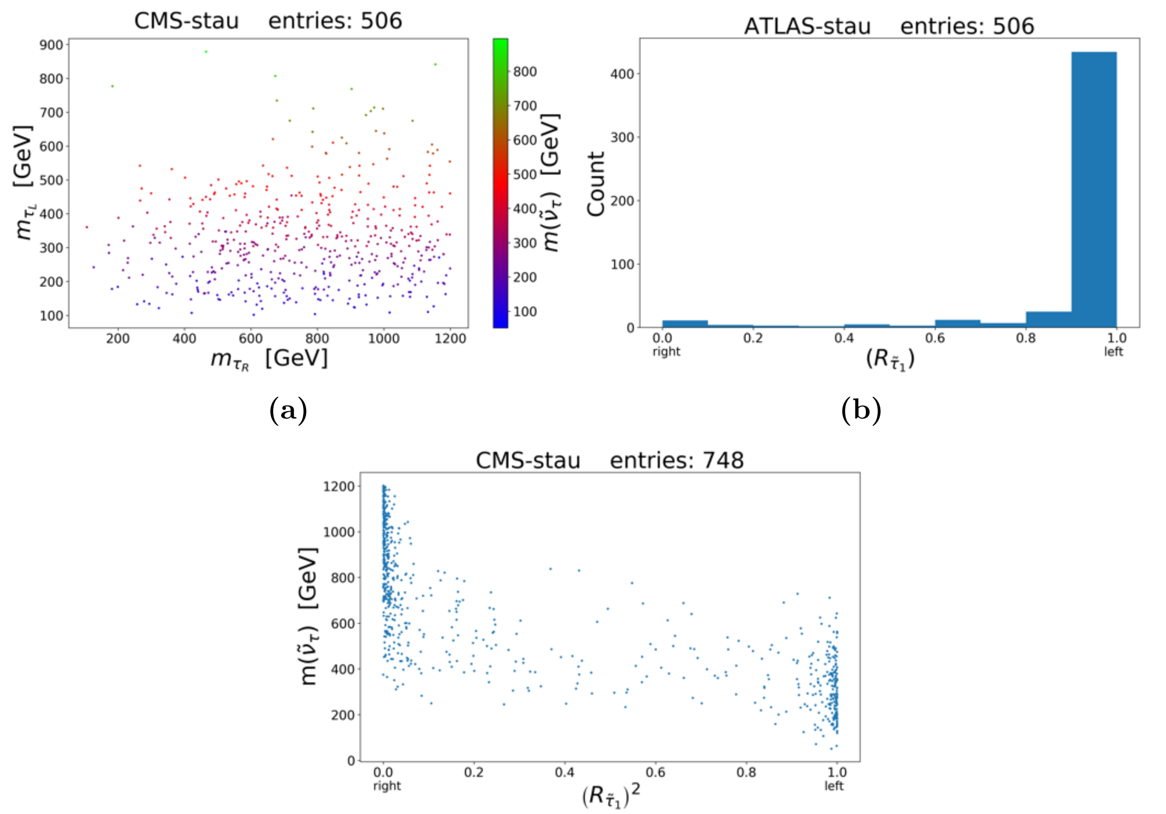

(c)

Figure 5.18: (a) Phase space of m_{τ_L} and m_{τ_R} with relation to the $\tilde{\nu}_\tau$ mass. (b) Distribution of the mixture of the $\tilde{\tau}_1$. (c) Visualisation of the relation between the mixture of the $\tilde{\tau}_1$ and the mass of the $\tilde{\nu}_\tau$ using model points containing the CMS-stau simplified model. Selection criteria: (a), (b) CMS-sneutrino simplified model, (c) CMS-stau simplified model.

The three parameters with the most noticeable differences are M_2, μ and m_{τ_L}. The shape of the distributions are very similar for certain sections of the phase space, implying that both simplified models are found in most model points in these sections. But, for smaller values of μ and m_{τ_L} and for larger values of M_2 there are many more model points containing the CMS-sneutrino model. Since the tau-sneutrino is left-handed, it is not too surprising to see that there are many model points with CMS-sneutrino with small values for m_{τ_L}. Small values for μ and large values for M_2 imply that the difference between the number of model points between the two simplified models could have something to do with the chargino, specifically higgsino-like charginos.

Fig. 5.20 shows the relation between the mixture of the chargino and the mixture of the stau. Fig. 5.20a and Fig. 5.20b depict model points that contain the CMS-stau simplified model, whereas in the latter, the model points also allow for the CMS-sneutrino simplified model kinematically. The first plot shows that the branching ratio of the chargino to the stau when the chargino is wino-like and the stau right-like is mostly > 0.9. Model points with higgsino-like charginos and right-like staus and points with wino-like charginos and left-like staus do not generally have very high branching ratios, but model points with higgsino-like charginos and left-like staus are suppressed,

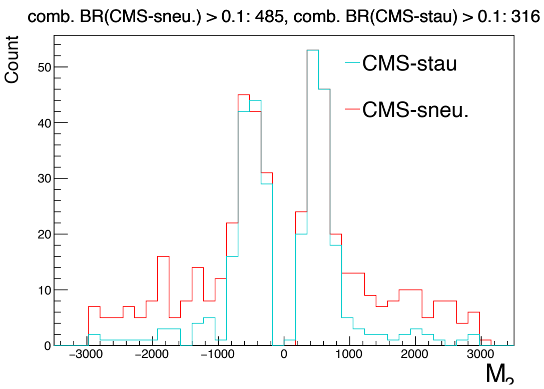

(a)

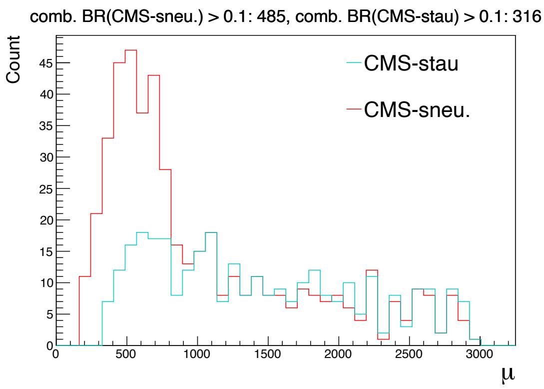

(b)

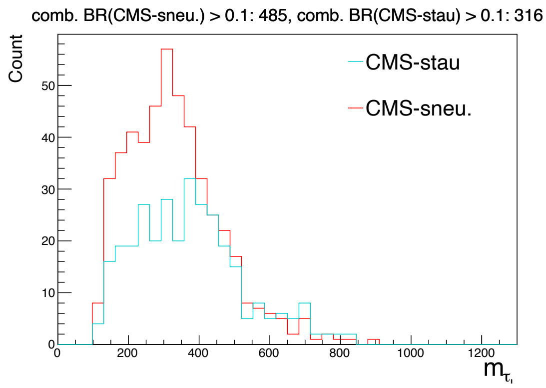

(c)

Figure 5.19: Selection criteria: Model points in which both CMS-stau and CMS-sneutrino are kinematically possible. Graphs represent model points in which the respective simplified models are found.

which was discussed with Fig. 5.9. Once the chargino is required to be heavier than the tau-sneutrino (and the tau-sneutrino to be heavier than the neutralino), most model points with a right-like stau are removed. The fact that the CMS-sneutrino model also exists when the chargino is higgsino-like and the stau is left-like (see Fig. 5.20d) explains why this simplified model is found in many more model points in which both models are kinematically possible.

The phase space for model points containing the CMS-sneutrino simplified model with $122 < \mathrm{m}(h) < 128$ GeV is the same as the CMS-stau model, which is in return the same as the ATLAS-stau model. It could be expected that there would be a difference in the the phase space for μ, but the statistics are even lower for the CMS-sneutrino model, thus a comparison can not be made. The CMS-sneutrino model has the same problems as the CMS-stau model when it comes to the dark matter relic density.

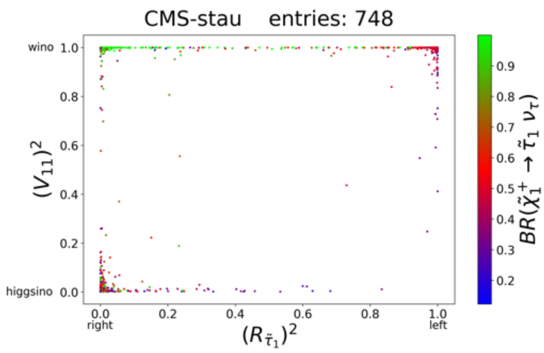

(a)

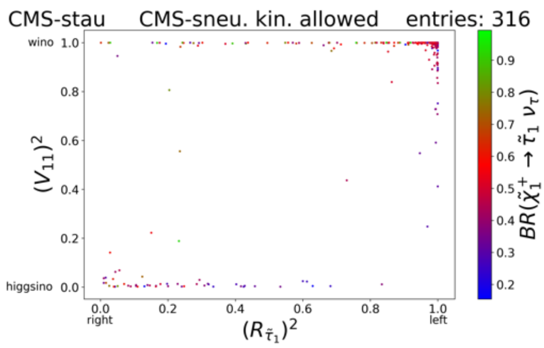

(b)

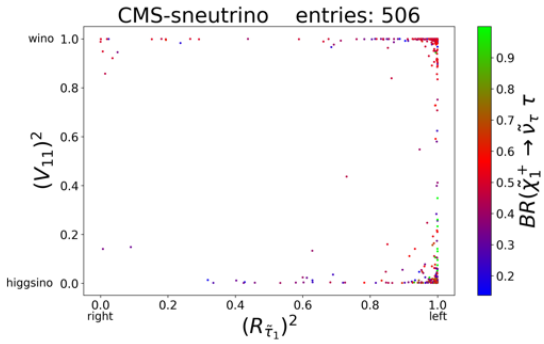

(c)

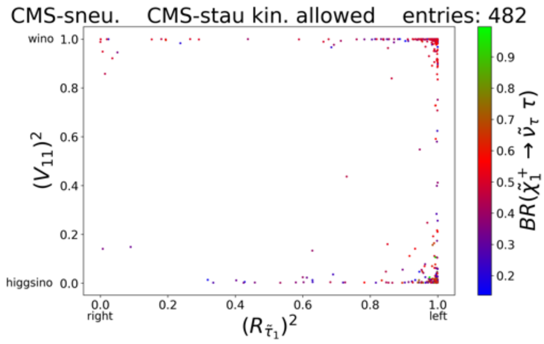

(d)

Figure 5.20: V_{11} is the $\tilde{\chi}_1^+$, $R_{\tilde{\tau}_1}$ is the $\tilde{\tau}_1$ mixture. Selection criteria: (a) CMS-stau simplified model, (b) CMS-stau simplified model, but CMS-sneutrino is kinematically possible, (c) CMS-sneutrino simplified model (d) CMS-sneutrino simplified model, but CMS-stau is kinematically possible.

Chapter 6

Conclusion

This work has compared three simplified models in the context of the pMSSM, with the goal of achieving a better understanding of how the parameters of the pMSSM influence the particle spectrum. This was done by scanning over all 19 parameters, allowing for the generation of model points, where each point represents a configuration of particle masses and decay modes.

Apart from having problems with the Higgs boson's mass, the ATLAS-stau model has shown to have a large phase space without many constraints on the sparticles' masses or mixtures. Having only two decay steps, where the second step has a branching ratio of nearly exclusively 1, results in 10626 of the 81132 physical model points with light gravitinos containing the simplified model. Optimising the pMSSM's phase space to increase the likelihood for a model point to contain this simplified model mostly relies on limiting five parameters: A_t, m_{t_R}, $m_{Q_{L3}}$, m_{τ_L} and m_{τ_R}. Limiting $|A_t| \leq 2000$ would greatly increase the number of physical model points, and would also increase the number of model points containing the simplified model. m_{t_R}, $m_{Q_{L3}}$, m_{τ_L} have all been limited to 1200 GeV, to generate $\tilde{t}_1$ with masses that are within the limits of the ATLAS detector. The simplified model does not show a clear preference for the mixture of the $\tilde{t}_1$, but it does prefer right-like $\tilde{\tau}_1$. The main competing decay modes are $\tilde{\tau}_1 \to \tilde{G}\, \tau$ and $\tilde{\tau}_1 \to \tilde{\nu}_{\tau_1}\, \tau\, b$, the first being difficult to suppress. While model points containing the simplified model are generally within the bounds of the dark matter relic density, very few model points contain Higgs bosons with $122 < \mathrm{m}(h) < 128$ GeV. Due to the large phase space and few constraints, the ATLAS-stau simplified model has proven to be a much more promising model for a search with real experimental data.

The CMS-stau model has the disadvantage that it has three decay steps, which makes the mass hierarchy much more restrictive. Implementing mass hierarchy by itself reduces the 83594 physical model points down to 2737. Only 748 of those model points contain the CMS-stau simplified model. However, the phase space used for the generation of the model points was not optimised for the mass of the $\tilde{\chi}_1^+$, meaning that the $\tilde{\chi}_1^+$ is heavier than the $\tilde{t}_1$ in many model points, greatly reducing the number of model points that can contain the simplified model. The simplified model is strongly influenced by the mixtures of the $\tilde{t}_1$, $\tilde{\chi}_1^+$ and $\tilde{\chi}_1^0$. Left-like $\tilde{t}_1$ and wino-like $\tilde{\chi}_1^+$ are strongly preferred for the first decay step $\tilde{t}_1 \to \tilde{\chi}_1^+\, b$ to have a high branching ratio.

For $\tilde{\chi}_1^+ \to \tilde{\tau}_1\, \nu_\tau$, right-like $\tilde{\tau}_1$ are preferred along with the wino-like $\tilde{\chi}_1^+$. The $\tilde{\chi}_1^0$ is almost exclusively bino-like, which has to do with how the mixture and mass of the $\tilde{\chi}_1^0$ are influenced by one another. The strongest competing decay for the CMS-stau simplified model is $\tilde{t}_1 \to \tilde{\chi}_1^0\, t$, which can be partially suppressed by the mixture of the $\tilde{\tau}_1$. The phase space for model points that contain a HIggs boson with $122 < \mathrm{m}(h) < 128$ GeV is the same as for the ATLAS-stau model. Model points that contain the CMS-stau simplified model tend to have dark matter relic densities that are much larger than the observed value.

The CMS-sneutrino model shares most of the same phase space as the CMS-stau model. Three parameters, M_2, μ and m_{τ_L}, have many more model points in certain regions of their phase spaces, but otherwise there isn't much difference in terms of the complete phase space. Since the mass of the $\tilde{\nu}_\tau$ is strongly dependent on the mixture of the $\tilde{t}_1$, the phase space of m_{τ_L} is reduced. Model points that contain the CMS-sneutrino model are more likely to kinematically allow for the CMS-stau model than vice-versa. Model points with Higgs bosons masses within $122 < \mathrm{m}(h) < 128$ GeV share the same phase space as those with the CMS-stau model and the dark matter relic density has the same problems. The phase spaces of the CMS-stau and CMS-sneutrino models are much more limited compared to the ATLAS-stau and combined with the fact that model points containing either simplified model struggle to stay within the bounds of the dark matter relic density suggests that these two simplified models are less optimal for a search with real experimental data.

Bibliography

[1] ATLAS Collaboration. "Observation of a new particle in the search for the Standard Model Higgs boson with the ATLAS detector at the LHC". *Physics Letters B*, 716(1):129, Sep 2012. ISSN 0370-2693. doi: 10.1016/j.physletb.2012.08.020. URL http://dx.doi.org/10.1016/j.physletb.2012.08.020. Discovery of the Higgs boson.

[2] D. J. Griffiths. *"Introduction to elementary particles; 2nd rev. version"*. Physics textbook. Wiley, New York, NY, 2008. URL https://cds.cern.ch/record/111880.

[3] Michael E Peskin and Daniel V Schroeder. *"An introduction to quantum field theory"*. Westview, Boulder, CO, 1995. URL https://cds.cern.ch/record/257493.

[4] S.M. Bilenky and J. Hoek. "Glashow-Weinberg-Salam theory of electroweak interactions and the neutral currents". *Physics Reports*, 90(2):73 – 157, 1982. ISSN 0370-1573. doi: https://doi.org/10.1016/0370-1573(82)90016-3. URL http://www.sciencedirect.com/science/article/pii/0370157382900163.

[5] C. N. Yang and R. L. Mills. "Conservation of Isotopic Spin and Isotopic Gauge Invariance". *Phys. Rev.*, 96:191–195, Oct 1954. doi: 10.1103/PhysRev.96.191. URL https://link.aps.org/doi/10.1103/PhysRev.96.191.

[6] P. Bagnaia et al. "Evidence for $Z^0 \to e^+e$ at the CERN *pp* collider". *Physics Letters B*, 129(1):130 – 140, 1983. ISSN 0370-2693. doi: https://doi.org/10.1016/0370-2693(83)90744-X. URL http://www.sciencedirect.com/science/article/pii/037026938390744X.

[7] G. Arnison et al. "Experimental observation of isolated large transverse energy electrons with associated missing energy at s=540 GeV". *Physics Letters B*, 122(1):103 – 116, 1983. ISSN 0370-2693. doi: https://doi.org/10.1016/0370-2693(83)91177-2. URL http://www.sciencedirect.com/science/article/pii/0370269383911772.

[8] P.A. Zyla et al. (Particle Data Group). "Review of Particle Physics". *Progress of Theoretical and Experimental Physics*, 2020(8), 08 2020. ISSN 2050-3911. doi: 10.1093/ptep/ptaa104. URL https://doi.org/10.1093/ptep/ptaa104. 083C01.

[9] D. Schaile. Lecture Notes on "Advanced Particle Physics", Summer Term 2019.

[10] Y. et al Fukuda. “Evidence for Oscillation of Atmospheric Neutrinos”. *Physical Review Letters*, 81(8):15621567, Aug 1998. ISSN 1079-7114. doi: 10.1103/physrevlett.81.1562. URL http://dx.doi.org/10.1103/PhysRevLett.81.1562.

[11] S. P. Martin. “A Supersymmetry Primer”. *Advanced Series on Directions in High Energy Physics*, page 198, Jul 1998. ISSN 1793-1339. doi: 10.1142/9789812839657_0001. URL http://dx.doi.org/10.1142/9789812839657_0001.

[12] N. et al Aghanim. “Planck 2018 results”. *Astronomy and Astrophysics*, 641: A6, Sep 2020. ISSN 1432-0746. doi: 10.1051/0004-6361/201833910. URL http://dx.doi.org/10.1051/0004-6361/201833910.

[13] A. et al Djouadi. “The Minimal supersymmetric standard model: Group summary report”. In *GDR (Groupement De Recherche) - Supersymetrie*, 12 1998.

[14] Daniele et al Alves. “Simplified models for LHC new physics searches”. *Journal of Physics G: Nuclear and Particle Physics*, 39(10):105005, Sep 2012. ISSN 1361-6471. doi: 10.1088/0954-3899/39/10/105005. URL http://dx.doi.org/10.1088/0954-3899/39/10/105005.

[15] ATLAS Collaboration. “Search for top squarks decaying to tau sleptons in pp collisions at $\sqrt{s} = 13$ TeV with the ATLAS detector”. *Phys. Rev. D*, 98:032008, Aug 2018. doi: 10.1103/PhysRevD.98.032008. URL https://link.aps.org/doi/10.1103/PhysRevD.98.032008.

[16] CMS Collaboration. “Search for top squark pair production in a final state with two tau leptons in proton-proton collisions at s

$$\sqrt{s}$$

= 13 TeV”. *Journal of High Energy Physics*, 2020(2):15, 2020. ISSN 1029-8479. URL https://doi.org/10.1007/JHEP02(2020)015.

[17] CERN. “Facts and figures about the LHC”. URL https://home.cern/resources/faqs/facts-and-figures-about-lhc. Visited on 21/10/2020.

[18] ATLAS Collaboration. “The ATLAS Experiment at the CERN Large Hadron Collider”. *JINST*, 3:S08003. 437 p, 2008. doi: 10.1088/1748-0221/3/08/S08003. URL http://cds.cern.ch/record/1129811. Also published by CERN Geneva in 2010.

[19] CMS Collaboration. “Highlights from the Compact Muon Solenoid (CMS) Experiment”. *Universe*, 5:28, 01 2019. doi: 10.3390/universe5010028.

[20] CMS Collaboration. “Validation of the CMS Magnetic Field Map”. *Journal of Superconductivity and Novel Magnetism*, 28(2):701–704, 2015. ISSN 1557-1947. URL https://doi.org/10.1007/s10948-014-2809-4.

[21] Junjie Cao et al. “EasyScan HEP”. URL https://easyscanhep.hepforge.org. Visited on 22/10/2020.

[22] B.C. Allanach. "SOFTSUSY: A program for calculating supersymmetric spectra". *Computer Physics Communications*, 143(3):305331, Mar 2002. ISSN 0010-4655. doi: 10.1016/s0010-4655(01)00460-x. URL http://dx.doi.org/10.1016/S0010-4655(01)00460-X.

[23] W. Porod and F. Staub. "SPheno 3.1: extensions including flavour, CP-phases and models beyond the MSSM". *Computer Physics Communications*, 183(11):24582469, Nov 2012. ISSN 0010-4655. doi: 10.1016/j.cpc.2012.05.021. URL http://dx.doi.org/10.1016/j.cpc.2012.05.021.

[24] W. Porod. "SPheno, a program for calculating supersymmetric spectra, SUSY particle decays and SUSY particle production at e^+e^- colliders". *Computer Physics Communications*, 153:275–315, 2003. doi: 10.1016/S0010-4655(03)00222-4.

[25] Henning Bahl, Thomas Hahn, Sven Heinemeyer, Wolfgang Hollik, Sebastian Paehr, Heidi Rzehak, and Georg Weiglein. "Precision calculations in the MSSM Higgs-boson sector with FeynHiggs 2.14“", 2019.

[26] Henning Bahl, Sven Heinemeyer, Wolfgang Hollik, and Georg Weiglein. "Reconciling EFT and hybrid calculations of the light MSSM Higgs-boson mass. *The European Physical Journal C*, 78(1), Jan 2018. ISSN 1434-6052. doi: 10.1140/epjc/s10052-018-5544-3. URL http://dx.doi.org/10.1140/epjc/s10052-018-5544-3.

[27] Henning Bahl and Wolfgang Hollik. "Precise prediction for the light MSSM Higgs-boson mass combining effective field theory and fixed-order calculations. *The European Physical Journal C*, 76(9), Sep 2016. ISSN 1434-6052. doi: 10.1140/epjc/s10052-016-4354-8. URL http://dx.doi.org/10.1140/epjc/s10052-016-4354-8.

[28] T. Hahn, S. Heinemeyer, W. Hollik, H. Rzehak, and G. Weiglein. "High-Precision Predictions for the LightCP-Even Higgs Boson Mass of the Minimal Supersymmetric Standard Model". *Physical Review Letters*, 112(14), Apr 2014. ISSN 1079-7114. doi: 10.1103/physrevlett.112.141801. URL http://dx.doi.org/10.1103/PhysRevLett.112.141801.

[29] Meikel Frank, Thomas Hahn, Sven Heinemeyer, Wolfgang Hollik, Heidi Rzehak, and Georg Weiglein. "The Higgs boson masses and mixings of the complex MSSM in the Feynman-diagrammatic approach". *Journal of High Energy Physics*, 2007 (02):047047, Feb 2007. ISSN 1029-8479. doi: 10.1088/1126-6708/2007/02/047. URL http://dx.doi.org/10.1088/1126-6708/2007/02/047.

[30] G. Degrassi, S. Heinemeyer, W. Hollik, P. Slavich, and G. Weiglein. "Towards high-precision predictions for the MSSM Higgs sector". *The European Physical Journal C*, 28(1):133143, May 2003. ISSN 1434-6052. doi: 10.1140/epjc/s2003-01152-2. URL http://dx.doi.org/10.1140/epjc/s2003-01152-2.

[31] S. Heinemeyer, W. Hollik, and G. Weiglein. "The masses of the neutral $\mathcal{CP}$ -even Higgs bosons in the MSSM: Accurate analysis at the two-loop level". *The European Physical Journal C*, 9(2):343366, Jun 1999. ISSN 1434-6052. doi: 10.1007/s100529900006. URL http://dx.doi.org/10.1007/s100529900006.

[32] S. Heinemeyer, W. Hollik, and G. Weiglein. "FeynHiggs: a program for the calculation of the masses of the neutral -even Higgs bosons in the MSSM". *Computer Physics Communications*, 124(1):7689, Jan 2000. ISSN 0010-4655. doi: 10.1016/s0010-4655(99)00364-1. URL http://dx.doi.org/10.1016/S0010-4655(99)00364-1.

[33] G. Blanger, F. Boudjema, A. Pukhov, and A. Semenov. "micrOMEGAs: Version 1.3". *Computer Physics Communications*, 174(7):577604, Apr 2006. ISSN 0010-4655. doi: 10.1016/j.cpc.2005.12.005. URL http://dx.doi.org/10.1016/j.cpc.2005.12.005.

[34] P et al Skands. "SUSY Les Houches Accord: Interfacing SUSY Spectrum Calculators, Decay Packages, and Event Generators". *Journal of High Energy Physics*, 2004(07):036036, Jul 2004. ISSN 1029-8479. doi: 10.1088/1126-6708/2004/07/036. URL http://dx.doi.org/10.1088/1126-6708/2004/07/036.

[35] Andy Buckley. "PySLHA: a Pythonic interface to SUSY Les Houches Accord data". *The European Physical Journal C*, 75(10), oct 2015. doi: https://doi.org/10.1140/epjc/s10052-015-3638-8.

[36] Fons Rademakers. "root-project/root: v6.20/04", April 2020. URL https://doi.org/10.5281/zenodo.3895855.

[37] Jim Pivarski et al. "scikit-hep/uproot: 3.11.3", feb 2020. URL https://doi.org/10.5281/zenodo.3662720.

[38] J. D. Hunter. "Matplotlib: A 2D graphics environment". *Computing in Science & Engineering*, 9(3):90–95, 2007. doi: 10.1109/MCSE.2007.55.

[39] Michael Waskom and the seaborn development team. "mwaskom/seaborn", September 2020. URL https://doi.org/10.5281/zenodo.592845.

Appendix A

A.1 Configuration for EasyScan_HEP

Configuration for `EasyScan_HEP` for generating model points with a light gravitino. This includes the configurations for `SoftSusy` and `SPheno`:

```
BLOCK MODSEL  # Model selection
     1     0   #  nonUniversal
#
BLOCK SMINPUTS  # Standard Model inputs
         1     1.27908970E+02   # alpha_em^-1(M_Z)^MSbar
         2     1.16637870E-05   # G_F [GeV^-2]
         3     1.18400000E-01   # alpha_S(M_Z)^MSbar
         4     9.11876000E+01   # M_Z pole mass
         5     4.18000000E+00   # mb(mb)^MSbar
         6     1.73200000E+02   # mt pole mass
         7     1.77700000E+00   # mtau pole mass
#
BLOCK MINPAR  # Input parameters - minimal models
#
BLOCK EXTPAR  # Input parameters - non-minimal models
         0    -1.00000000E+00   # Set
         1     ES_M_1 # M_1(MX)
         2     ES_M_2 # M_2(MX)
         3     ES_M_3 # M_3(MX)
        11     ES_AT # At(MX)
        12     ES_Ab # Ab(MX)
        13     ES_Atau # Atau(MX)
        23     ES_MU # mu(MX)
        25     ES_tanb # tanb(MX)
        26     ES_mA # mA(pole)
        31     ES_meL # meL(MX)
        32     ES_meL # mmuL(MX)
        33     ES_mtauL # mtauL(MX)
        34     ES_meR # meR(MX)
        35     ES_meR # mmuR(MX)
        36     ES_mtauR # mtauR(MX)
        41     ES_mqL1 # mqL1(MX)
        42     ES_mqL1 # mqL2(MX)
        43     ES_mqL3 # mqL3(MX)
```

```
        44     ES_muR # muR(MX)
        45     ES_muR # mcR(MX)
        46     ES_mtR # mtR(MX)
        47     ES_mdR # mdR(MX)
        48     ES_mdR # msR(MX)
        49     ES_mbR # mbR(MX)
1000039     1.00000000E-09 # gravitino
#
Block SOFTSUSY               # Optional SOFTSUSY-specific parameters
    0   1.000000000e+00      # Calculate decays in output (only for RPC (N)MSSM)
# The default is that without this, SOFTSUSY will only calculate the spectrum
    1   1.000000000e-03      # Numerical precision: suggested range 10^(-3...-6)
    2   0.000000000e+00      # Quark mixing parameter: see manual
    3   0.000000000e+00      # Additional verbose output?
    4   1.000000000e+00      # Change electroweak symmetry breaking scale?
    5   1.000000000e+00      # Include 2-loop scalar mass squared/trilinear RGEs
    6   1.000000000e-04      # Numerical precision
    7   3.000000000e+00      # Number of loops in Higgs mass computation
   10   0.000000000e+00      # Force it to SLHA***1*** output?
   11   1.000000000e-09      # Gravitino mass
   12   0.000000000e+00      # Print spectrum even when point disallowed
   13   0.000000000e+00      # Set a tachyonic A^0 to zero mass
#   19   1.000000000e+00      # Include 3-loop SUSY RGEs
#   20   3.100000000e+01      # Include 2-loop g/Yuk corrections: 31 for all
#   22   1.000000000e+00      # Include 2-loop sparticle mass thresholds
#   23   0.000000000e+00      # No expansion of 2-loop gluino terms
   24   1.000000000e-06      # If decay BR is below this number, don't output (default: 1.0e
   25   1.000000000e+00      # If set to 0, don't calculate 3-body decays (1=default)
#
Block SPhenoInput       # SPheno specific input
 1  -1                  # error level
 2   0                  # SPA conventions
11   1                  # calculate branching ratios
12   1.00000000E-04     # write only branching ratios larger than this value
21   0                  # calculate cross section
```

Configuration for EasyScan_HEP for generating model points with a heavy gravitino:

```
BLOCK MODSEL  # Model selection
     1     0   #  nonUniversal
#
BLOCK SMINPUTS  # Standard Model inputs
         1     1.27908970E+02   # alpha_em^-1(M_Z)^MSbar
         2     1.16637870E-05   # G_F [GeV^-2]
         3     1.18400000E-01   # alpha_S(M_Z)^MSbar
         4     9.11876000E+01   # M_Z pole mass
         5     4.18000000E+00   # mb(mb)^MSbar
         6     1.73200000E+02   # mt pole mass
         7     1.77700000E+00   # mtau pole mass
```

```
#
BLOCK MINPAR  # Input parameters - minimal models
#
BLOCK EXTPAR  # Input parameters - non-minimal models
         0    -1.00000000E+00   # Set
         1     ES_M_1 # M_1(MX)
         2     ES_M_2 # M_2(MX)
         3     ES_M_3 # M_3(MX)
        11     ES_AT # At(MX)
        12     ES_Ab # Ab(MX)
        13     ES_Atau # Atau(MX)
        23     ES_MU # mu(MX)
      25     ES_tanb # tanb(MX)
        26     ES_mA # mA(pole)
        31     ES_meL # meL(MX)
        32     ES_meL # mmuL(MX)
        33     ES_mtauL # mtauL(MX)
        34     ES_meR # meR(MX)
        35     ES_meR # mmuR(MX)
        36     ES_mtauR # mtauR(MX)
        41     ES_mqL1 # mqL1(MX)
        42     ES_mqL1 # mqL2(MX)
        43     ES_mqL3 # mqL3(MX)
        44     ES_muR # muR(MX)
        45     ES_muR # mcR(MX)
        46     ES_mtR # mtR(MX)
        47     ES_mdR # mdR(MX)
        48     ES_mdR # msR(MX)
        49     ES_mbR # mbR(MX)
   1000039    1.00000000E+19 # gravitino
#
Block SOFTSUSY               # Optional SOFTSUSY-specific parameters
    0   1.000000000e+00      # Calculate decays in output (only for RPC (N)MSSM)
# The default is that without this, SOFTSUSY will only calculate the spectrum
    1   1.000000000e-03      # Numerical precision: suggested range 10^(-3...-6)
    2   0.000000000e+00      # Quark mixing parameter: see manual
    3   0.000000000e+00      # Additional verbose output?
    4   1.000000000e+00      # Change electroweak symmetry breaking scale?
    5   1.000000000e+00      # Include 2-loop scalar mass squared/trilinear RGEs
    6   1.000000000e-04      # Numerical precision
    7   3.000000000e+00      # Number of loops in Higgs mass computation
   10   0.000000000e+00      # Force it to SLHA***1*** output?
   11   1.000000000e+19      # Gravitino mass
   12   0.000000000e+00      # Print spectrum even when point disallowed
   13   0.000000000e+00      # Set a tachyonic A^0 to zero mass
#   19   1.000000000e+00      # Include 3-loop SUSY RGEs
#   20   3.100000000e+01      # Include 2-loop g/Yuk corrections: 31 for all
#   22   1.000000000e+00      # Include 2-loop sparticle mass thresholds
#   23   0.000000000e+00      # No expansion of 2-loop gluino terms
   24   1.000000000e-06      # If decay BR is below this number, don't output (default: 1
   25   1.000000000e+00      # If set to 0, don't calculate 3-body decays (1=default)
```

```
#
Block SPhenoInput        # SPheno specific input
 1  -1                   # error level
 2   0                   # SPA conventions
11   1                   # calculate branching ratios
12   1.00000000E-04      # write only branching ratios larger than this value
21   0                   # calculate cross section
```

A.2 Phase space of Physical Model Points

In the following plots, the left plots are for $\mathrm{m}(\tilde{G}) = 10^{-9}$ GeV and (the right plots are for $\mathrm{m}(\tilde{G}) = 10^{19}$ GeV.

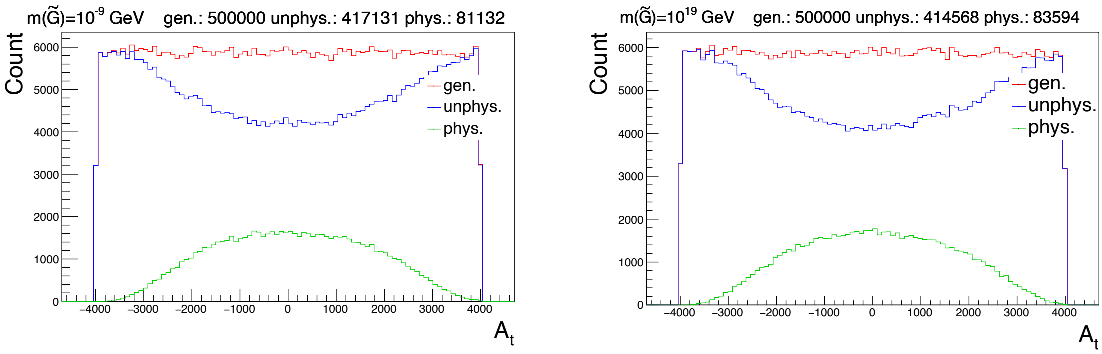

Figure A.1

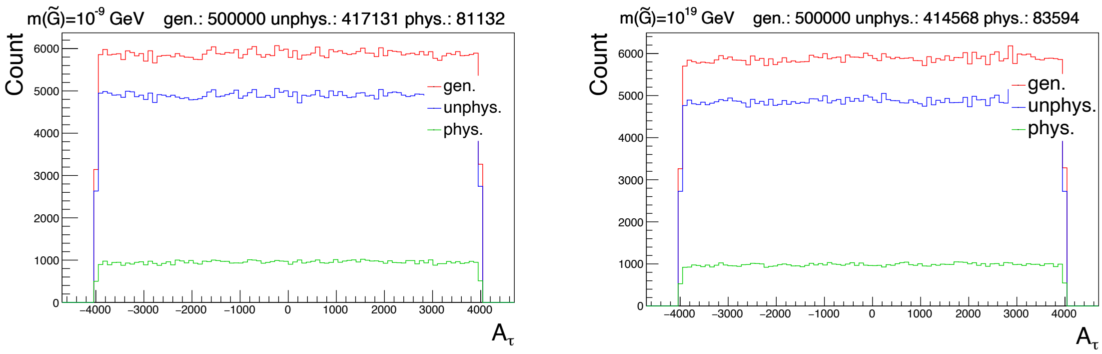

Figure A.2

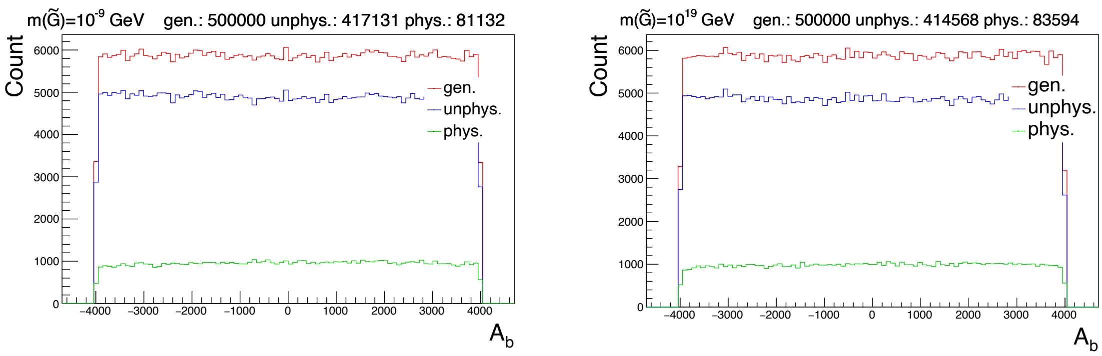

Figure A.3

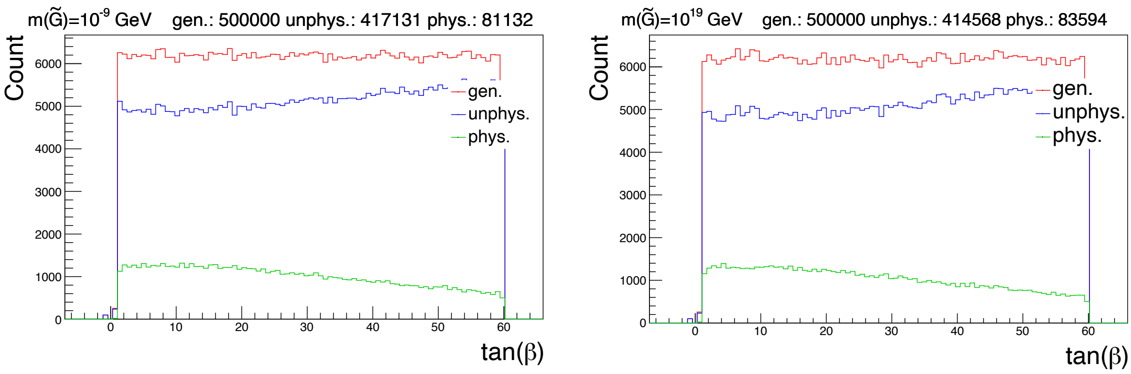

Figure A.4

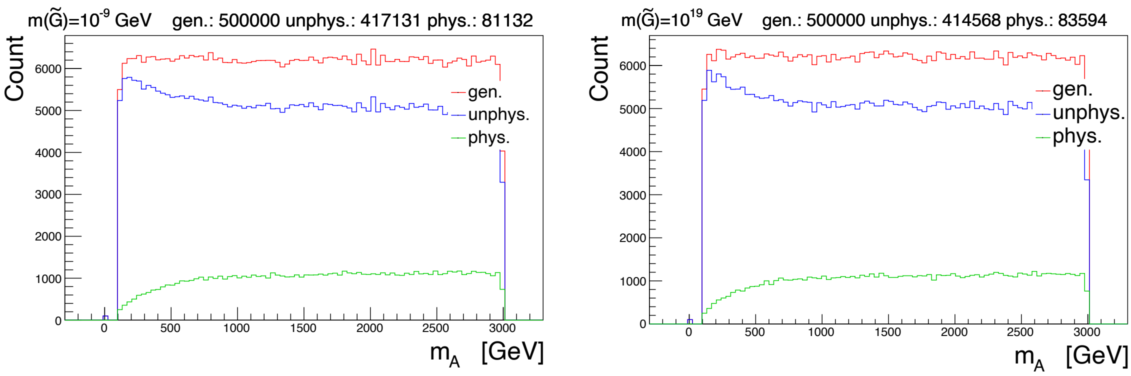

Figure A.5

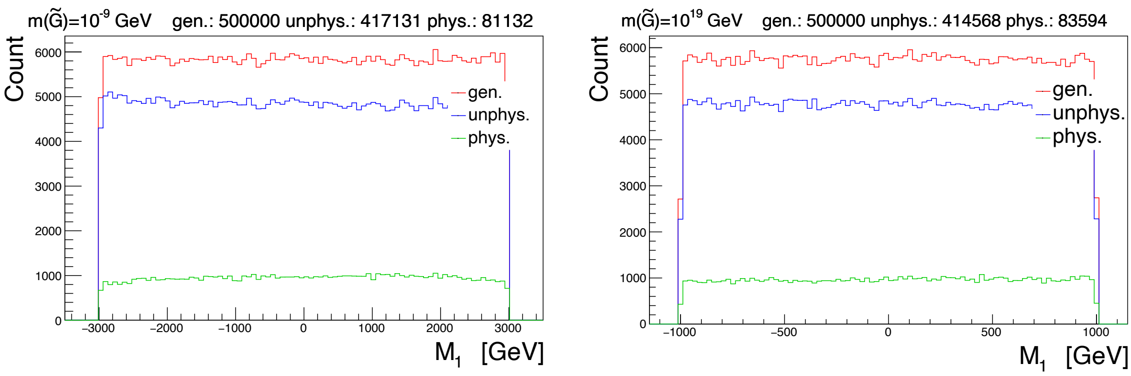

Figure A.6

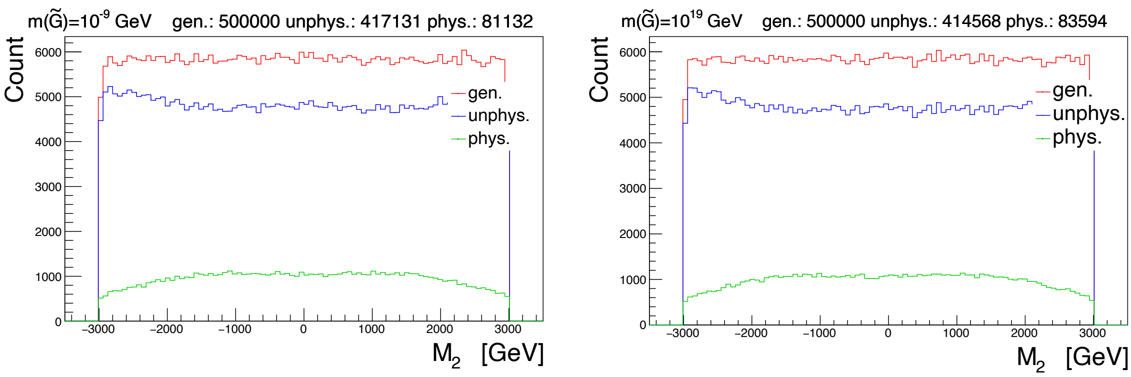

Figure A.7

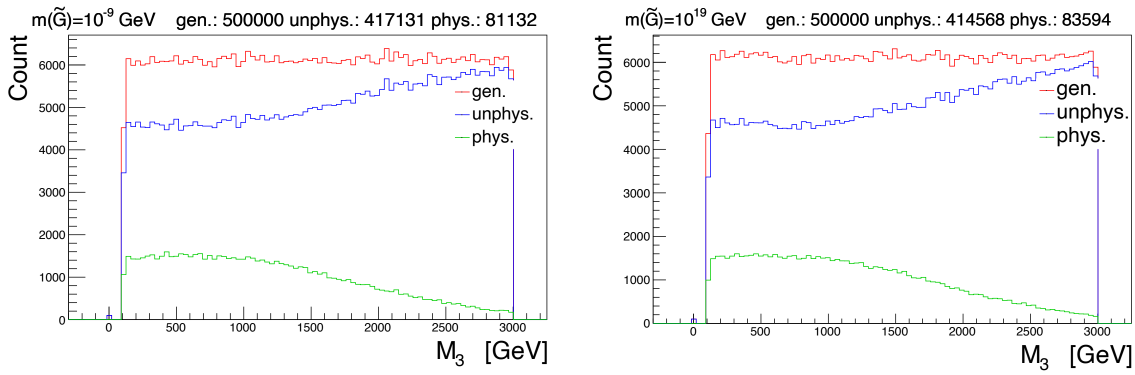

Figure A.8

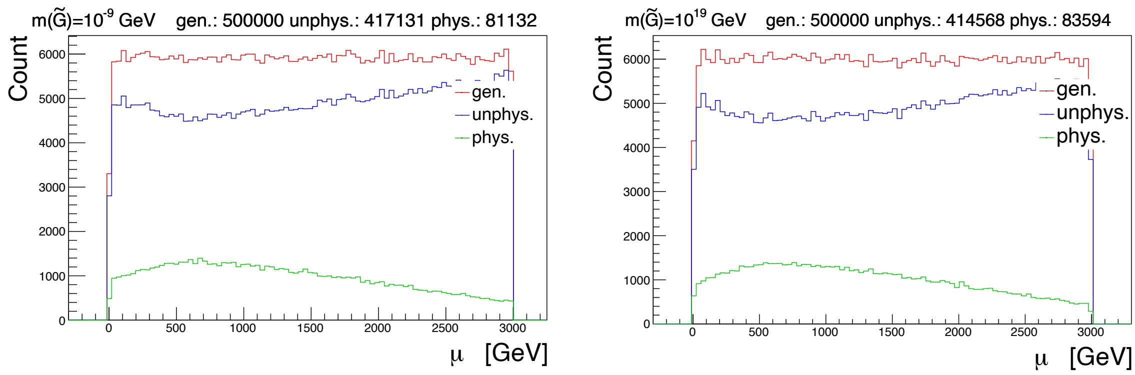

Figure A.9

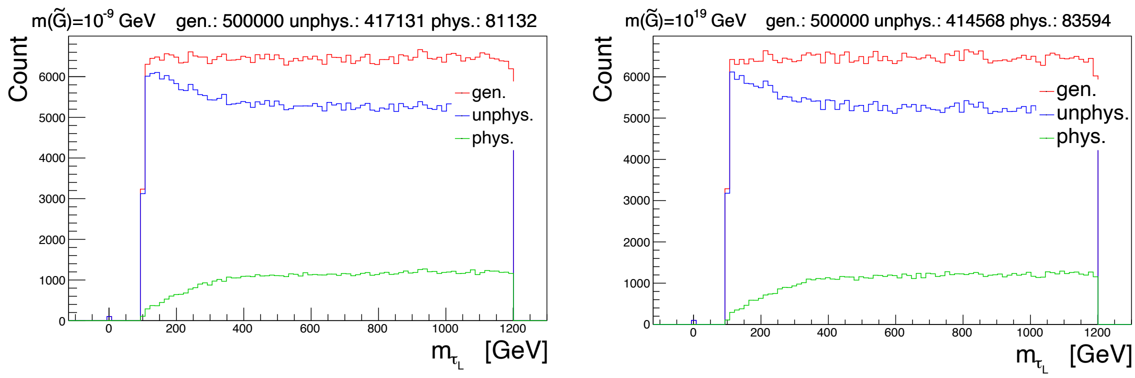

Figure A.10

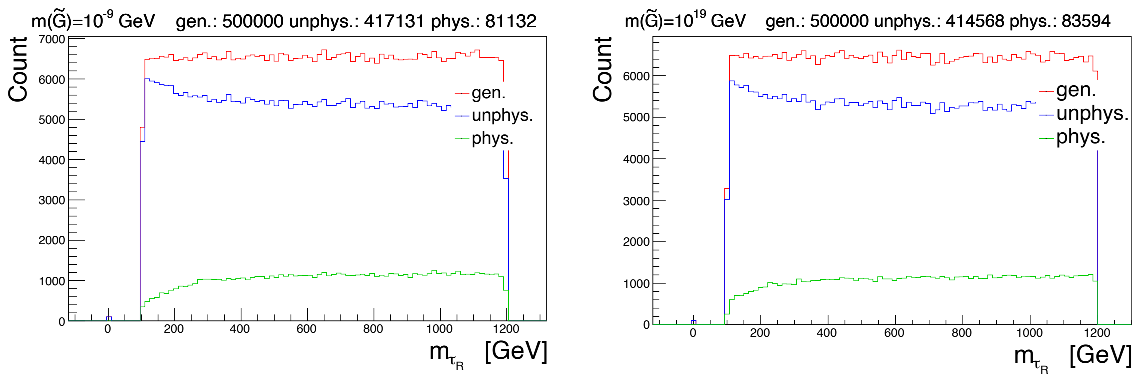

Figure A.11

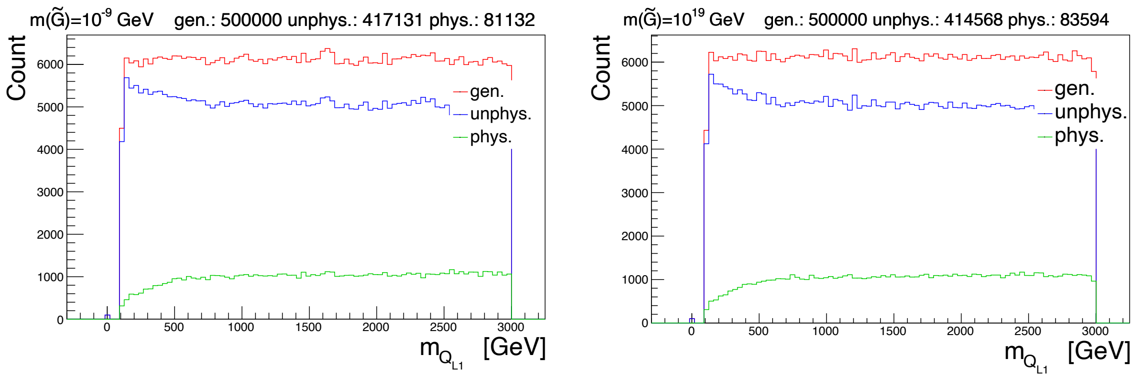

Figure A.12

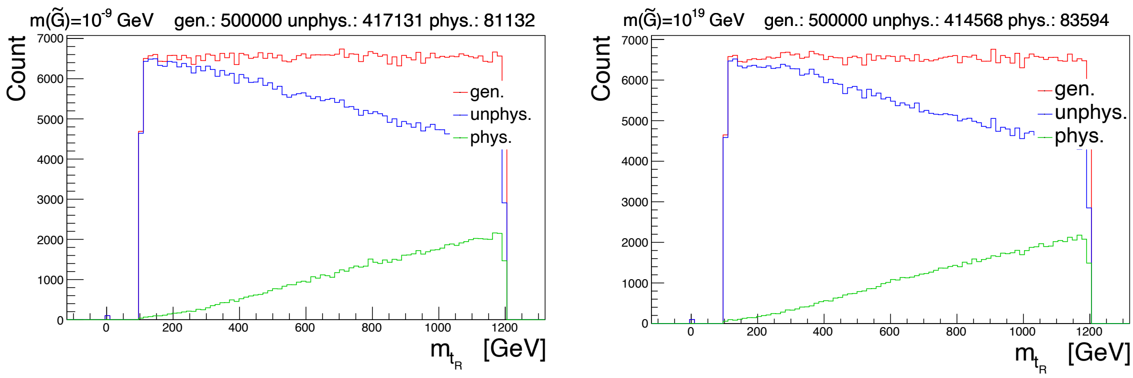

Figure A.13

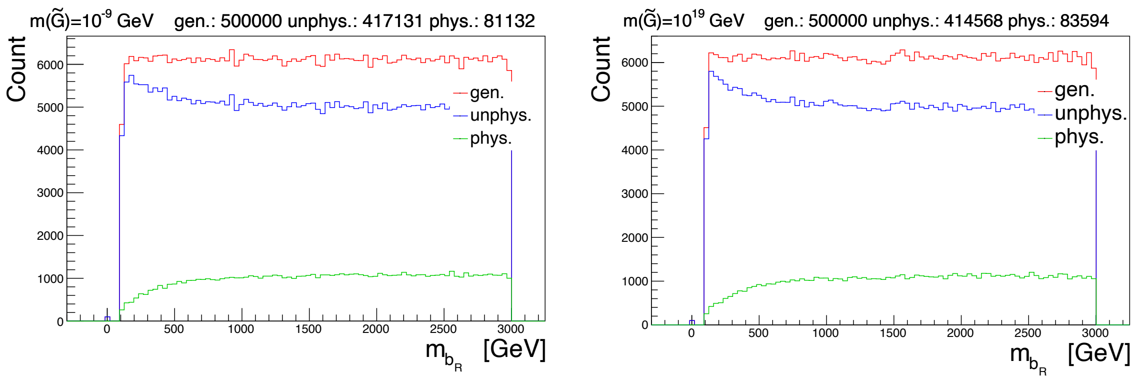

Figure A.14

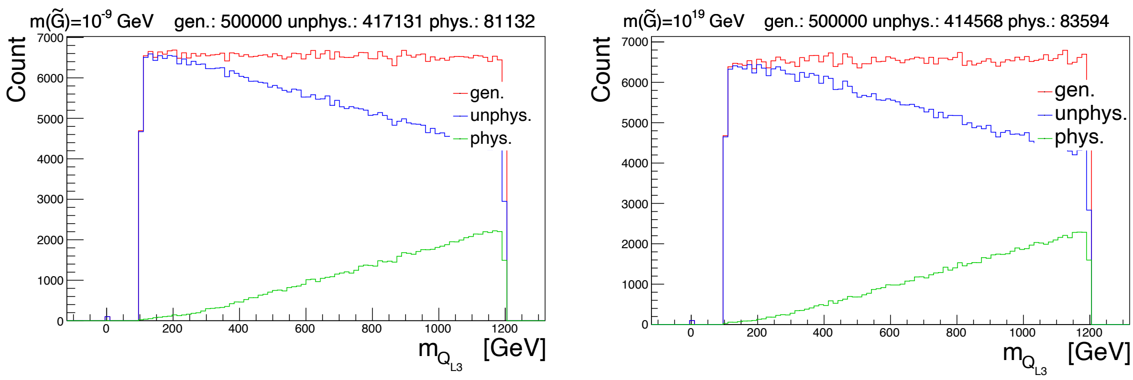

Figure A.15

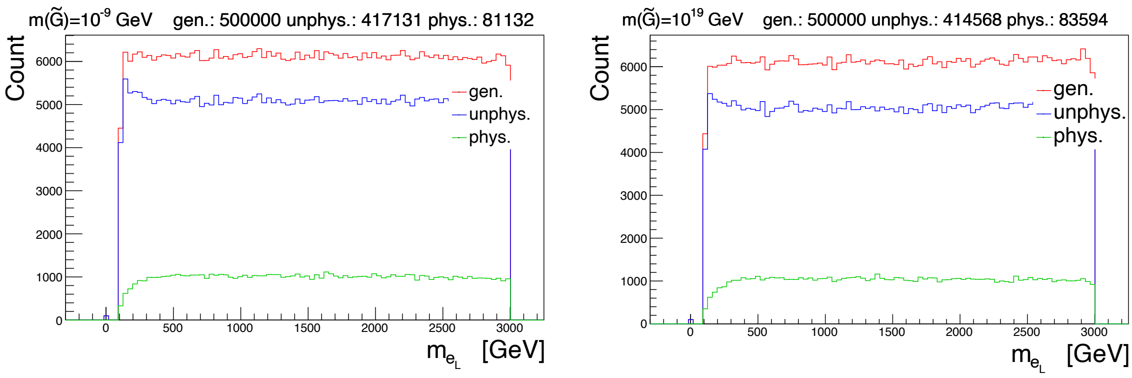

Figure A.16

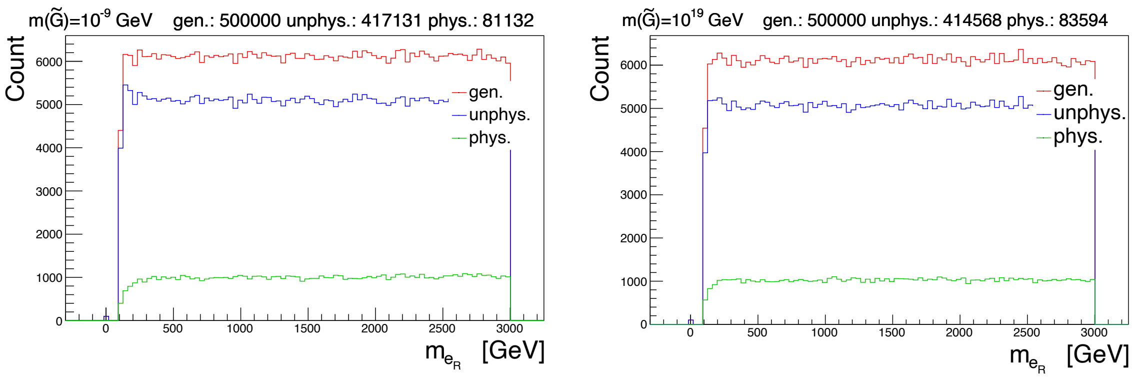

Figure A.17

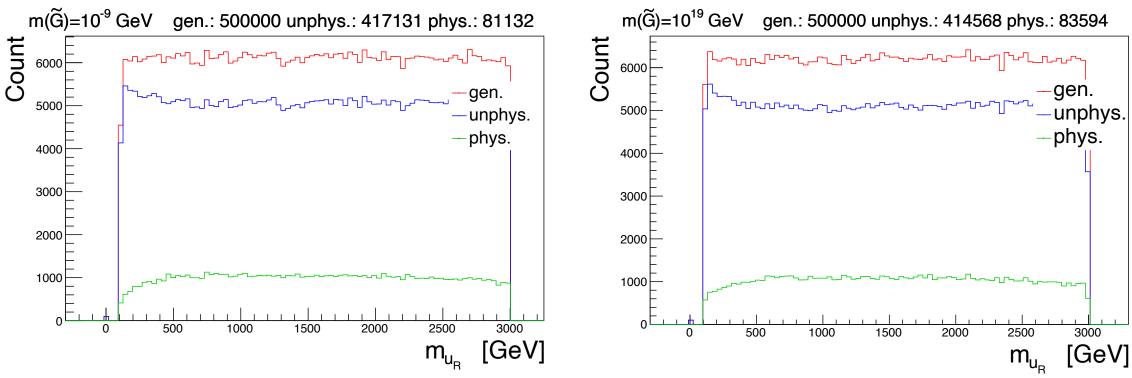

Figure A.18

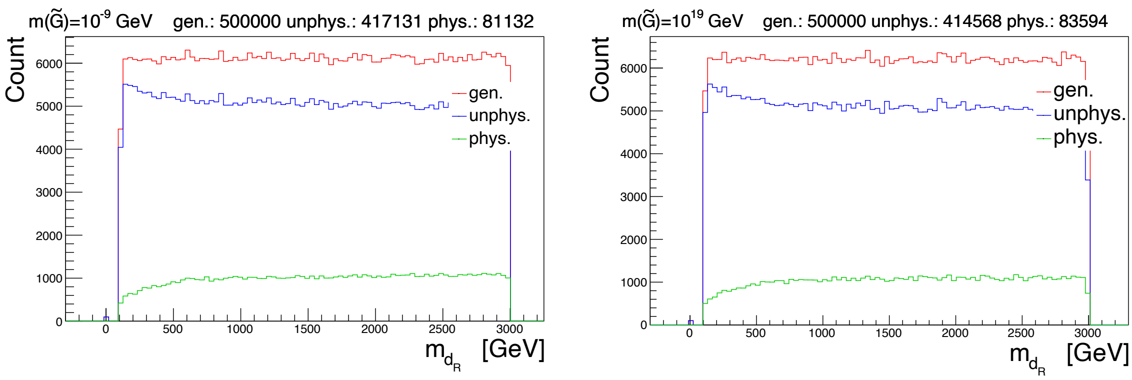

Figure A.19

Acknowledgements

I would like to thank everyone that supported me throughout the last year with the making of this thesis. Special thanks go to

- Prof. Dr. Dorothee Schaile, for giving me the opportunity of working in her group.
- PD Dr. Alexander Mann, for the help and guidance that was provided throughout my time working on this thesis, without which none of this would have been possible.
- Eric Schanet, for reviewing this work and giving very helpful feedback.
- Everyone in the ETP group, for the fun and inclusive atmosphere.
- Anna Bertolini, for being a good friend.
- My family, for supporting me throughout the entire process, especially during the last seven months in which I've been working from home due to COVID-19.

Selbständigkeitserklärung

Ich versichere hiermit, die vorliegende Arbeit mit dem Titel

Modelling Pair Production of Top Squarks with Decays via Tau Sleptons in the pMSSM

selbständig verfasst zu haben und keine anderen als die angegebenen Quellen und Hilfsmittel verwendet zu haben.

Christoph Ames

München, den 30. Oktober 2020